Functional Aligned Porous Materials via Directional Freezing and Frozen UV Initiated Polymerization

By Michael Barrow

UNIVERSITY OF LIVERPOOL

Thesis submitted in accordance with the requirements of the University of Liverpool for the degree of Doctor of Philosophy by Michael Barrow

July 2013

Abstract

Thesis title: Functional Aligned Porous Materials via Directional Freezing and Frozen UV Initiated Polymerization.

The work in this thesis is split into three experimental chapters:

The first section involves the development of the directional freezing and frozen polymerization method to prepare crosslinked aligned porous polymers with improved mechanical stability. Monomer solutions were directionally frozen in liquid nitrogen to orientate the growth of solvent crystals and the frozen samples are polymerized by UV irradiation. The solvent is removed under vacuum at room temperature to produce aligned porous structure. The mechanical stability is improved by two orders of magnitude compared to the usually freeze-dried porous materials. The materials are modified with graphene and a conducting polymer to make conducting monoliths, whilst maintaining the aligned porous structure. The aligned porous monolith is also assessed by high performance liquid chromatography (HPLC), showing fast separation of hydrocarbon compounds with low back-pressure. The second section uses directional freezing and frozen UV initiated polymerization to prepare aligned porous stimuli-responsive hydrogels. Oligo-ethylene glycol methacrylates and dimethylamino ethyl methacrylate monomers were used to produce temperature and pH-responsive hydrogels respectively. Aligned porous morphologies are observed in both dry and hydrated states. The hydrogels exhibit stimuli-responsive behaviour in aqueous conditions and anisotropic compressive strength and diffusion behaviour with respect to freezing direction. Section three uses directional freezing and frozen UV polymerization method to prepare aligned porous monoliths containing silica. The surface of the materials was post-functionalized to make two different types of aligned porous composites. Hydrothermal synthesis using Teflon lined autoclaves was used to functionalize monoliths separately with silver and metal organic frameworks (MOFs). The MOF composite materials were used as a stationary phase to try and separate a mixture of organic compounds.

Acknowledgements

I would like to thank my supervisor Dr Haifei Zhang for giving me the opportunity to study within his group. I thank the EPSRC for funding my work and the Centre of Materials Discovery at the University of Liverpool for access to state of the art facilities. I would also like to say a special thanks to Dr Adham Ahmed for his constant help and enthusiasm during the project.

I would like to acknowledge everybody who has helped me at some point during my research and say thanks to all my friends for making my time at the university enjoyable and wish them all the best for the future.

Also, a big thank you to my Mum, Dad and Nicola for their support.

Publications

1. **"Frozen polymerization for aligned porous structures with enhanced mechanical stability, conductivity and as a stationary phase for HPLC"** Barrow, M.; Eltmimi, A.; Ahmed, A.; Myers, P.; Zhang, H. *Journal of Materials Chemistry.* **2012**, *22*, 11615.
2. **"Aligned porous stimuli-responsive hydrogels via directional freezing and frozen UV polymerization"** Barrow, M.; Zhang, H. *Soft Matter* **2013**, *9*, 2723.
3. **"Aligned porous MOF monoliths via multiple loading technique on a surface functionalized scaffold"** Barrow, M.; Ahmed, A.; Clowes, R.; Zhang, H. *Manuscript in preparation* **2013**

GLOSSARY

ATRP	atom transfer radical polymerization
CGP	chain growth polymerization
FRP	free radical polymerization
FTIR	fourier transform infrared spectroscopy
GC	gas chromatography
GPC	gel permeation chromatography
HETP	height equivalent theoretical plate
HIPE	high internal phase emulsion
HIPIC	hydrophilic interaction chromatography
HPLC	high performance liquid chromatography
IEX	ion exchange chromatography
m/m	mass to mass ratio
LCST	lower critical solution temperature
M_n	number average molecular weight
MP	mobile phase
M_w	weight average molecular weight
NPC	normal phase chromatography
O/W	oil in water
Poly/P	polymerized
PDI	polydispersity index
pXRD	powder X-ray diffraction
RAFT	radical addition-fragmentation chain transfer polymerization
RPC	reverse phase chromatography
RT	room temperature
SEC	size exclusion chromatography
SEM	scanning electron microscopy
SGP	step growth polymerization
SP	stationary phase
TGA	thermogravimetric analysis
UV	ultraviolet
v/v	volume to volume ratio
W/O	water in oil

CHEMICAL GLOSSARY

APTES	(3-aminopropyl)triethoxysilane
BTC	trimesic acid/benzene-1,3,5-tricarboxylic acid
CNT	carbon nanotube
DEAEMA	(2-diethyl amino) ethyl methacrylate
DMAEMA	(2-dimethyl amino) ethyl methacrylate
DMSO	dimethylsulfoxide
DVB	divinylbenzene
EGDMA	ethylene glycol dimethacrylate
GO	graphene oxide
HCl	hydrochloric acid

HEMA	(hydroxyethyl) methacry==late
HKUST-1	metal organic framework made from copper nitrate and trimesic acid
MOF	metal organic framework
MPTMS	(3-mercaptopropyl)trimethoxysilane
MWCNT	multi-walled carbon nanotube
NaOH	sodium hydroxide
NIPAAm	N-isopropylacrylamide
OEGMA	oligo-ethylene glycol methacrylate
PCS	polycarbosilane
PCL	poly(caprolactone)
PEDOT-PSS	poly(3,4 ethylene dioxythiphene) poly(styrene sulfonate)
PEG	poly(ethylene glycol)
PEGDA	poly(ethylene glycol) diacrylate
PEGMA	poly(ethylene glycol) dimethacrylate
PLA	poly(lactic acid)
PLGA	poly(lactic acid co-glycolic acid)
PVA	poly(vinyl alcohol)
PVP	poly(vinyl pyrrolidone)
SCMC	sodium carboxymethylcellulose
SWCNT	single walled carbon nanotube
TEGDMA	tetraethylene glycol dimethacrylate
TMPSMA	trimethoxysilyl propyl methacrylate

CONTENTS

Chapter 1 - Introduction

Chapter 2 – Characterization Methods and Equipment

Chapter 4 - Aligned porous stimuli-responsive hydrogels *via* directional freezing and frozen UV initiated polymerization

Chapter 5 – Aligned Porous Composites

Chapter 6 – Conclusions and Outlook

Chapter 1

Introduction

List of Figures

List of Schemes

The target of this work is to produce aligned macroporous material with different functionality. This material is produced by combining two techniques: directional freezing and frozen ultraviolet (UV) initiated polymerization. We aim to show the versatility of this new procedure for making aligned porous material.

1.1 Porous Materials

A porous material is defined as a material that contains voids or cavities. They are generally separated into 3 categories: microporous (< 2 nm), mesoporous (2-50 nm) and macroporous (> 50 nm).[1]

Microporous materials can be prepared as extended networks or discrete molecules.[2] They can be composed of organic, inorganic or hybrid building blocks and have functions in gas storage,[3] molecular separations[4-7] and heterogeneous catalysis.[8-10] Ordered mesoporous materials that allow facile diffusion of bulky molecules are used for catalysis[11-13] and adsorption technologies such as chromatography.[14,15] Mesoporous materials are normally prepared *via* self-assembly of sol-gel precursors and structure directing amphiphiles such as block copolymers or surfactants.[16-18]

This study focuses primarily on ordered macroporous materials. Macroporous materials are widely investigated due to their relatively large pore size, fast mass transport and pore accessibility. They are used in a wide range of applications, such as drug delivery,[19] catalysis,[20] separation processes[21] and as scaffolds for tissue engineering.[22] A more detailed overview of these materials is given in section 1.2.

1.2 Macroporous Materials

Production of macroporous materials is most commonly achieved using templating methods,[23] however other methods do exist such as self-assembly of polymers,[24] electrochemistry,[25] etching[26] and soft lithography.[27] The types of templates used for production of macroporous materials can be split into hard and soft categories. Ice has also been widely used as a template where aqueous polymer solutions are frozen and freeze-dried to produce macroporous material.

1.2.1 Hard Templates

Macropores can be produced using *hard* templates or prefabricated materials such as polymers,[28,29] colloidal particles[30,31] or pre-formed natural structures.[32] The pores are generated after solid material is formed around the template that is subsequently removed by heat, washing or etching techniques.

Walsh *et al*. used the polysaccharide dextran as a sacrificial template to prepare macroporous zeolites[28] (Figure 1.1) and metal sponges[29]. Dextran was used because of its easy-handling, water solubility and aldehyde functionality, which reduce metal

ions *in-situ*. During thermal degradation dextran expands creating macropores before being removed.

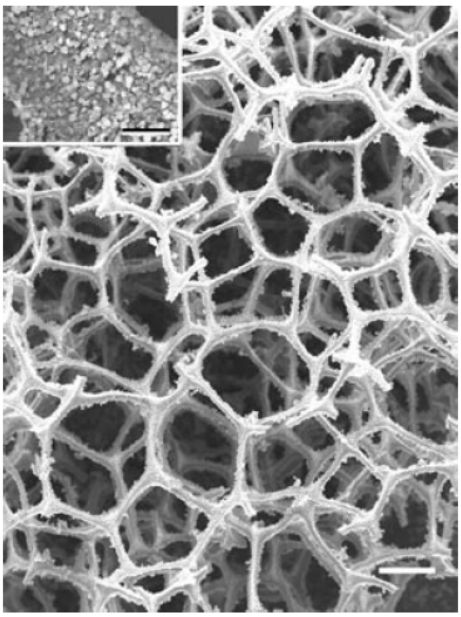

Figure 1.1 SEM image of macroporous zeolite/silica framework prepared by dextran templating, scale bar = 100 µm. Inset; high magnification image of pore wall containing NaY crystals, scale bar = 5 µm.[28]

Macroporous $LiMn_2O_4$ thin films have been prepared using a sol-gel technique on $Pt/Ti/SiO_2/Si$ substrates. Polystyrene microspheres were used as a template to develop the ordered macroporous network. The spheres were removed using calcination to yield a three dimensional (3D) electrode material.[33]

Colloidal crystal templating uses spherical latex or silica particles to prepare ordered macroporous material.[34] This method was first used to make porous silica[35] however it has since been used to make macroporous metals,[31] carbon[36] and polymers.[37] Scheme 1.1 outlines the method where particles are first isolated by filtration before loading of material takes place via reactions such as polymerization, particle infusion or sol gel hydrolysis. Latex particles are removed by calcination and silica particles are washed away with hydrofluoric acid (HF). Materials produced by this method were used as scaffolds to prepare photonic crystals[38] and thought to be a desirable surface for catalysis.[34]

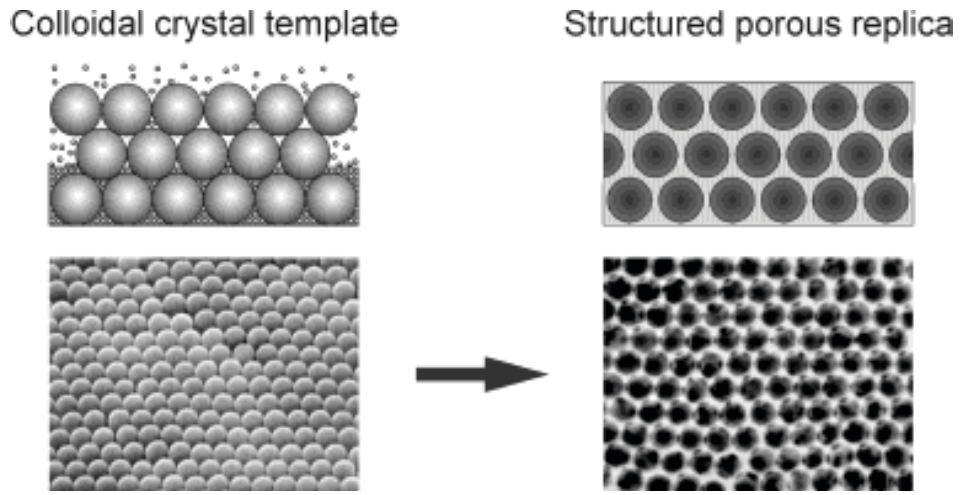

Scheme 1.1 Preparation of macroporous material using colloidal crystal templating.[34]

1.2.2 Soft Templates

Using a *soft* template is considered to be a more facile route to produce macroporous material. A *soft* template such as gas, water, supercritical fluid or the oil phase of an emulsion can be removed by washing or under vacuum.

An advantage of using soft templates is less energy intensive steps to generate the macropores. In particular, using water or gas as a solvent leads to easier handling of samples and removes the need for using volatile organic solvents. A method for preparing macroporous chitosan was developed that involves dissolving high-pressure carbon dioxide into an aqueous solution acting as a foaming agent. Removing the need for toxic solvent resulted in increased cell proliferation.[39] Dense macroporous poly 2-hydroxyethyl methacrylate (HEMA) was prepared by thermal polymerization. This was carried out in water using radical polymerization; varying concentration to investigate different physical and mechanical properties.[40]

1.2.2.1 Emulsion Templated Materials

Emulsion templating is a widely used technique for the preparation of macroporous materials. An emulsion is a mixture of two immiscible liquids in the form of droplets.[41] They are often referred to as either an oil-in-water (O/W) emulsion or a water in oil (W/O) emulsion, where the first phase mentioned refers to the droplet/internal phase.[41] Scheme 1.2 shows three ways polymerization can be used in emulsions. For preparation of macroporous material an O/W emulsion is used that contains oil droplets in the micrometer size range. The water (continuous) phase

containing monomer and initiator is polymerized to prepare macroporous material. The oil phase is removed by washing, or if volatile, using vacuum techniques.[19,42] In 1982, Unilever patented a process for the production of macroporous material by polymerizing the continuous phase of HIPE (high internal phase emulsion). The resulting materials are commonly known as polyHIPEs.[43]

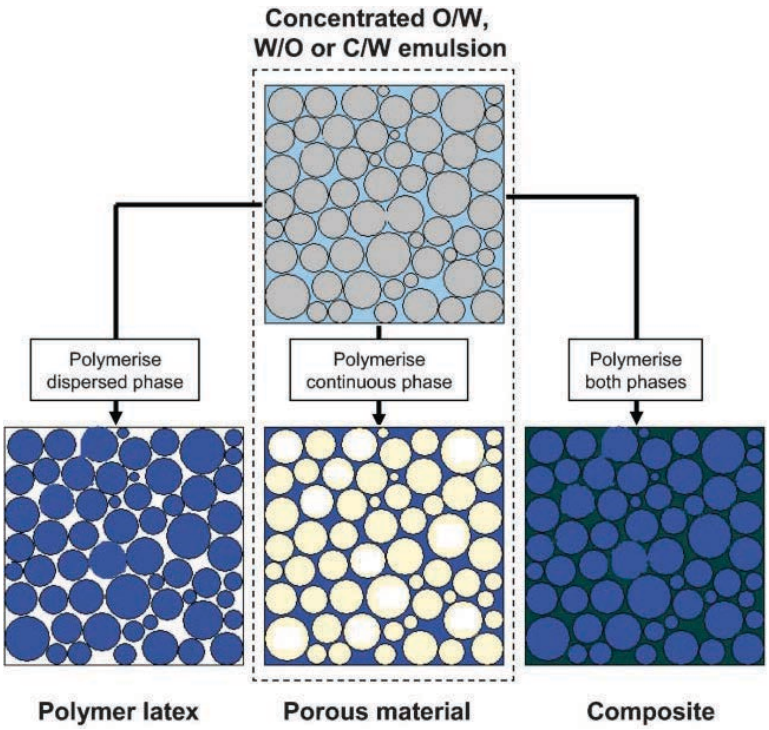

Scheme 1.2 Schematic showing polymerization in emulsions. Left - Polymerization of the dispersed phase to yield latex/colloid particles. Centre - polymerization of continuous phase to produce macroporous material. Right – polymerization of both phases to yield composite materials.[41]

There are now a vast number of publications regarding emulsion templated materials. Hydrophobic, hydrophilic and inorganic composite polyHIPE materials can be prepared by polymerizing the continuous phase of a HIPE.[41] The most widely studied hydrophobic material is based on polymers made from styrene and divinylbenzene.[44,45] Figure 1.2 shows an SEM image of this material, in which a highly porous, interconnected network is obtained. Pore morphology is governed by the size and shape of oil droplets, which are removed after polymerization. Therefore, polyHIPE materials always contain characteristic spherical voids. Other types of hydrophobic macroporous polyHIPEs have been prepared from methyl methacrylate,[46] ethylene glycol dimethacrylate (EGDMA)[47] and butyl acrylate.[48]

Hydrophilic polyHIPEs based on HEMA[49] and acrylic acid[50] monomers have also been investigated, as well as macroporous metals[51] and silica.[52]

Numerous reviews have been published regarding polyHIPEs.[41,53,54] The primary aim of most studies is to fine tune or control the macroporous size range for specific applications.[49,55] Mainly, polyHIPEs are used in tissue engineering for cell growth, but other applications include drug delivery,[19,42] purification[56] and separation.[57]

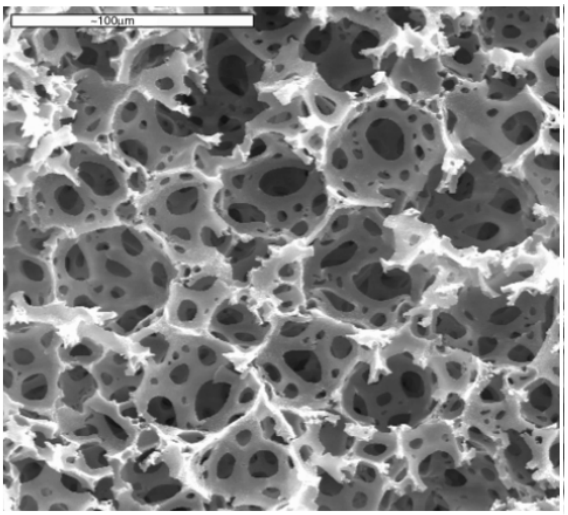

Figure 1.2 SEM image of a polystyrene/divinylbenzene foam (pore volume approximately 90%).[44]

For tissue engineering, different styrene/ divinyl benzene (DVB) systems have been used for cell growth,[58] bone formation,[59] and neurone growth[60] as the porous crosslinked scaffolds demonstrate considerable cell adhesion and growth. More recently, degradable polyHIPEs have been prepared by photopolymerization of emulsions containing multifunctional arcylates and thiols.[61] Human skin cells were successfully cultured on the thiolene polyHIPEs suggesting that the materials are biocompatible. However, cell growth was mainly on the surface and penetration into the porous scaffold was limited.[61]

Another interesting use of emulsions is for the preparation of drug nanoparticles.[62,63] Due to the low solubility of drugs in water, polyHIPEs were prepared with the drug component dissolved in the droplet phase. After freeze-drying, the drug molecules formed nanoparticles on the surface of the macroporous polymer material, which then collapse in water to form a dispersed organic nanoparticle (Scheme 1.3). When

aqueous nanodispersions containing an antimicrobial agent were prepared using this method showed greater activity than typical organic aqueous solutions.[62]

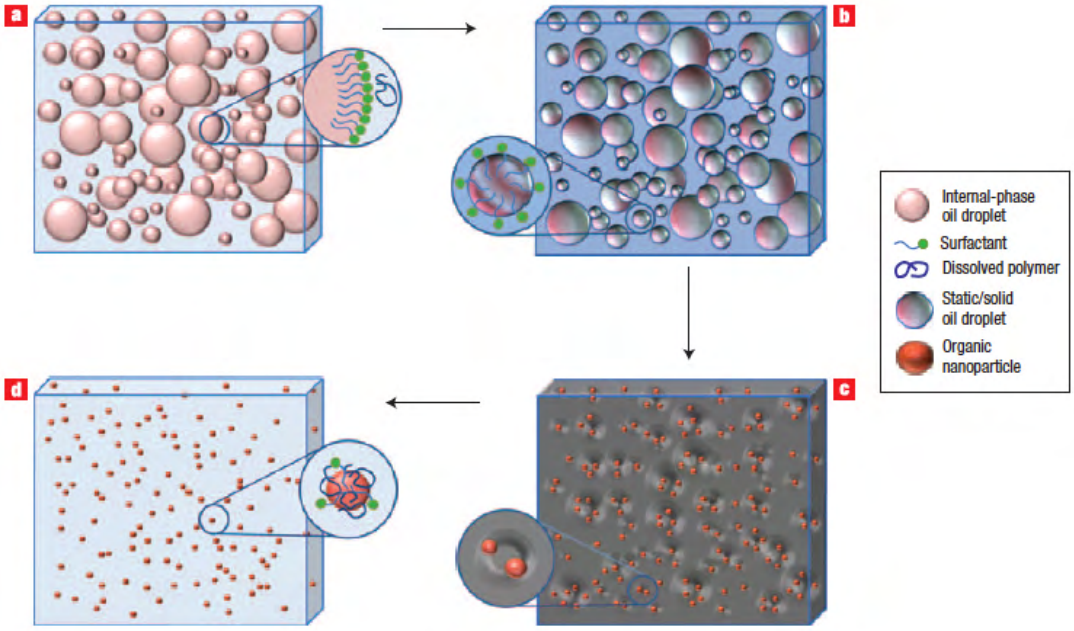

Scheme 1.3 Schematic showing organic nanoparticle formation on a macroporous scaffold after freeze drying A) O/W emulsion with active drug phase dispersed in internal phase B) frozen O/W emulsion C) macroporous solid obtained after freeze drying with organic nanoparticles formed on the surface. D) organic nanodispersion after addition of water.[62]

1.2.3 Ice Template

Ice has been used as a template to produce a range of macroporous materials. Typically, an aqueous solution (e.g., polymer solution) is frozen and the ice crystals are removed by a sublimation technique known as freeze-drying. The macropores are formed by a phase separation between ice crystals and the solute which have low solubility in ice crystals.[64,65] This method is also seen as a *green* route to macroporous material as the use of organic solvents is avoided, however, some freeze dried materials are prepared using organic solvents with relatively high melting points.[66,67]

Predominantly, macroporous structures made using this method consist of polymer[68] or ceramic material.[69] The pore morphology is largely dependent on freezing conditions or concentration of solutions. Figure 1.3 demonstrates this with aqueous solutions of polymer sodium carboxymethylcellulose (SCMC). A random freezing

procedure (Figure 1.3A) was compared with a directional freezing technique (Figure 1.3B) to obtain different pore morphology. When the solution was diluted a more porous material was obtained (Figure 1.3C). In this particular study pore volumes and sizes of macroporous polymers were systematically tuned using a combination of emulsion templating and freeze-drying. Both organic and inorganic materials were investigated.[68]

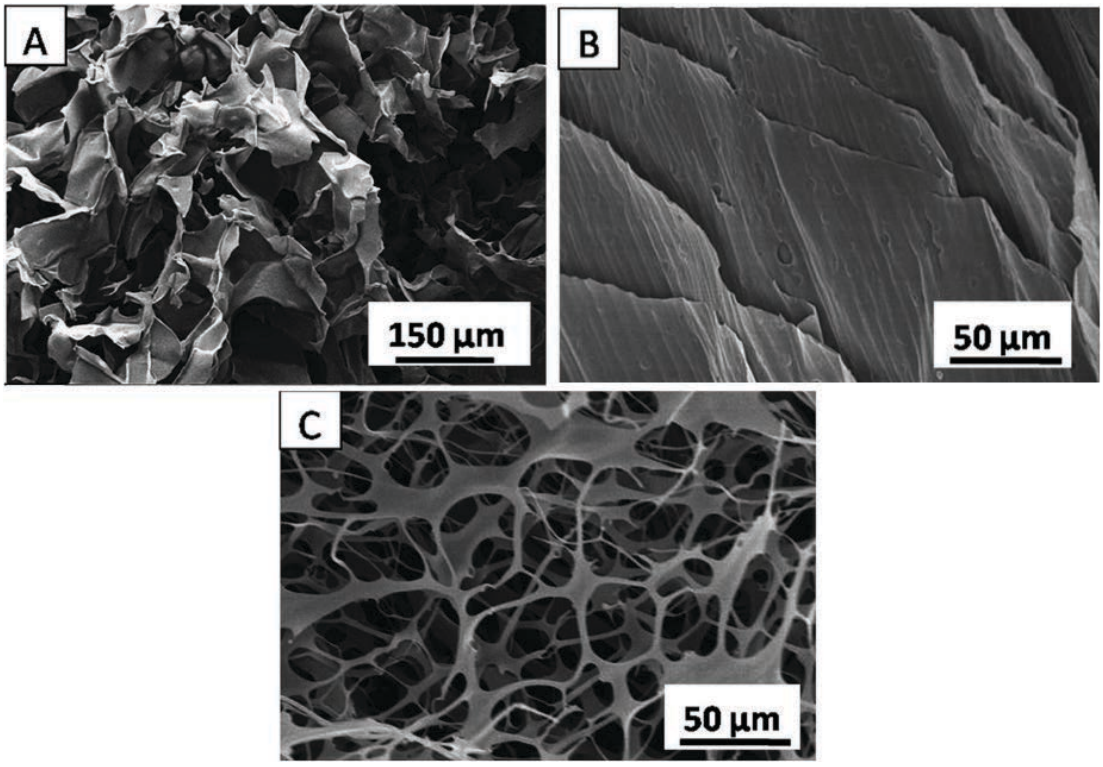

Figure 1.3 SEM images of freeze dried SCMC. A) Randomly porous structure by freeze drying 3 wt% aqueous solution frozen in freezer B) layered structure after same solution was directionally frozen in liquid nitrogen C) highly porous structure obtained after freeze drying 1 wt% solution after directional freezing.[68]

Macroporous monolithic gels can also be prepared using cryopolymerisation where monomer solutions are frozen and polymerized in a frozen or semi-frozen state. These materials have potential applications in chromatography, water purification and cell culturing.[70-72] A more detailed description of cryopolymerization is given in section 1.7.

An ongoing challenge for preparing macroporous materials is the control of pore size, volume, morphology and interconnectivity for specific applications. A

directional freezing method was introduced to produce aligned porous materials with ordered structure throughout.

1.3 Aligned Macroporous Material

Aligned macroporous materials are often preferred, as their anisotropic properties allow for more efficient mass transport compared to regular macroporous materials.[73,74] Therefore this type of material is widely investigated for tissue engineering[75] and for conductive flow through electrodes.[76] Colloidal and emulsion templating are the still the main method for production of macroporous material, although a directional freezing method was introduced to produce aligned porous material,[73,77,78] where polymer solutions are submerged in liquid nitrogen at a controlled rate, resulting in a uniform phase separation between solvent and solute. The solvent (water is used most commonly) could then be removed by freeze-drying, leaving an interconnected aligned porous structure. This method is viewed as a more economical route to produce aligned porous materials and various parameters such as freezing rate, freezing temperature and solvent viscosity can be altered to control pore size.[79]

Aligned porous polycaprolactone (PCL) and polyvinylalcohol (PVA) were prepared using the directional freezing method. Tuning of pore size was achieved by varying freezing rate.[78,80,81] An on-going challenge for freeze-dried materials is lack of mechanical stability. Polymer samples are normally very fragile and will dissolve in certain solvents.

1.3.1 Tissue Engineering

In terms of tissue engineering, desirable properties of a scaffold include:

1) Three dimensional and highly interconnected pore network for cell growth and mass transport
2) Biocompatibility with a controllable degradation and resorption rate to match cell/tissue growth
3) Suitable surface chemistry for cell attachment, proliferation, differentiation.

4) Mechanical properties to match those of the tissues at the site of implantation.[82,83]

Aligned porous materials have been made from polylactic acid (PLA) dissolved in dioxane via directional freezing and washing in ethanol.[84] Highly interconnecting structures were observed. These structures were used to seed bone marrow stromal cells on the surface. Lack of perfusion and lack of vascular networks often prevent regularly porous polymeric scaffolds from being suitable for tissue engineering, however aligned porous poly(lactic-co-glycolic acid) (PLGA) (also prepared using dioxane) was used as a blood vessel scaffold.[67] These scaffolds could be prepared with different wall thickness and diameter corresponding to the type of mould used (Figure 1.4) and contained an aligned structure throughout. They showed rapid proliferation of A10 cells derived from rat's vascular muscles.[67] Many polymers and natural minerals are now investigated for use as aligned porous scaffolds for cell growth *e.g.,* gelatin[85] and hydroxyapatite.[86]

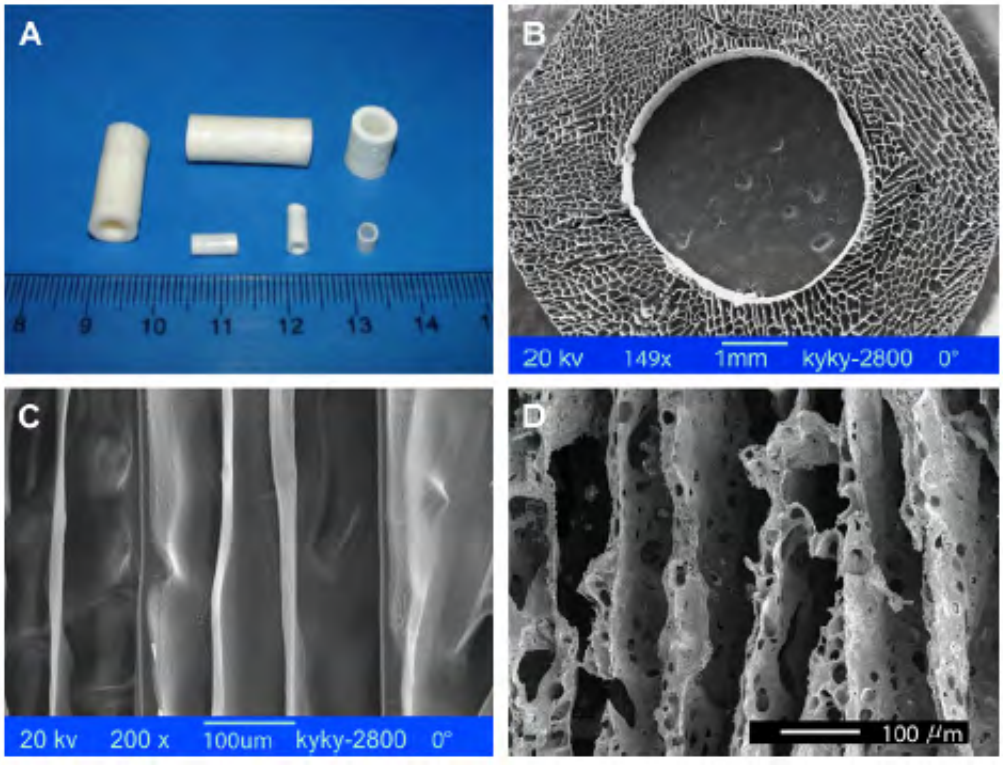

Figure 1.4 View of a microtubular orientation-structured blood vessel scaffold: A) physical appearance B) SEM image of cross section C) SEM magnified vertical section of a smooth microtubular stuctured blood vessel scaffold (x 200 magnification) D) SEM vertical section of a porous microtubular structured blood vessel sod vessel scaffold (x 200 magnification).[67]

For regeneration of load bearing bones, use of polymer scaffolds is often difficult because of the low mechanical stability of the polymer scaffold.[83] Bioactive glasses or ceramics generally have larger compressive strength than polymer scaffolds.[83] Aligned porous alumina has been prepared by freeze-casting ceramic slurries.[74] Also, aligned silica carbide ceramics were prepared using polycarbosilane (PCS) in camphene. Porous SiC ceramics were then produced by pyrolysis of the porous PCS at 1400°C under an argon atmosphere.[87] An alternative to ceramic material for increased mechanical stability is the use of polymer nanocomposites. A nanomaterial such as carbon nanotubes (CNT) can be incorporated into polymer solutions before directional freezing takes place and the resulting material will have characteristics owing to the CNTs. Even though some contradictory results have been reported with regards to the cytotoxicity of CNTs,[88-90] aligned porous chitosan/multiwalled-carbon nanotubes (MWCNT) composites have been used successfully for bone formation in muscle tissue (Figure 1.5).[75]

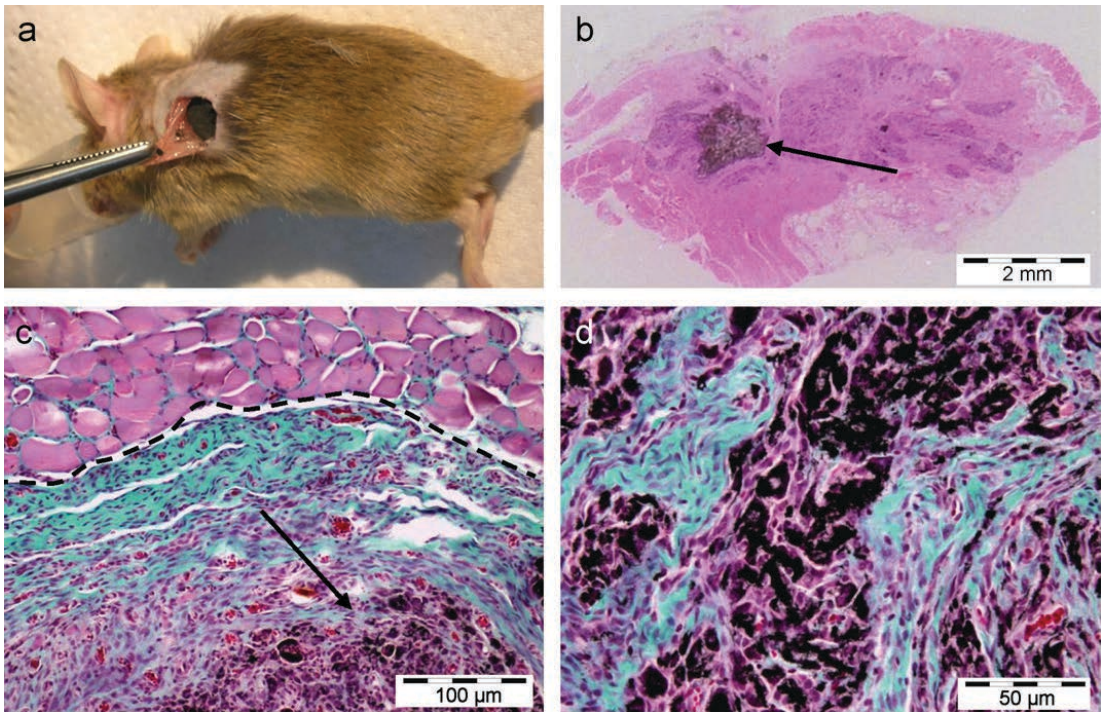

Figure 1.5 Optical images A) shows surgical implantation of rhBMP-2 absorbed onto MWCNT/chitosan scaffolds into subcutaneous muscular pocket of a mouse. Optical microscope images showing B) regenerated bone tissue and a fraction of MWCNT/chitosan scaffold remaining. C) Detail of regenerated bone tissue (collagen expressing cells blue-green coloured) after disassembly of scaffold. Black colour indcates remaining scaffold. D) Detail of scaffold (black colour) prior to its disassembly and colonization by collagen expressing cells (blue-green colour).[75]

This was achieved by implantation of the scaffold loaded with bone morphogenetic protein 2 (rhBMP-2) into the subcutaneous muscular pocket of a mouse (Figure 1.5A). The bone tissue was regenerated, with only a fraction of the scaffold remaining after degradation (Figure 1.5B-D).[75]

1.3.2 Aligned Porous Material with Enhanced Conductivity and Mechanical Stability

Introducing conductivity into aligned 3D polymeric scaffolds can increase the range of potential applications, mainly as flow-through electrodes but also as scaffolds for catalysis.[91] Aligned macroporous structures can be fabricated by direction freezing and lyophilization of conducting polymer solutions.[92] For example, aligned honeycomb structures were observed when conductive polymer poly(3,4-ethylenedioxythiophene) polystyrene sulfonate (PEDOT-PSS) was treated in this manner. Conductive cryogels were prepared using PEDOT-PSS in solution and a PEDOT-PSS hydrogel. The hydrogel was formed using iron nitrate oxidizing agent instead of ammonium persulfate, which increased the amount of crosslinking but decreased the resulting porosity of the cryogel. Also when the hydrogel was freeze-dried, no aligned structure was observed. The conductivities of these materials are 10^{-2} S/cm for the hydrogel and 10^{-3} (axial) 10^{-4-6} (radial) S/cm for the polymer structure.[92] Silver nanowires stabilized by polyvinylpyrrolidone (PVP) were imbedded into aligned PVA structures by mixing both components in aqueous solutions before directional freezing. The composite material exhibit electrical conductivity to the order 1.4 x 10^{-4} S/cm.[93] Alternatively, an aligned scaffold containing PVA and iron chloride ($FeCl_3$) was prepared. The $FeCl_3$ within the material could oxidatively polymerize aromatic monomers to produce conductive composites.[94] This method could have advantages as various water-soluble polymers could be investigated (e.g., poly ethylene glycol) and various aromatic monomers. In this case pyrrole and 3,4 ethyldioxythiophene were studied. After functionalization with pyrrole, the monoliths turned from yellow to black (Figure 1.6A &B). Also, the polymerization reaction did not compromise the aligned structure (Figure 1.6C &D). The conductivity of the PVA-PPy composites reached up to 0.1 S/cm.[94] The disadvantage associated with these freeze-dried materials is the lack of mechanical stability and dissolution in aqueous environments.

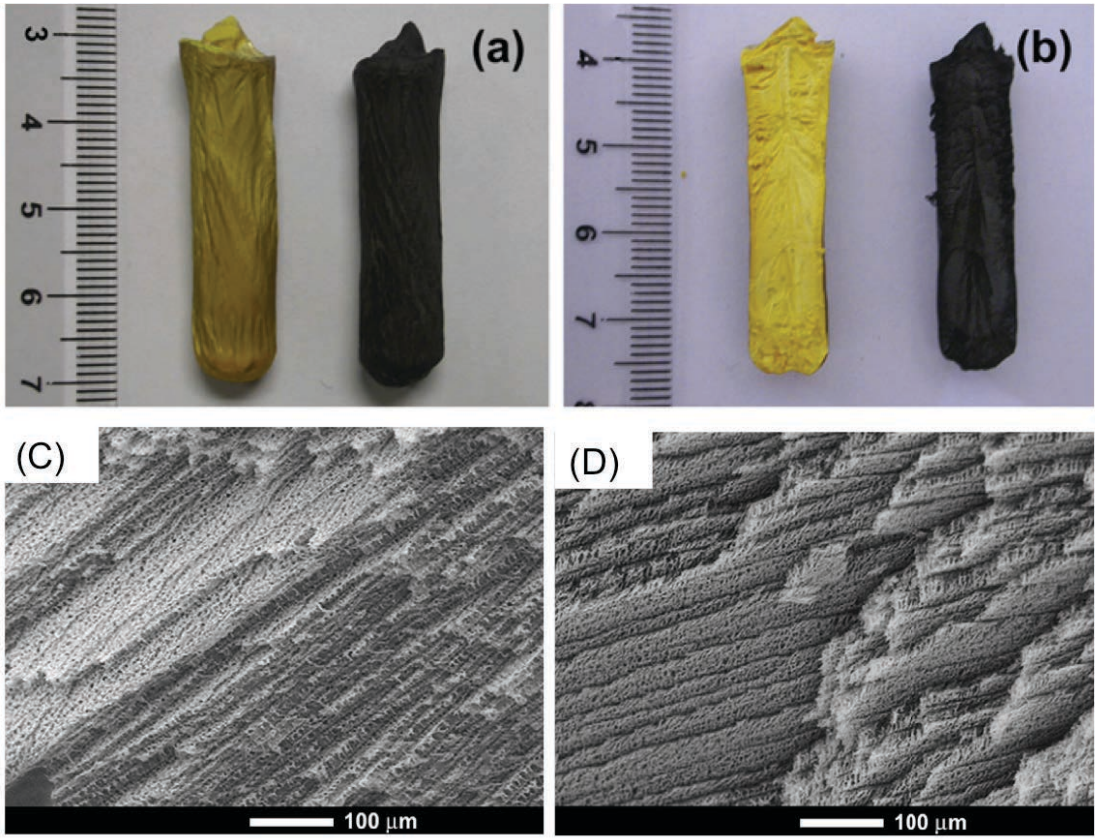

Figure 1.6 Optical images of A) monoliths B) cross-section of PVA-$FeCl_3$ (left) and PVA-PPy composite (right). SEM images C) before and after D) modification. Figure amended from reference.[94]

Since the discovery of CNTs in 1991[95] and isolation of pristine graphene in 2004,[96] polymer nanocomposites have been intensely investigated. The two different allotropes of carbon receive lots of interest due to their unique properties: high thermal and electrical conductivity and superior mechanical stability.[91] When incorporated into porous structures, materials can experience performance enhancements resulting from these properties. This is only possible if the nanomaterial is accessible or arranged in a manner where their properties can be exploited.[91]

CNTs are a cylindrical hollow nanomaterial with walls consisting of an atom thick layer of carbon atoms rolled into specific angles. They are split into three categories depending on the number of rolled walls: single, double or multiwalled (SWCNT, DWCNT, MWCNT).[91] Graphene is a two dimensional (2D) planar monolayer of carbon atoms arranged in a honeycomb lattice-like structure. It is essentially a single layer of graphite.[91] The most common route to polymer nanocomposites with CNTs

and graphene is chemical modification.[88,97] Treating these materials with heavily oxidative acidic solutions, transforms the carbon from a chemically inert insoluble material to a soluble material that can undergo further modification. This allows for direct reactions with polymers, or formation of homogenous solutions with polymers which can be freeze dried to produce macroporous composites.[91,97]

1.3.2.1 Carbon Nanotubes

The most common functionalization method of CNTs is using nitric acid.[98-100] This introduces carboxylic acid groups to the surface of the CNTs which can then be dispersed in aqueous solutions. They can be further functionalized for different functions or applications. Scheme 1.4 shows how further modification of oxidized CNTs can be used to make polymer nanocomposites. Thionyl chloride is used to introduce an acyl chloride functionality which then reacts with a conductive polythiophene polymer.[101]

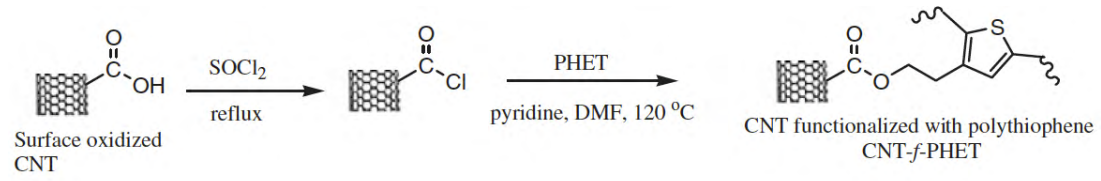

Scheme 1.4 Schematic of functionalized CNTs further modification with a conductive polythiophene polymer.[101]

Due to the biocompatibility of the polymer chitosan, chitosan/CNT composites are widely investigated for functions in living systems.[76,102,103] Porous chitosan/CNT composites can be prepared by freeze drying mild acetic acid solutions containing chitosan and functionalized CNTs.[75,104] Alternatively, a preformed macroporous structure is soaked in a functionalized CNT dispersion and freeze-dried.[105] After drying, the material has a homogenous layer of CNTs on the surface that forms a conductive network throughout the material.[105] As previously stated, aligned porous chitosan/CNT scaffolds were used for bone engineering as the aligned microchannels were ideal for cell proliferation and the CNTs provide mechanical properties that can support bone growth.[75] Due to the high loading of CNTs (up to 85 %) the composites

have conductivities of 2.5 S/cm (Figure 1.7). This property makes the material an ideal candidate as an anode for a direct methanol fuel cell.[106]

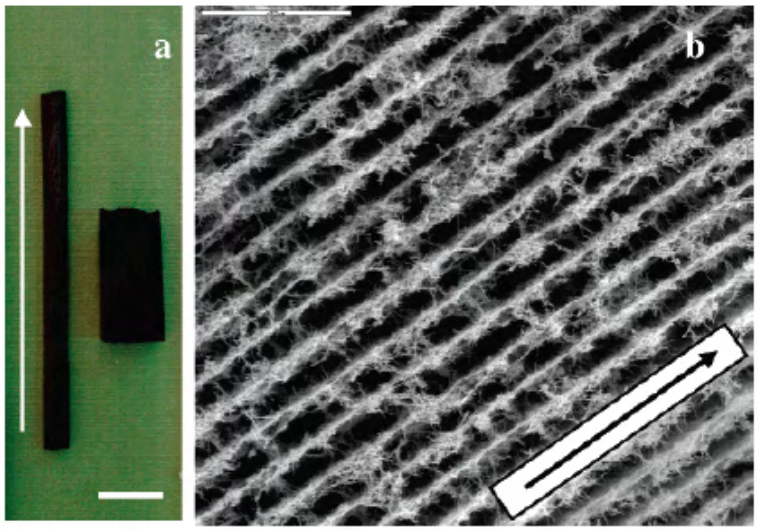

Figure 1.7 Aligned porous MWCNT/chitosan composites prepared by directional freezing of MWCNT/chitosan suspensions. A) Monoliths prepared using different disposable vessels (scale bar is 1 cm). B) SEM images of pore morphology of the material. The MWCNT content of all samples is 85%.[106] The arrow points towards the freezing direction.

1.3.2.2 Graphene

Ever since mechanical exfoliation of graphene was achieved and the fascinating properties were reported,[96] there has been intensive research trying to incorporate individual graphene sheets into various materials systems.[107-110] The most common route to graphene is through the oxidation of graphite to produce graphene oxide, then chemically reduced to produce individual graphene sheets.[111] The first report of oxidation of graphite oxide was in 1859, when Brodie added potassium chlorate ($KClO_3$) to a slurry of graphite and fuming nitric acid (HNO_3).[112] Staudemaier then improved the method by adding the potassium chlorate in portions during the course of the reaction.[113] In 1958, Hummers and Offeman developed another oxidation reaction using potassium permanganate and concentrated sulfuric acid.[114] Hummer's method is now the most commonly used method for producing graphite oxide and can be altered slightly to increase the degree of oxidation.[115] After oxidation is complete, individual sheets can be exfoliated by ultrasonication in aqueous conditions or in certain organic solvents where hydrogen bonding can take place.[116,117] The reaction scheme and structure of graphene oxide are shown in Scheme 1.5.

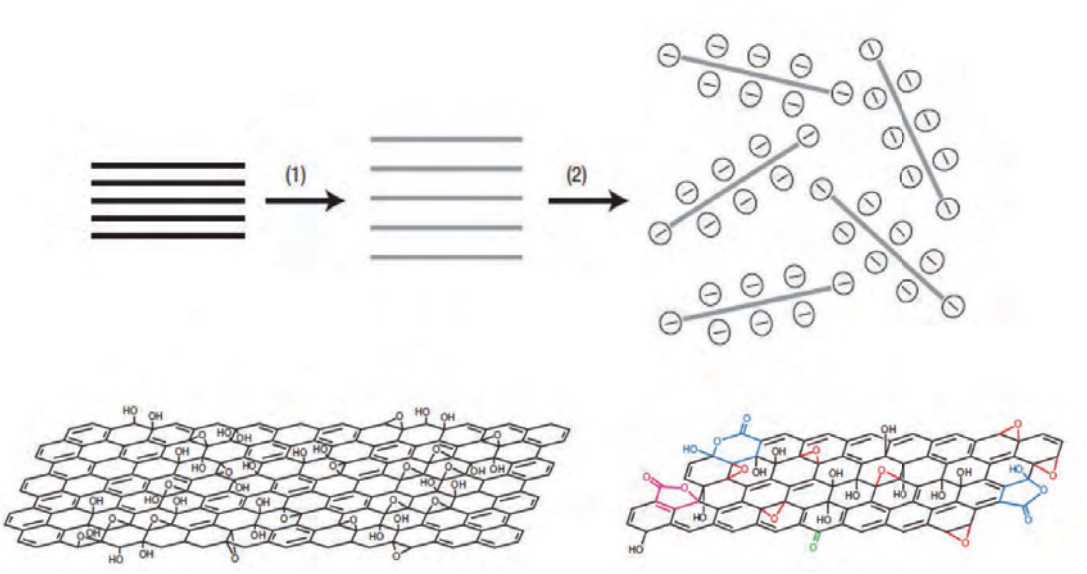

Scheme 1.5 Top - schematic of exfoliation of graphene oxide 1) graphite is treated chemically to make graphene oxide 2) separated into individually layers by ultrasonic agitation in water.[116] Bottom - structure of graphene oxide (left) Lerf-Klinowski model[118] (right) Gao model.[119]

There have been many models proposed for the structure of graphene oxide.[97] Even though the exact structure is not widely agreed upon, the most accepted is the Lerf and Klinowski model.[118,120] Originally the model contained carboxylic acid groups on the edge of the basal plane of the platelets, and there are still arguments to suggest that GO does contain acidic sites.[121] More recently, Gao *et al.* suggested that GO could contain 5 and 6 membered lactol rings on the edge of the platelets as well as esters of tertiary alcohols on the surface (Scheme 1.5).[119]

A problem with graphene oxide is that it is an electrical insulator. To reap all the benefits of single layered graphene, graphene oxide needs to be reduced to remove the oxygen groups and restore aromaticity and conductivity.[97] During the reduction reaction (typically using hydrazine) the solution turns from a brown suspension to a black precipitate owing to the hydrophobicity of the sheets after removal of oxygen functionality.[122] To counter this problem material scientists have used polymer stabilization during the reduction process,[123] or an *in situ* polymerization of a monomer stabilized graphene dispersion.[107,124]

There have been various successful methods published for production of 3D macroporous materials containing graphene. One approach used involved templating

a stable graphene dispersion around sacrificial PS beads.[125] Another method used sol-gel polymerization in the presence of GO, and then chemically reduced the structure afterwards.[126] Self-assembled conductive graphene hydrogels were prepared by one-pot hydrothermal reduction of graphene oxide solutions. Concentration and reduction time were varied to investigate compression strength of the gels.[127]

There have been very few reports of aligned porous conductive structures containing graphene. GO has been used to reinforce aligned porous chitosan/gelatin scaffold, increasing the mechanical strength.[128] Vickery *et al.* produced aligned structures by mixing a PSS stabilized graphene dispersion with PVA and directional freezing.[129] The main focus of this study was to increase mechanical stability, so conductivity values were not quoted. The monoliths did exhibit a compressive strength of 3 MPa which was a significant increase over aligned porous structure containing only polymer.[129] Directional freezing of GO solutions alone was employed, and post reduced to produce ultra-light super-elastic monoliths with conductivities close to 0.1 S/cm.[130]

1.3.3 Aligned Composites and Fibres

Natural structures such as nacre can be mimicked by directional freezing of ceramic slurries.[131] Even though the inorganic ice templated scaffolds exhibited remarkable compressive strength alone, an organic or metal phase could be added to further increase the strength. Porous scaffolds filled with an epoxy layer created the hybrid organic-inorganic phases observed in nacre. It was speculated that filling the pores of the hydroxyapatite scaffolds with a biodegradable phase could be ideal for bone growth where porosity could be created *in situ* via degradation.[131] Following on from this study, aligned alumina scaffolds were filled with poly methyl methacrylate (PMMA) polymer to further replicate these bio inspired structures. The composite "bricks and mortar" materials had strength and toughness which surpassed nacre, matching those of metallic alloys.[132] The lamellar structures shown in Figure 1.8A were pressed perpendicular to the freezing direction to collapse them, followed by sintering to make the material more dense and form ceramic bridges between the "bricks".[132]

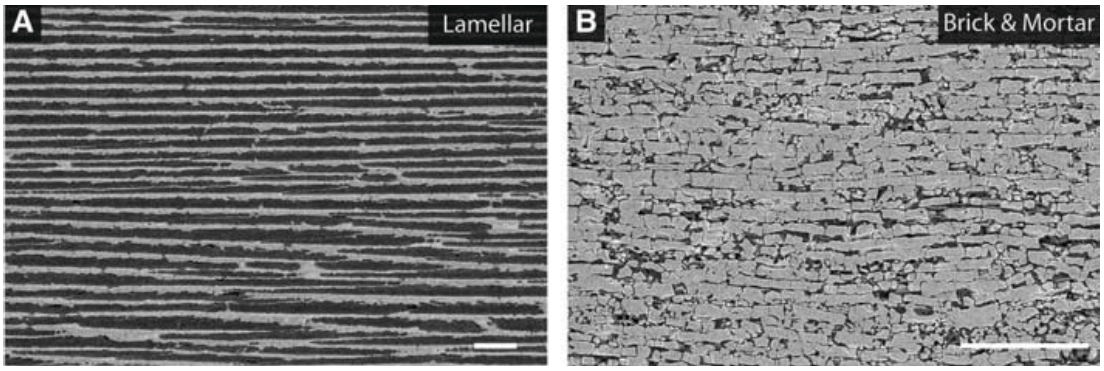

Figure 1.8 A) Aligned Al_2O_3/PMMA composite prepared by freeze casting of ceramic suspensions of ceramic suspensions followed by infiltration of polymer. Dark phase - polymer light phase - ceramic. B) Brick and mortar structure prepared pressing lamellar materials and sintering, they contain larger amount of ceramic (up to 80%).[132]

Aligned biodegradable nanofibrous structures are commonly prepared using electrospinning and have potential as scaffolds for blood vessel engineering.[133] Production of chitosan via electrospinning is often challenging because the viscosity of aqueous chitosan solutions is too high. To avoid this problem, concentrated acid solutions or toxic organic solvents have been used.[134,135] Due to these issues, a *green* method for producing chitosan nanowires was investigated. Dilute solutions were freeze-dried resulting in fibres with diameters ranging between 100 and 700 nm. Although the materials were not aligned throughout they did contain some aligned features (Figure 1.9). They showed higher absorbance capacity of Cu^{2+} compared to electrospun nanofibres and faster release profiles than regular macroporous chitosan structures.[136]

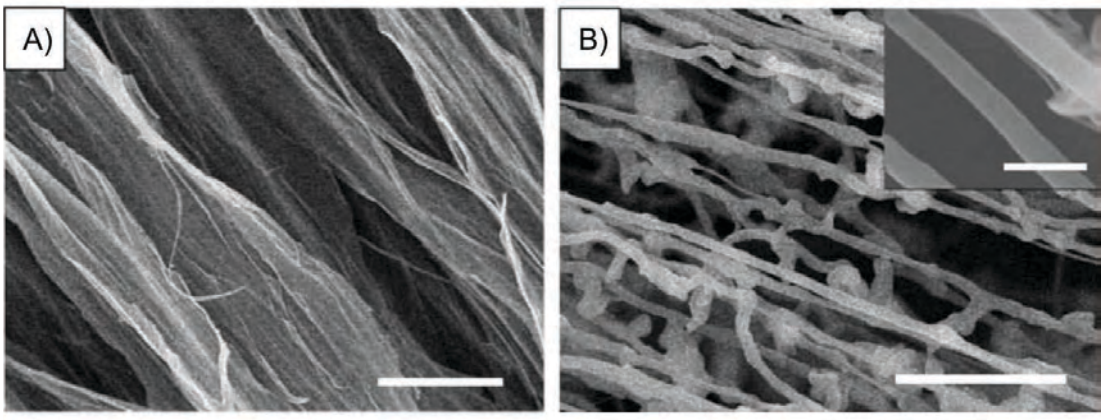

Figure 1.9 SEM images of fibres prepared by freeze drying chitosan solutions. A) 1 wt%, scale bar 50 µm B) 0.02 wt%, scale bar 5 µm, inset scale bar 500 nm. Figure adapted from reference.[136]

1.4 Chromatography

Chromatography is a physical method of separation in which components to be separated are distributed between two phases: a stationary phase (SP) and a mobile phase (MP) that moves in a definite direction. The technique was first used by Mikhail Tswett who used a calcium carbonate column (SP) to separate plant pigments using a petroleum ether/ethanol (MP) mixture under the flow of gravity.[137] The two different types of interactions are adsorption and partitioning. Adsorption chromatography works on the basis that analytes chemically interact with the surface of the SP causing retention. Partition chromatography is a technique where the analyte dissolves into a bonded phase, which forms a solvated layer into which the analytes partition.[138,139]

There are five different modes of chromatography: normal phase (NPC), reversed phase (RPC), size exclusion (SEC), hydrophilic interaction (HILIC) and ion exchange (IEX). The two most widely used modes are NPC and RPC. Scheme 1.6 shows a diagram of a typical NPC setup; molecules are separated in order of the strength of their interaction with the SP. The SP contains polar functional groups such as silanol, cyano or amino.

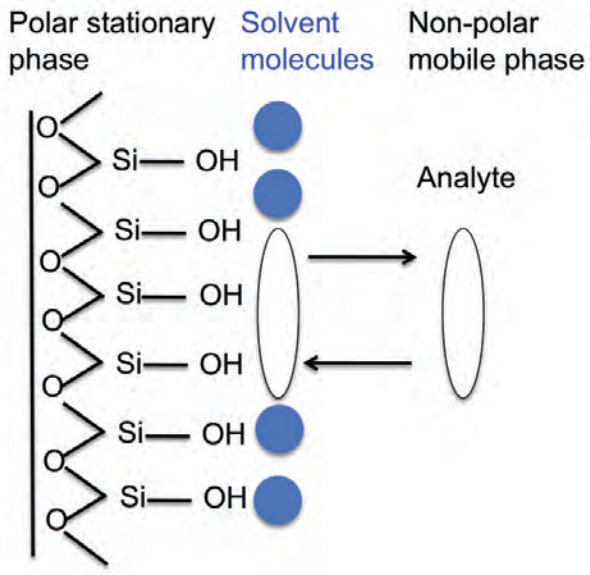

Scheme 1.6 Diagram of normal phase chromatography

The MP in NPC contains mostly non-polar solvents such as heptane or hexane. The non-polar solvent molecules on the surface of the SP are replaced by analyte molecules which have a higher affinity for the polar functional groups. This setup is normally used to separate polar molecules such as sugars and proteins. RPC works on the opposite basis, using a polar MP and non-polar stationary phase. The polar mobile phase (e.g., water, methanol or acetonitrile) elutes analytes in order of the hydrophilicity. The non-polar SP is used where the surface is functionalized with aliphatic carbon chains containing between 4 and 18 carbon atoms, with the longer carbon chains resulting in the largest retention due to greater hydrophobic interactions.[138,139]

SEC separates molecules through porous systems in order of size. For example, linear rod like molecules will be eluted before large globule molecules such as proteins. This method relies on minimal interactions with the stationary phase and cannot be used to separate small molecules. HILIC uses hydrophilic stationary phase and mostly organic mobile phase to retain hydrophilic molecules (sugars, oligosaccharides etc.) that are not retained using reversed phase chromatography. IEX is a process that allows the separation of ions or polar molecules depending on their charge.[138,139] This process is commonly used for water and protein purification.[140,141]

Microsphere packed columns are typically used as stationary phase for chromatography. For selective and efficient separation of analytes a sufficiently large surface area and a large number of interactive sites is required. Also, the monodisperse spherical morphology of silica particles allows for efficient column packing. Column efficiency can be improved by controlling morphology, porosity and particle size. The efficiency, (N) also referred to as the plate number (of theoretical plates), is a measure of the dispersion of peaks. When a column is more efficient, more complex separation mixtures can be resolved as the narrow peaks take up less area. The plate number can be used to calculate the height equivalent theoretical plate (HETP) (Equation 1.1), which is a measure of band broadening brought on by different flow velocities throughout a column.[142]

$$HETP = H = L/N \tag{1.1}$$

HETP or H = height equivalent theoretical plate, L= column length, N = efficiency or plate number. A smaller HETP value indicates more efficient chromatography. The band shape of a chromatography peak is affected by the rate of elution and different paths that the solute can travel through the SP. The van Deetmer equation takes into account these variables and is shown below (Equation 1.2).[142]

$$HETP = A + B/u + Cu \tag{1.2}$$

Where u is the average velocity of the mobile phase and A, B, and C are all factors that contribute to band broadening. A = Eddy diffusion – Solute molecules take different paths through SP so travel different overall distance resulting in broadening.[143] B = Longitudinal diffusion – The analyte diffuses from the centre to the edges of column, the concentration of analyte is less at the edges which causes broadening. If the MP travels quicker through the column the effects of longitudinal diffusion are less, resulting in narrower peaks.[143] C = Resistance to mass transfer - If the analyte has a high affinity for the SP and the flow rate of the MP is too high, the MP will travel ahead of the analyte resulting in peak broadening. For a small HETP value and a more efficient column, a compromised flow rate must be used to balance out the effects of longitudinal diffusion and resistance to mass transfer.[143]

1.4.1 Macroporous Monolithic Stationary Phases.

Typically, for high performance liquid chromatography (HPLC) silica spheres 2-5 μm in diameter are used. Whilst the smaller particles give more resolving power, they increase the column backpressure by a factor of four. Monolithic porous polymer monoliths are investigated as an alternative to particulate columns because the interconnected porous system allows the use of high flow rates with relatively low back-pressures generated. Production of monolithic material was first reported in 1967 by Kubin *et al.*[144] and later by Schneko.[145] The macroporous gels had limitations such as solvent degradation and mechanical stability under pressure. In 1989 Hjertan *et al.* reported a continuous macroporous amphiphilic polymer bed

made from bulk polymerization of monomers acrylic acid and N,N-methylenebisacrylamide.[146] This material was assessed for use in IEX. In the early 1990s monolithic columns were investigated more intensively when Svec *et al.* used porous monolithic columns made from glycidyl methacrylate and ethylene glycol dimethacrylate to separate proteins.[147] Minakuchi[148] and Fields[149] were the first to prepare monolithic columns containing silica. These earlier methods of production of monolithic columns led to the production of the first commercially available Chromolith™ columns, which were opened up to the market in 2000.[150,151] Figure 1.10 shows the bare monolithic silica rod (Figure 1.10A) and a covered rod placed inside a HPLC column. (Figure 1.10B).

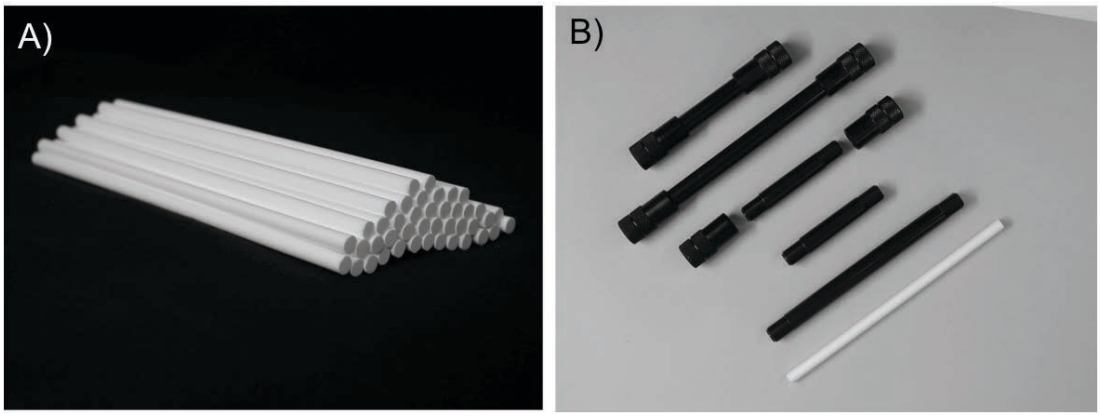

Figure 1.10 A) Monolithic silica rods B) Chromolith™ columns clad with poly(ether ether ketone) and equipped with column end fittings.[151]

More recent studies have focused on different methods of polymerization, control of pore morphology, use of different functional monomers and also grafting of functional groups to monomer surfaces.[152,153] Free radical polymerization is the most widely used method for producing porous monolith materials and initiation can be achieved via temperature or radiation polymerization such as UV light,[154] gamma rays[155] or electron beams.[156] Various methods exist for controlling the porous structure. A simple difference in temperature of solution during polymerization can affect the overall pore size.[157] Cryopolymerization was found to be an interesting alternative where polymerization takes place in the frozen state and is induced by water-soluble redox system.[70] When a dextran solution was frozen and polymerized in the frozen state, the porous structure obtained after solvent removal had a very

open interconnected pore structure. This was different to a dextran gel prepared in solution which exhibited a virtually featureless non-porous structure (Figure 1.11).[70]

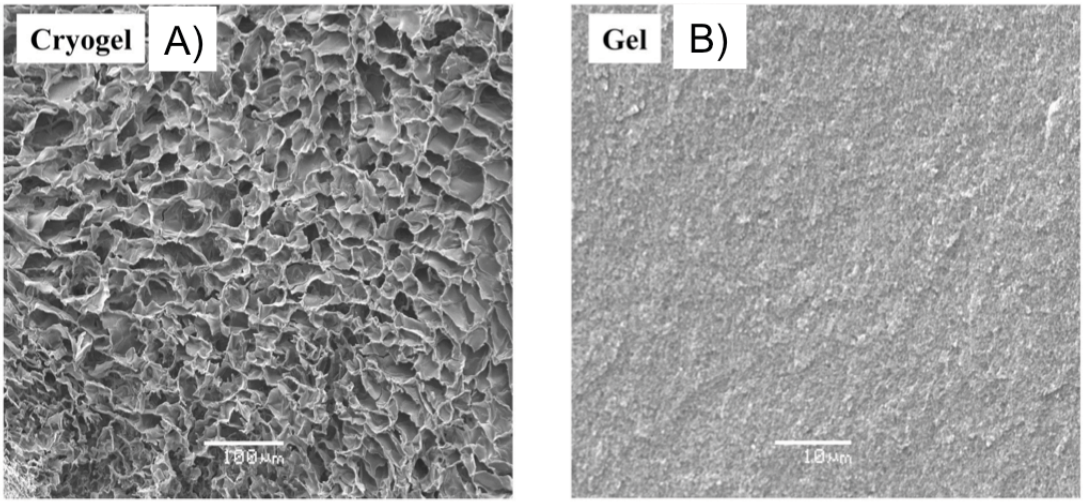

Figure 1.11 SEM of dextran based cryogel prepared at -20°C and conventional dextran gel prepared at room temperature.[70]

For solution polymerization, solvent selection is of high importance as it contains the pore generating properties through the solvation of monomer and polymer chains.[158] For this reason solvents are often referred to as porogens. In general, the more solvent used with respect to monomer, the larger porosity obtained in the resulting monolith. The monolith will also have a higher overall porosity.[158] The use of certain solvents can lead to properties with undesirable properties. Zhu *et al*. found that the use of porogens cyclohexanol, dodecanol, dimethylsulfoxide (DMSO), 1-propanol and 1,4-butanediol produced poly(glycidyl methacrylate-co-ethylene dimethacrylate) (PGMA co-EGDMA) monoliths with poor permeability or cracks in the structure.[159] However, when DMSO and 1,4-butanediol were used in combination, monoliths with excellent permeability were obtained.[159] PGMA co-EGDMA monoliths have also been prepared as polyHIPE monoliths and used for separation of a standard protein mixture.[160] Monolithic columns were prepared within thin capillary tubes with 90% overall porosity containing a crosslinked isodecylacrylate with DVB. Successful separations of alkylbenzenes were achieved through this system.[57]

Now that there are many facile routes for preparing porous monolithic materials, more studies are focused on the selection of specific monomers, or polymer grafting for a certain mode of chromatography. Two novel polymeric monoliths were

prepared for anion exchange liquid chromatography of proteins. Monoliths were prepared using 2-(dimethylamino) ethyl methacrylate (DEAEMA) and 2-(acryloyloxy) ethyl trimethylammonium chloride (AETAC) and polyethylene glycol diacrylate (PEGDA) as the crosslinking agent. The material was photopolymerized inside the HPLC column then attached to HPLC pump and flushed. The separation results were comparable to other stationary phases used for separation of proteins.[140] Two other polymer monoliths were designed and synthesized with commercially available monomers with an attempt to increase hydrophobicity for strong cation-exchange chromatography.[141] This was done using sulfonic acid containing monomers and crosslinker PEGDA. To avoid shrinkage, the fused silica capillaries are silanized to anchor a pendant vinyl group for the monomers to polymerize off.[141] This is a common method used to grow polymers from silanized surfaces to stop any leakage in columns.

Modification of the surface of porous monoliths can be achieved in solution as the materials are highly crosslinked and will not dissolve in common organic solvents. Glycidyl methacrylate monoliths have been modified with diethylamine to replace the epoxide group with tertiary amine and alcohol, allowing the material to be used as an anion exchanger (Scheme 1.7A).[147]

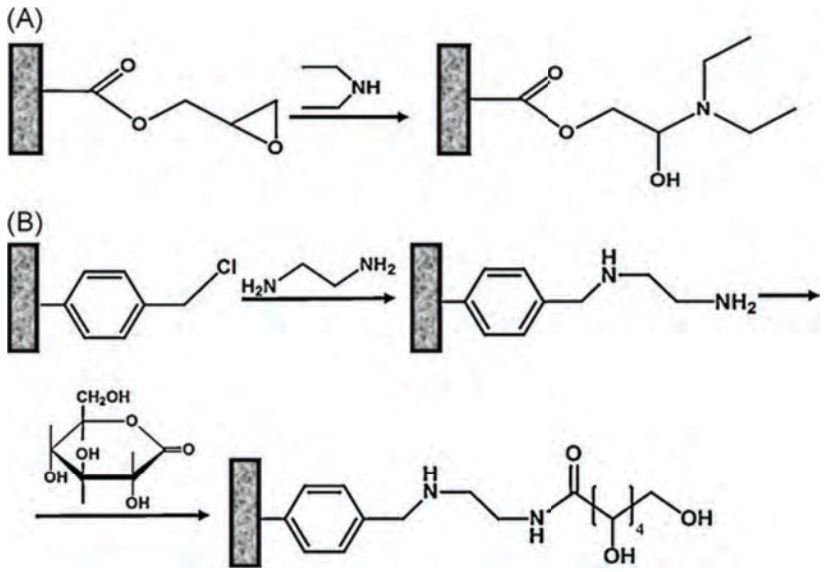

Scheme 1.7 Examples of modification of the surface of porous crosslinked polymer scaffolds A) modification with tertiary amines B) two step modification with diamine, then ring opening procedure to make surface hydrophilic. Image taken from reference.[152]

A poly(chloromethylstyrene-co-DVB) surface could also be modified by reacting with ethylenediamine which changes the surface from hydrophobic to hydrophilic (Scheme 1.7B).[161] The advantages of such modifications are the reaction simplicity and the ability to completely transform the columns functionality for different types of chromatography. When this study began in October 2009 there were no reports of aligned porous materials used as stationary phases for chromatography.

HPLC and gas chromatography (GC) will be discussed in more detail in chapter 2.

1.5 Freezing theory, Directional freezing and Freeze drying

Solidification of any pure liquid is governed entirely by heat flow. The rate of solidification at any point on the liquid-solid interface is determined by the latent heat generated (or absorbed) at that point that can be conducted into the bulk of the sample.[162]

When an aqueous solution is frozen, ice crystals form and solute molecules are excluded because they have very low solubility within these crystals.[80] This causes an increase in concentration of solute to form in front of the ice front.[74,131] The increase in concentration of solute reduces the melting point of the solution, resulting in the formation of a constitutional supercooling zone that can break down the planar interface causing ice crystals to grow.[64,79,163,164] This phenomenon is known as the Mullins-Sekerka instability, which states that the primary ice structure depends on the destabilizing solute interfacial concentration gradient and the surface energy which opposes cell formation.[79] Figure 1.12 shows a diagram of how directional freezing works and actual observations of the process using a microscope.

Directional freezing is a cheap, simple method used to prepare aligned porous materials. It involves lowering a vessel containing a liquid solution into a cold bath (e.g. liquid nitrogen or organic solvent cooled with dry ice) at a controlled rate causing the ice crystals to grow upwards in a uniform manner, producing aligned 3-dimensional (3D) structures after removal of solvent. Solvent removal is normally achieved by freeze drying also known as lyophilization. The pore morphology of

these structures can be controlled to a certain extent by changing the initial slurry/polymer composition and freezing conditions,[74,81] and properties of the solvent used. As mentioned above, this technique can be used to make a variety of porous materials with aligned features.[79]

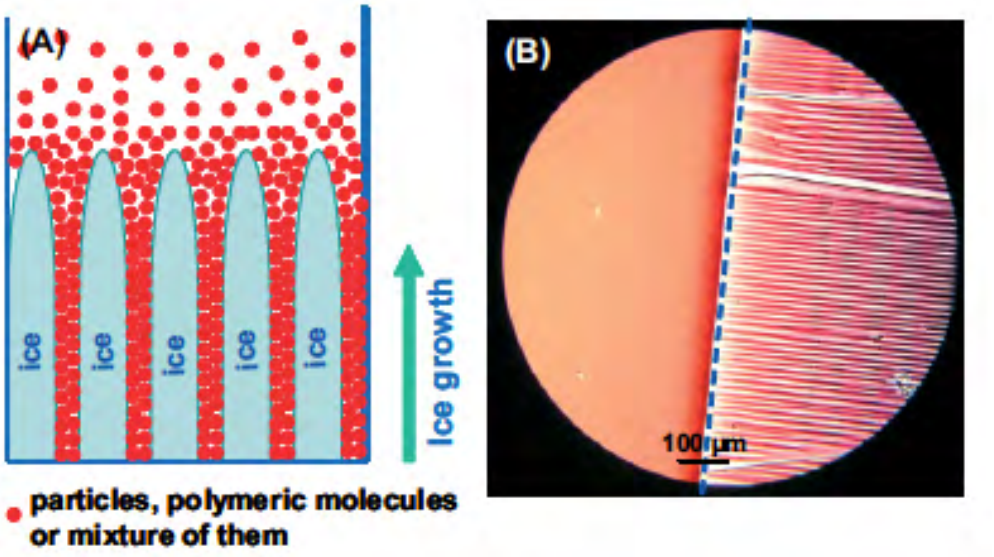

Figure 1.12 A) Diagram showing the directional freezing process. Particles (including nanaoparticles and microparticles) and polymeric molecules are excluded from the ice and aggregate between the growing ice crystals. After freezing is complete ice is removed by freeze drying to produce aligned porous material. B) Optical microscope image showing directional freezing of gold nanoparticle sol.[78]

1.5.1 Freeze Drying

Freeze drying is a process of making porous materials where solutions are crystallized at low temperatures and the solvent is sublimed from a solid phase to a gas phase at low pressure under vacuum. Scheme 1.8 shows a simplified phase diagram of the process where A) to B) represents the initial freezing, B) to C) represents the sublimation of solvent at low pressure and C) to D) is a possible sintering process used to make porous ceramics.[165,166] Freeze drying is mostly carried out using aqueous solutions but can be used to remove organic solvents with relatively high melting points. The process usually consists of three different stages: freezing, primary drying and secondary drying. The sample must be kept below the glass transition temperature or melting point of the solvent under vacuum to make porous structures. The frozen solvent acts as a porogen as the pores are created by the voids left over after removal of solvent.[79] The process is viewed as being quite

energy intensive as it requires keeping the chamber at low temperatures for up to 48 hours.

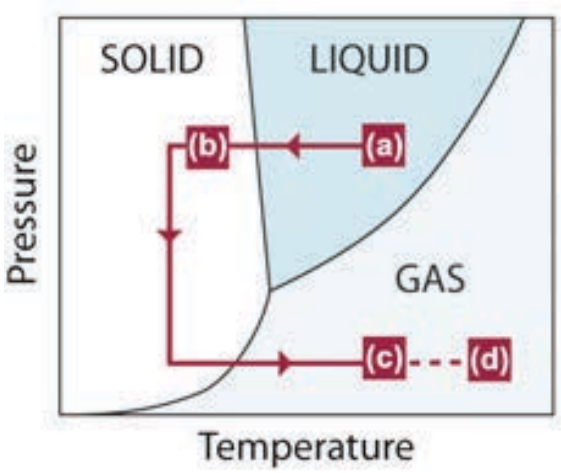

Scheme 1.8 Simplified phase diagram for a given liquid showing how the phase can be altered by varying temperature and pressure.[166]

Drying of a frozen material is governed by two mechanisms: The energy required to transform a frozen solvent into vapour and transport of the sublimed solvent into a drying chamber for condensation.[167,168] There are two stages of drying known as the primary and secondary drying. During the primary drying stage the chamber of a freeze dryer is lowered to the millibar region under vacuum. At this time the temperature should be high enough for the solvent to sublime but also low enough so that the structure of the porous material is not compromised. In this initial phase 95% of the solvent is removed. The condenser of a freeze dryer is used to stop the solvent vapour from entering the vacuum pump, which could cause damage. Secondary drying removes any unfrozen solvent molecules adsorbed to the surface of the porous material. This phase is governed by the materials adsorption isotherm. At this stage, the temperature is increased slightly higher than the primary drying stage, to break any physical or chemical interaction between the solvent and the material. In some cases the pressure can be lowered to encourage desorption. After secondary drying only 1-4 % of solvent remains.[167,168]

1.6 Polymers and Polymerization

German chemist Hermann Staudinger was the first to propose the idea of polymers as large macromolecules composed of 10,000 or more atoms.[169] This was in contrast

to previous claims which suggested that polymers were aggregates of small molecules.[170] Monomer and polymer are terms derived from Greek: poly (many), mono (one) and meros (parts). Staudinger formulated the structure of rubber from the monomeric structure of isoprene,[169] and later won the Nobel prize in 1953 for contributions to chemistry. Wallace H. Carothers was the first person to synthesize nylon and lay the groundwork for the production of synthetic rubbers.[171,172] Carothers was also the first to distinguish the methods of formation of polymers by categorizing polymers through method of production or type of product formed.[172] Condensation reactions resulted in a polymer and molecules of low molecular weight, while addition polymerization resulted in formation of polymer alone.[172] Paul. J Flory further categorized polymerization reactions in 1953.[173] Condensation and addition reactions taking place via the reaction of functional groups were named "step growth polymerization" and polymerizations initiated by free radicals or ions were named "chain growth polymerization".[173]

1.6.1 Step Growth Polymerization

Step growth polymerization (SGP) is a type of reaction where monomers react via functional groups to form dimers, trimers, oligomers and eventually polymers. SGP reactions are used to form many natural and synthetic polymers such as polyesters,[174] polyamides[175] and polyurethanes[176] (Scheme 1.9). It is also possible to have a difunctional monomer with reactive groups at each end, as with the formation of polyesters from hydroxycarboxlic acids (Scheme 1.9 C).

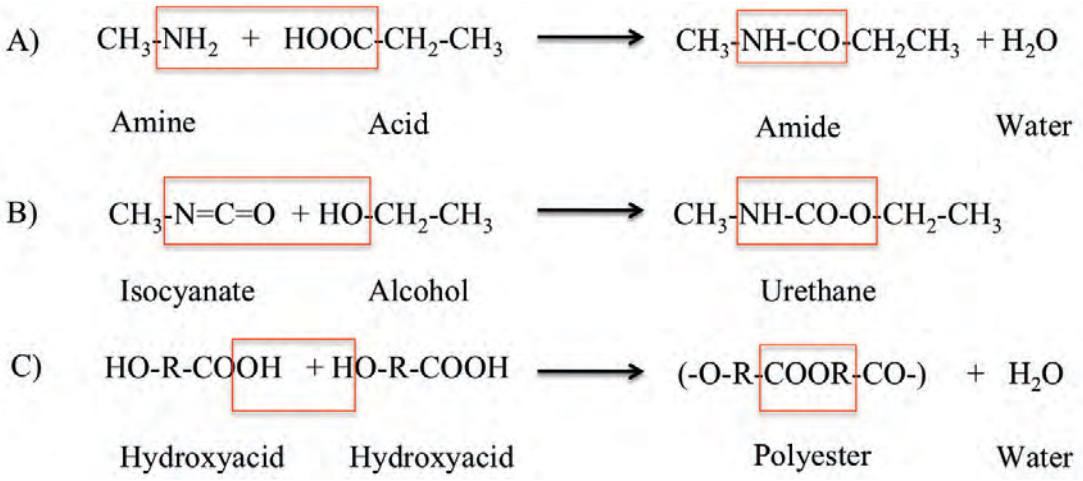

Scheme 1.9 Reaction schemes for various SGP procedures.

Due to the nature of the mechanism long reaction times are required to achieve polymers with high molecular weights.

1.6.2 Chain Growth Polymerization

Chain growth polymerization (CGP) is a polymerization technique where unsaturated molecules add on to an active site of a growing polymer chain. The limited amount of active sites at any given time gives this method its key characteristics. In contrast to SGP, CGP can increase chain length rapidly resulting in high molecular weight polymers being formed at low conversion. Another difference to SGP is that polymerization only occurs at one end of the chain. The five steps involved in CGP are: 1) decomposition of initiator 2) initiation of polymerization 3) propagation of the polymer chains 4) chain transfer 5) chain termination. Initiator molecules are available in a variety of forms such as ions or free radicals and the decomposition to this active state can brought on by temperature,[19] radiation[156] or electron transfer.[177] Initiation is a chemical reaction between a reactive species and a monomer that will lead to further reactions. The cascade of reactions that follow are known as chain propagation and ultimately lead to the formation of a polymer. Chain propagation involves continuous regeneration of a reactive species (ion or free radical) after a reaction with a monomer at one end of the polymer or oligomer chain. Chain transfer is a reaction during the polymerization where the reactivity of the polymer chain is transferred to another molecule. This can be induced deliberately using chain transfer agents (CTA) or via unavoidable side reactions with components of the polymerization. Common CTAs include thiols[178] and halocarbons[179] because they contain weak chemical bonds. Chain termination is a chemical reaction that terminates propagation bringing polymerization to a stop. The final weight of polymer is determined by the rate of propagation against the rate of chain termination.

1.6.2.1 Free Radical Polymerization

Free radical polymerization (FRP) is a form of CGP by which a polymer forms via addition of free radical building blocks. A free radical is an atomic or molecular species which contains an unpaired electron. The unpaired electron causes radicals to be highly chemically reactive. This is the most widely used polymerization technique for the formation of polymers and composites. Firstly, a primary radical is generated

by homolytical cleavage of a chemical bond and addition on to a monomer. Scheme 1.10 shows the decomposition of photoinitiator 2,2-dimethoxy phenyl acetophenone (DMPA) used widely for photopolymerization of methacrylate monomers.[180] The C-C bond is homolytically cleaved to form benzoyl and acetal radicals. The benzoyl component is highly effective at adding on to monomers, however the acetal is less effective due to stabilizing effects brought on by the phenyl groups.[181,182] DMPA is used for all polymerizations presented in this work. Scheme 1.10B shows how a free radical initiator adds on to a vinyl monomer via electron transfer.

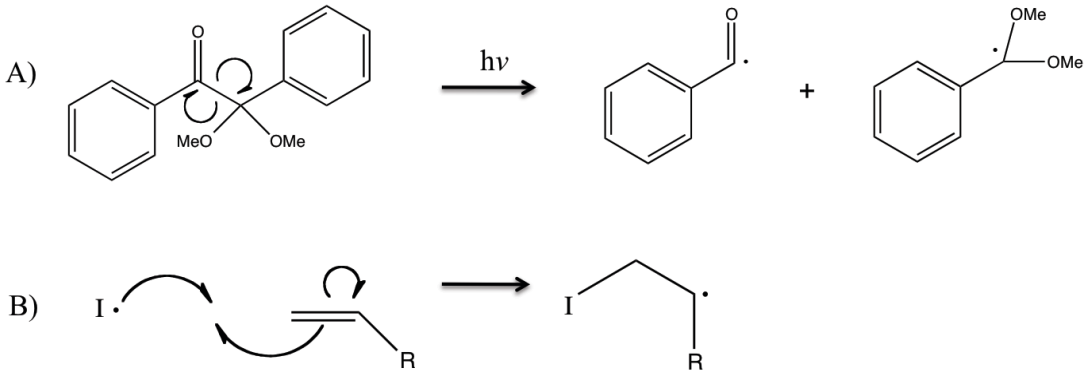

Scheme 1.10 A) Decomposition of photoinitiator DMPA to form benzoyl and acetal radicals B) addition of initiator on to a generic vinyl monomer. Arrows indicate transfer or single electrons.

Due to the reactivity of free radicals, propagation occurs rapidly until depletion of the monomer or termination occurs. Scheme 1.11A shows how an initiated monomer propagates with another monomer molecule. This propagation will continue until termination occurs. This could happen due to depletion of monomer resulting in two active radicals reacting to terminate the polymerization (Scheme 1.11B).

Other causes of termination include radical disproportionation brought on by extraction of a hydrogen atom from one chain to another, leaving one polymer molecule with an an alkene group at the end and one polymer with an alkane group at the end. Chain transfer of a hydrogen atom from solvent molecules is another possible route to termination. This can happen during the polymerization of styrene, resulting in a terminated polymer and a solvent radical.[183]

FRP polymerization is the mode of polymerization used for the entirety of this thesis.

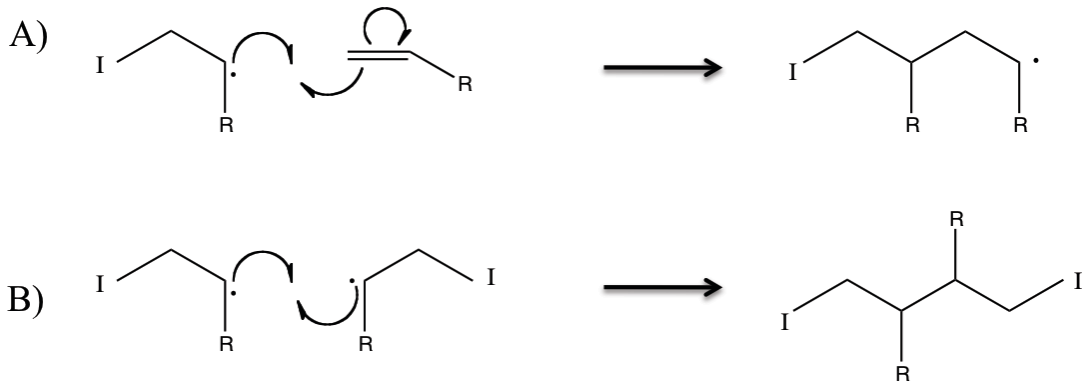

Scheme 1.11 A) Propagation of an initiated monomer radical with a monomer molecule. B) An example of a termination reaction where two propagating radicals meet to terminate polymerization.

1.6.2.2 UV- and Cryo-polymerization

Ultra-violet initiated polymerization uses UV radiation (wavelength 10-400 nm) to create free radicals for polymerization. The reactions are normally completed in the presence of a UV generated light source (UV lamp). A photoinitiator is a compound added to a formulation to convert light energy, UV or visible light into chemical energy in the form of initiating species.[184] An efficient photoinitiator must exhibit a large absorption in the emission range of the light source. Thermal curing requires higher activation energy and is influenced strongly by the decomposition of the initiator, whereas UV induced polymerization requires low activation energy as the decomposition of the initiator is a near instantaneous process, resulting in polymers forming quicker.[185-187] UV polymerization can be used to prepare macroporous materials via solution polymerization or coat surfaces containing ionic liquids.[188]

Cryopolymerization is a technique where a monomer solution in a frozen or semi frozen state is polymerized at subzero temperature to produce polymers or macroporous material.[71,72,189] When a monomer solution containing initiator is frozen the solute molecules are excluded from the growing ice crystals into a small concentrated non-frozen liquid phase (phase separation).[189] These can be polymerized in a freezer using a water-soluble redox system to produce free radicals,[70] or irradiation using electron beams[156] or UV.[190]

1.6.2.3 Living Polymerizations, Controlled Radical Polymerization and Polymer Architecture

A living polymerization (LP) is a polymerization reaction where the termination steps are restricted and the rate of initiation is larger than the rate of propagation. LP is a popular method for making block co-polymers because the polymer is constructed in stages and after propagation the chains remain active. Anionic[191] and cationic[192] polymerizations are examples of LPs, however they require strict reaction conditions. Controlled radical polymerizations such as atom transfer radical polymerization (ATRP)[193] and reverse addition fragmentation chain transfer (RAFT)[194] can overcome these problems by use of co-ordination catalysts, creating an equilibrium between a polymer chain in its dormant and active state. The equilibrium is crucial to the polymerization as it slows propagation, and theoretically adds only one monomer at a time.[193,194] This leads to the formation of polymers with low polydispersity index and can aid the design of polymers with specific molecular weights and architecture. Some of the most commonly reported polymer architectures are listed in Scheme 1.12 including: regular linear polymer, branched, network, graft/comb polymer, star polymer and various types of block co-polymers.[194,195] In this work, crosslinked polymer networks are the type of polymer produced.

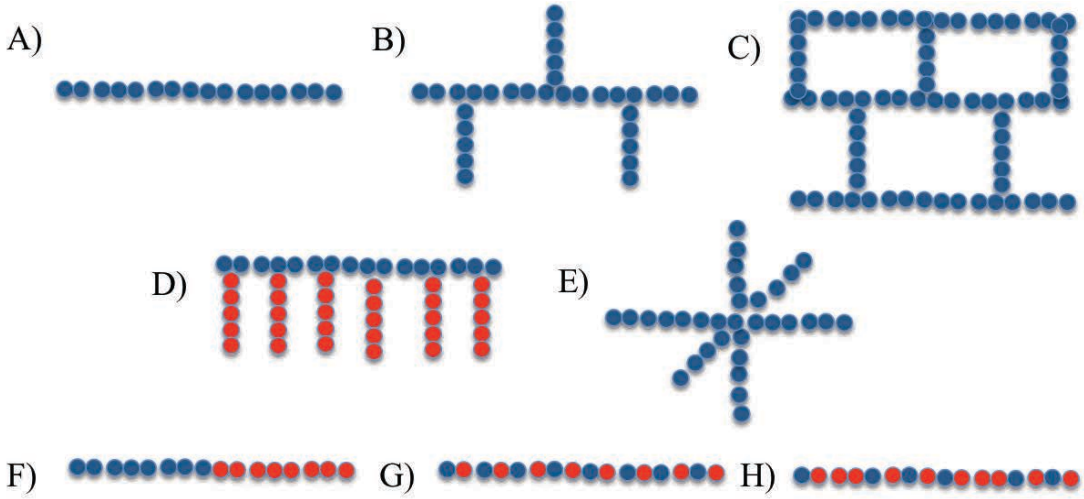

Scheme 1.12 Different forms of polymers that have been reported: A) linear B) branched C) network D) graft E) star F) block co-polymer G) alternating copolymer H) random copolymer.

1.6.3 Stimuli Responsive Polymers

A stimuli-responsive polymer (SRP) is a polymer that can respond to their external environment. The stimulus can be provided in an aqueous solution in terms of temperature or pH, or specific chemical triggers. Intensity of light[196,197] or external magnetic field[198] can also be used to manipulate certain polymers behaviour. SRPs have a massive scope of applications from drug delivery[199] and tissue engineering[200] to oil recovery.[201]

For macroporous material containing SRP a lot of work has been focused on poly(N-isopropylacrylamide) also known as poly(NIPAAm) that has a lower critical solution temperature (LCST) of 32 °C.[202,203] The LCST is the critical temperature below which components are soluble, while above it they are desolvated. The reversible phase change comes from the fact that water soluble polymers contain polar groups such as hydroxy, amide or ether groups which can hydrogen bond to water molecules. Above the LCST hydrogen bonds are decreased as polymer-polymer interactions are favoured and phase separation occurs (Figure 1.13). This causes crosslinked macroporous systems containing polymers such poly(NIPAAm) to swell below the LCST and contract above it.[204,205] Porous poly(NIPAAm) can easily be prepared using free-radical methods and is usually completed containing crosslinker.[19,204] This crosslinker effectively ties the polymer strands together stopping the solvation, but the inherent properties of the polymer remain. Also because the LCST is very close to body temperature it means that porous poly(NIPAAm) materials are useful for drug delivery in biomimetic conditions.[204]

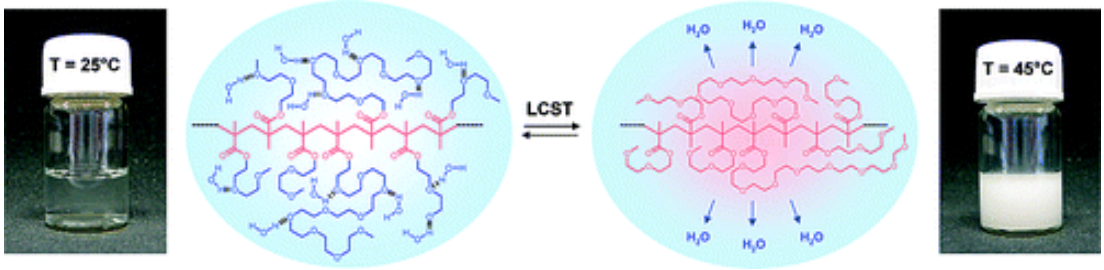

Figure 1.13 Optical image and scheme showing how poly(OEGMA)-water interactions change at different temperatures.[206]

Temperature responsive systems containing poly(oligo-ethylene glycol methacrylate) polyOEGMA have been prepared.[206-208] The advantage of preparing poly(OEGMA)

over poly(NIPAAm) is that the LCST can be tuned by varying co-monomer ratios of OEGMA monomers with different amounts of ethylene glycol units. The solubility and LCST is determined by three factors: length of PEG side chain, length of polymer chain and the nature of the end group. Not only can the LCST be tuned between 27 - 60 °C it can be tuned to match body temperature directly, making this type of polymer interesting for biological applications. There are not many reports of porous poly(OEGMA) membranes because precision polymerization is normally required for specific LCST, however the use of this type of polymer is growing in the biomaterial area.[209] Porous poly(NIPAAm) can be produced via free-radical methods.

Macroporous pH responsive materials are often sought after for drug delivery vehicles within pH extremities in the body and are tested *in vitro*.[199,210-212] pH responsive polymer hydrogels are often separated into anionic and cationic categories. For example polymers such as poly 2-(dimethylamino) ethyl methacrylate (polyDMAEMA) and 2-(diethylamino) ethyl methacrylate (polyDEAMA) are called cationic because at low pH they are protonated and carry a positive charge making them more hydrophilic and at high pH they are neutral and are said to be less hydrophilic.[213,214] Poly methacrylic acid is an example of an anionic polymer because at high pH the carboxylic acid group is deprotonated and carries a negative charge making it more hydrophilic.[215] At low pH the polymer is a neutral species and carries no charge making it less hydrophilic. Scheme 1.13 shows how crosslinked anionic and cationic hydrogels react to external pH of solution. There are also reports combining pH and temperature responsive polymers.[205,216,217]

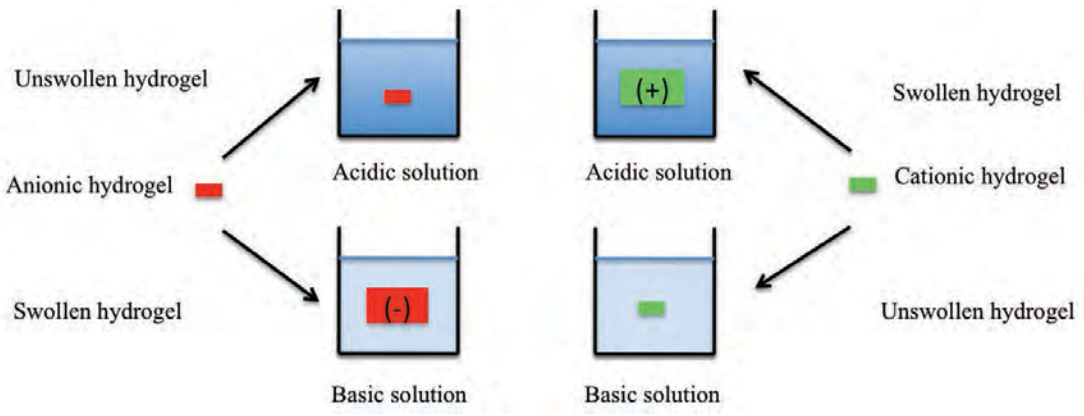

Scheme 1.13 pH responsive swelling of anionic and cationic hydrogels.

1.7 Targets and Layout of Thesis

The aim of this piece of work is to develop a new method for producing functional aligned porous materials. This was achieved using a combination of directional freezing and frozen UV-initiated polymerization. When this study began in October 2009 there was no reports of combining directional freezing and frozen polymerization methods to produce aligned porous material. Firstly, some of the experimental methods are discussed in chapter 2 and the theory behind the most important techniques. The experimental work is separated into 3 chapters.

In chapter 3 the directional freezing and frozen UV polymerization method is introduced. Aligned porous material is produced from crosslinker monomer tetraethylene glycol dimethacrylate with enhanced mechanical stability, and removes the need for freeze-drying. The material is post-functionalized with conductive polymer and graphene nanosheets to further improve mechanical stability and conductivity. Production of monolithic columns for HPLC is also demonstrated using this method. Further studies following on from this extend the amounts of methacrylates that can be polymerized using this method. In chapter 4 Oligo-ethylene glycol methacrylates and dimethylamino ethyl methacrylate monomers are used to produce aligned porous temperature- and pH-responsive hydrogels respectively. The hydrogels exhibit stimuli-responsive behaviour in aqueous conditions and anisotropic compressive strength and diffusion behaviour with respect to freezing direction. Aligned porous monoliths containing silica are produced in chapter 5 from the monomer trimethoxysilane propyl methacrylate. The surface of the materials can be post functionalized to make two different types of aligned porous composites. Hydrothermal synthesis using Teflon lined autoclaves is used to functionalize monoliths separately with silver and metal organic frameworks (MOFs). The MOF composite materials are used as a stationary phase to try and separate a mixture of organic compounds.

1.8 References

(1) Zdravkov, B.; Čermák, J.; Šefara, M.; Janků, J. *cent.eur.j.chem.* **2007**, *5*, 385.

(2) Holst, J. R.; Cooper, A. I. *Adv. Mater.* **2010**, *22*, 5212.

(3) Grant Glover, T.; Peterson, G. W.; Schindler, B. J.; Britt, D.; Yaghi, O. *Chem. Eng. Sci.* **2011**, *66*, 163.

(4) Chang, N.; Gu, Z.-Y.; Yan, X.-P. *J. Am. Chem. Soc.* **2010**, *132*, 13645.

(5) Xie, S.-M.; Zhang, Z.-J.; Wang, Z.-Y.; Yuan, L.-M. *J. Am. Chem. Soc.* **2011**, *133*, 11892.

(6) Liu, S.-S.; Yang, C.-X.; Wang, S.-W.; Yan, X.-P. *Analyst* **2012**, *137*, 816.

(7) Mitra, T.; Jelfs, K. E.; Schmidtmann, M.; Ahmed, A.; Chong, S. Y.; Adams, D. J.; Cooper, A. I. *Nat Chem* **2013**, *5*, 276.

(8) Mueller, U.; Schubert, M.; Teich, F.; Puetter, H.; Schierle-Arndt, K.; Pastre, J. *J. Mater. Chem.* **2006**, *16*, 626.

(9) Bradshaw, D.; Garai, A.; Huo, J. *Chem Soc Rev* **2012**, *41*, 2344.

(10) Sachse, A.; Ameloot, R.; Coq, B.; Fajula, F.; Coasne, B.; De Vos, D.; Galarneau, A. *Chem. Commun.* **2012**, *48*, 4749.

(11) Bartoszek, M.; Eckelt, R.; Jäger, C.; Kosslick, H.; Pawlik, A.; Schulz, A. *J. Mater. Sci.* **2009**, *44*, 6629.

(12) Kamegawa, T.; Yamahana, D.; Yamashita, H.; *J. Phys. Chem C* **2010**, *114*, 15049.

(13) Parida, K. M.; Rath, D. *Appl. Catal,; A: General* **2007**, *321*, 101.

(14) Guiochon, G. *J. Chromatogr. A* **2007**, *1168*, 101.

(15) Gallis, K. W.; Araujo, J. T.; Duff, K. J.; Moore, J. G.; Landry, C. C. *Adv. Mater.* **1999**, *11*, 1452.

(16) Ehlert, N.; Mueller, P. P.; Stieve, M.; Lenarz, T.; Behrens, P. *Chem. Soc. Rev.* **2013**, *42*, 3847.

(17) Kresge, C. T.; Leonowicz, M. E.; Roth, W. J.; Vartuli, J. C.; Beck, J. S. *Nature* **1992**, *359*, 710.

(18) Lebeau, B.; Galarneau, A.; Linden, M. *Chem. Soc. Rev.* **2013**, *42*, 3661.

(19) Grant, N. C.; Cooper, A. I.; Zhang, H. *ACS Appl. Mater. Interfaces* **2010**, *2*, 1400.

(20) Du, J.; Kang, D. J. *Mater. Lett.* **2008**, *62*, 3185.

(21) Ahmed, A.; Myers, P.; Zhang, H. *Anal. Meth.* **2012**, *4*, 3942.

(22) Studenovská, H.; Šlouf, M.; Rypáček, F. *J. Mater. Sci. - Mater. Med.* **2008**, *19*, 615.

(23) Jiang, P.; Hwang, K. S.; Mittleman, D. M.; Bertone, J. F.; Colvin, V. L. *J. Am. Chem. Soc.* **1999**, *121*, 11630.

(24) Noble, L.; Gray, A. I.; Sadiq, L.; Uchegbu, I. F. *Int. J. Pharm.* **1999**, *192*, 173.

(25) Li, Z.; Zhao, L.; Diao, H.; Li, H.; Zhou, C.; Wang, W. *ECS Journal of Solid State Science and Technology* **2013**, *2*, Q65.

(26) Bang, B. M.; Lee, J.-I.; Kim, H.; Cho, J.; Park, S. *Advanced Energy Materials* **2012**, *2*, 878.

(27) Qin, D.; Xia, Y.; Whitesides, G. M. *Nature Protocols* **2010**, *5*, 491.

(28) Walsh, D.; Kulak, A.; Aoki, K.; Ikoma, T.; Tanaka, J.; Mann, S. *Angew. Chem. Int. Ed.* **2004**, *43*, 6691.

(29) Walsh, D.; Arcelli, L.; Ikoma, T.; Tanaka, J.; Mann, S. *Nature Materials* **2003**, *2*, 386.

(30) Stein, A.; Li, F.; Denny, N. R. *Chem. Mater.* **2007**, *20*, 649.

(31) Chen, Z.; Zhan, P.; Wang, Z. L.; Zhang, J. H.; Zhang, W. Y.; Ming, N. B.; Chan, C. T.; Sheng, P. *Adv. Mater.* **2004**, *16*, 417.

(32) Meldrum, F. C.; Seshadri, R. *Chem. Commun.* **2000**, *0*, 29.

(33) Park, B.; Kim, S.; Kim, I.-D.; Park, Y. *J. Mater. Sci* **2010**, *45*, 3947.

(34) Velev, O. D.; Kaler, E. W. *Adv. Mater.* **2000**, *12*, 531.

(35) Velev, O. D.; Jede, T. A.; Lobo, R. F.; Lenhoff, A. M. *Nature* **1997**, *389*, 447.

(36) Zakhidov, A. A.; Baughman, R. H.; Iqbal, Z.; Cui, C.; Khayrullin, I.; Dantas, S. O.; Marti, J.; Ralchenko, V. G. *Science* **1998**, *282*, 897.

(37) He, H.; Zhong, M.; Konkolewicz, D.; Yacatto, K.; Rappold, T.; Sugar, G.; David, N. E.; Gelb, J.; Kotwal, N.; Merkle, A.; Matyjaszewski, K. *Adv. Funct. Mater.* **2013**, In print.

(38) Wijnhoven, J. E. G. J.; Vos, W. L. *Science* **1998**, *281*, 802.

(39) Ji, C.; Khademhosseini, A.; Dehghani, F. *Biomaterials* **2011**, *32*, 9719.

(40) Seidel, J. M.; Malmonge, S. n. M. *Materials Research* **2000**, *3*, 79.

(41) Zhang, H.; Cooper, A. I. *Soft Matter* **2005**, *1*, 107.

(42) Grant, N.; Zhang, H. *J. Colloid Interface Sci.* **2011**, *356*, 573.

(43) Barby, H.; Haq, Z. *Eur. Pat.* **1982**, 60 138.

(44) Barbetta, A.; Cameron, N. R.; Cooper, S. J. *Chem. Commun.* **2000**, *0*, 221.

(45) Cameron, N. R.; Sherrington, D. C.; Ando, I.; Kurosu, H. *J. Mater. Chem.* **1996**, *6*, 719.

(46) Xu, H.; Wang, N.; Qu, T.; Yang, J.; Yao, Y.; Qu, X.; Lovell, P. A. *J. Appl. Polym. Sci.* **2012**, *123*, 1068.

(47) Naves, A. F.; Carmona-Ribeiro, A. M.; Petri, D. F. S. *Langmuir* **2006**, *23*, 1981.

(48) Plessis, C.; Arzamendi, G.; Leiza, J. R.; Schoonbrood, H. A. S.; Charmot, D.; Asua, J. M. *Macromolecules* **2000**, *33*, 5041.

(49) Kovacic, S.; Stefanic, D.; Krajnc, P. *Macromolecules* **2007**, *40*, 8056.

(50) Kovačič, S.; Jeřabek, K.; Krajnc, P. *Macromol. Chem. Phys.* **2011**, *212*, 2151.

(51) Maekawa, H.; Esquena, J.; Bishop, S.; Solans, C.; Chmelka, B. F. *Adv. Mater.* **2003**, *15*, 591.

(52) Zhang, H.; Hardy, G. C.; Rosseinsky, M. J.; Cooper, A. I. *Adv. Mater.* **2003**, *15*, 78.

(53) Cameron, N. R. *Polymer* **2005**, *46*, 1439.

(54) Kimmins, S. D.; Cameron, N. R. *Adv. Funct. Mater.* **2011**, *21*, 211.

(55) Ahmed, A.; Smith, J.; Zhang, H. *Chem. Commun.* **2011**, *47*, 11754.

(56) Pulko, I.; Kolar, M.; Krajnc, P. *Sci. Total Environ.* **2007**, *386*, 114.

(57) Tunç, Y.; Gölgelioğlu, Ç.; Hasirci, N.; Ulubayram, K.; Tuncel, A. *J. Chromatogr. A* **2010**, *1217*, 1654.

(58) Busby, W.; Cameron, N. R.; Jahoda, C. A. B. *Biomacromolecules* **2001**, *2*, 154.

(59) Akay, G.; Birch, M. A.; Bokhari, M. A. *Biomaterials* **2004**, *25*, 3991.

(60) Hayman, M. W.; Smith, K. H.; Cameron, N. R.; Przyborski, S. A. *J. Biochem. Bioph. Methods* **2005**, *62*, 231.

(61) Caldwell, S.; Johnson, D. W.; Didsbury, M. P.; Murray, B. A.; Wu, J. J.; Przyborski, S. A.; Cameron, N. R. *Soft Matter* **2012**, *8*, 10344.

(62) Zhang, H.; Wang, D.; Butler, R.; Campbell, N. L.; Long, J.; Tan, B.; Duncalf, D. J.; Foster, A. J.; Hopkinson, A.; Taylor, D.; Angus, D.; Cooper, A. I.; Rannard, S. P. *Nature Nanotechnology* **2008**, *3*, 506.

(63) McDonald, T. O.; Martin, P.; Patterson, J. P.; Smith, D.; Giardiello, M.; Marcello, M.; See, V.; O'Reilly, R. K.; Owen, A.; Rannard, S. *Adv. Funct. Mater.* **2012**, *22*, 2469.

(64) Butler, M. F. *Crystal Growth & Design* **2002**, *2*, 541.

(65) Madihally, S. V.; Matthew, H. W. T. *Biomaterials* **1999**, *20*, 1133.

(66) Seager, H.; Taskis, C. B.; Syrop, M.; Lee, T. J. *J. Pharm. Sci.* **1985**, *39*, 161.

(67) Hu, X.; Shen, H.; Yang, F.; Bei, J.; Wang, S. *Biomaterials* **2008**, *29*, 3128.

(68) Qian, L.; Ahmed, A.; Foster, A.; Rannard, S. P.; Cooper, A. I.; Zhang, H. *J. Mater. Chem.* **2009**, *19*, 5212.

(69) Chen, R.; Wang, C.-A.; Huang, Y.; Ma, L.; Lin, W. *J. Am. Ceram. Soc.* **2007**, *90*, 3478.

(70) Plieva, F. M.; Galaev, I. Y.; Mattiasson, B. *J. Sep. Sci.* **2007**, *30*, 1657.

(71) Savina, I. N.; English, C. J.; Whitby, R. L. D.; Zheng, Y.; Leistner, A.; Mikhalovsky, S. V.; Cundy, A. B. *J. Hazard. Mater.* **2011**, *192*, 1002.

(72) Savina, I. N.; Cnudde, V.; D'Hollander, S.; Van Hoorebeke, L.; Mattiasson, B.; Galaev, I. Y.; Du Prez, F. *Soft Matter* **2007**, *3*, 1176.

(73) Zhang, H.; Hussain, I.; Brust, M.; Butler, M. F.; Rannard, S. P.; Cooper, A. I. *Nat Mater* **2005**, *4*, 787.

(74) Deville, S.; Saiz, E.; Tomsia, A. P. *Acta Mater.* **2007**, *55*, 1965.

(75) Abarrategi, A.; Gutiérrez, M. C.; Moreno-Vicente, C.; Hortigüela, M. J.; Ramos, V.; López-Lacomba, J. L.; Ferrer, M. L.; del Monte, F. *Biomaterials* **2008**, *29*, 94.

(76) Katuri, K.; Ferrer, M. L.; Gutiérrez, M. C.; Jiménez, R.; del Monte, F.; Leech, D. *Energy & Environmental Science* **2011**, *4*, 4201.

(77) Zhang, H.; Long, J.; Cooper, A. I. *J. Am. Chem. Soc.* **2005**, *127*, 13482.

(78) Zhang, H.; Cooper, A. I. *Adv. Mater.* **2007**, *19*, 1529.

(79) Qian, L.; Zhang, H. *J. Chem. Technol. & Biotechnol.* **2011**, *86*, 172.

(80) Zhang, H.; Hussain, I.; Brust, M.; Butler, M. F.; Rannard, S. P.; Cooper, A. I. *Nature Materials* **2005**, *4*, 787.

(81) Gutiérrez, M. C.; García-Carvajal, Z. Y.; Jobbágy, M.; Rubio, F.; Yuste, L.; Rojo, F.; Ferrer, M. L.; del Monte, F. *Adv. Funct. Mater.* **2007**, *17*, 3505.

(82) Dietmar W, H. *Biomaterials* **2000**, *21*, 2529.

(83) Fu, Q.; Saiz, E.; Rahaman, M. N.; Tomsia, A. P. *Mater. Sci. Eng.: C* **2011**, *31*, 1245.

(84) Mandoli, C.; Mecheri, B.; Forte, G.; Pagliari, F.; Pagliari, S.; Carotenuto, F.; Fiaccavento, R.; Rinaldi, A.; Di Nardo, P.; Licoccia, S.; Traversa, E. *Macromol. Biosci.* **2010**, *10*, 127.

(85) Wu, X.; Liu, Y.; Li, X.; Wen, P.; Zhang, Y.; Long, Y.; Wang, X.; Guo, Y.; Xing, F.; Gao, J. *Acta Biomaterialia* **2010**, *6*, 1167.

(86) Deville, S.; Saiz, E.; Tomsia, A. P. *Biomaterials* **2006**, *27*, 5480.

(87) Yoon, B.-H.; Lee, E.-J.; Kim, H.-E.; Koh, Y.-H. *J. Am. Ceram. Soc.* **2007**, *90*, 1753.

(88) Sun, Y.-P.; Fu, K.; Lin, Y.; Huang, W. *Acc. Chem. Res.* **2002**, *35*, 1096.

(89) Jia, G.; Wang, H.; Yan, L.; Wang, X.; Pei, R.; Yan, T.; Zhao, Y.; Guo, X. *Environ. Sci. Technol* **2005**, *39*, 1378.

(90) Hu, H.; Ni, Y.; Montana, V.; Haddon, R. C.; Parpura, V. *Nano Lett.* **2004**, *4*, 507.

(91) Nardecchia, S.; Carriazo, D.; Ferrer, M. L.; Gutierrez, M. C.; del Monte, F. *Chem. Soc. Rev.* **2013**, *42*, 794.

(92) Zhang, X.; Li, C.; Luo, Y. *Langmuir* **2011**, *27*, 1915.

(93) Romeo, H. E.; Hoppe, C. E.; López-Quintela, M. A.; Williams, R. J. J.; Minaberry, Y.; Jobbágy, M. *J. Mater. Chem.* **2012**, *22*, 9195.

(94) Bai, H.; Li, C.; Chen, F. e.; Shi, G. *Polymer* **2007**, *48*, 5259.

(95) Iijima, S. *Nature* **1991**, *354*, 56.

(96) Novoselov, K. S.; Geim, A. K.; Morozov, S. V.; Jiang, D.; Zhang, Y.; Dubonos, S. V.; Grigorieva, I. V.; Firsov, A. A. *Science* **2004**, *306*, 666.

(97) Dreyer, D. R.; Park, S.; Bielawski, C. W.; Ruoff, R. S. *Chem. Soc. Rev.* **2010**, *39*, 228.

(98) Rosca, I.; Watari, F.; Uo, M.; Akasaka, T. *Carbon* **2005**, *43*, 3124.

(99) Ramanathan, T.; Fisher, F. T.; Ruoff, R. S.; Brinson, L. C. *Chem. Mater.* **2005**, *17*, 1290.

(100) Ozarkar, S.; Jassal, M.; Agrawal, A. *Fibers and Polymers* **2008**, *9*, 410.

(101) Philip, B.; Xie, J.; Chandrasekhar, A.; Abraham, J.; Varadan, V. K. *Smart Mater. Struct.* **2004**, *13*, 295.

(102) Zhang, M.; Smith, A.; Gorski, W. *Anal. Chem.* **2004**, *76*, 5045.

(103) Qian, L.; Yang, X. *Talanta* **2006**, *68*, 721.

(104) Lau, C.; Cooney, M. J.; Atanassov, P. *Langmuir* **2008**, *24*, 7004.

(105) Petrov, P. D.; Georgiev, G. L. *Chem. Commun.* **2011**, *47*, 5768.

(106) Gutiérrez, M. C.; Hortigüela, M. J.; Amarilla, J. M.; Jiminez, R.; Ferrer, M. L.; del Monte, F. *J. Phys. Chem.; C* **2007**, *111*, 5557.

(107) Alzari, V.; Nuvoli, D.; Sanna, R.; Scognamillo, S.; Piccinini, M.; Kenny, J. M.; Malucelli, G.; Mariani, A. *J. Mater. Chem.* **2011**, *21*, 16544.

(108) Guo, P.; Song, H.; Chen, X. *J. Mater. Chem.* **2010**, *20*, 4867.

(109) Yang, H.; Li, F.; Shan, C.; Han, D.; Zhang, Q.; Niu, L.; Ivaska, A. *J. Mater. Chem.* **2009**, *19*, 4632.

(110) Cai, D.; Song, M. *J. Mater. Chem.* **2010**, *20*, 7906.

(111) Park, S.; Ruoff, R. S. *Nat. Nano.* **2009**, *4*, 217.

(112) Brodie, B. C. *Philos. Trans. R. Soc. London* **1859**, *149*, 249.

(113) Staudenmaier, L. *Berichte der deutschen chemischen Gesellschaft* **1898**, *31*, 1481.

(114) Hummers, W. S.; Offeman, R. E. *J. Am. Chem. Soc.* **1958**, *80*, 1339.

(115) Marcano, D. C.; Kosynkin, D. V.; Berlin, J. M.; Sinitskii, A.; Sun, Z.; Slesarev, A.; Alemany, L. B.; Lu, W.; Tour, J. M. *ACS Nano* **2010**, *4*, 4806.

(116) Li, D.; Müller, M. B.; Gilje, S.; Kaner, R. B.; Wallace, G. G. *Nat. Nano.* **2008**, *3*, 101.

(117) Li, F.; Bao, Y.; Chai, J.; Zhang, Q.; Han, D.; Niu, L. *Langmuir* **2010**, *26*, 12314.

(118) Lerf, A.; He, H.; Forster, M.; Klinowski, J. *J. Phys. Chem.; B* **1998**, *102*, 4477.

(119) Gao, W.; Alemany, L. B.; Ci, L.; Ajayan, P. M. *Nat. Chem.* **2009**, *1*, 403.

(120) He, H.; Klinowski, J.; Forster, M.; Lerf, A. *Chem. Phys. Lett.* **1998**, *287*, 53.

(121) Szabó, T.; Tombácz, E.; Illés, E.; Dékány, I. *Carbon* **2006**, *44*, 537.

(122) Stankovich, S.; Dikin, D. A.; Piner, R. D.; Kohlhaas, K. A.; Kleinhammes, A.; Jia, Y.; Wu, Y.; Nguyen, S. T.; Ruoff, R. S. *Carbon* **2007**, *45*, 1558.

(123) Stankovich, S.; Dikin, D. A.; Dommett, G. H. B.; Kohlhaas, K. M.; Zimney, E. J.; Stach, E. A.; Piner, R. D.; Nguyen, S. T.; Ruoff, R. S. *Nature* **2006**, *442*, 282.

(124) Xu, Z.; Gao, C. *Macromolecules* **2010**, *43*, 6716.

(125) Choi, B. G.; Yang, M.; Hong, W. H.; Choi, J. W.; Huh, Y. S. *ACS Nano* **2012**, *6*, 4020.

(126) Worsley, M. A.; Pauzauskie, P. J.; Olson, T. Y.; Biener, J.; Satcher, J. H.; Baumann, T. F. *J. Am. Chem. Soc.* **2010**, *132*, 14067.

(127) Xu, Y.; Sheng, K.; Li, C.; Shi, G. *ACS Nano* **2010**, *4*, 4324.

(128) Zhang, N.; Qiu, H.; Si, Y.; Wang, W.; Gao, J. *Carbon* **2011**, *49*, 827.

(129) Vickery, J. L.; Patil, A. J.; Mann, S. *Adv. Mater.* **2009**, *21*, 2180.

(130) Qiu, L.; Liu, J. Z.; Chang, S. L. Y.; Wu, Y.; Li, D. *Nat Commun* **2012**, *3*, 1241.

(131) Deville, S.; Saiz, E.; Nalla, R. K.; Tomsia, A. P. *Science* **2006**, *311*, 515.

(132) Munch, E.; Launey, M. E.; Alsem, D. H.; Saiz, E.; Tomsia, A. P.; Ritchie, R. O. *Science* **2008**, *322*, 1516.

(133) Xu, C. Y.; Inai, R.; Kotaki, M.; Ramakrishna, S. *Biomaterials* **2004**, *25*, 877.

(134) Schiffman, J. D.; Schauer, C. L. *Biomacromolecules* **2006**, *8*, 594.

(135) Min, B.-M.; Lee, S. W.; Lim, J. N.; You, Y.; Lee, T. S.; Kang, P. H.; Park, W. H. *Polymer* **2004**, *45*, 7137.

(136) Qian, L.; Zhang, H. *Green Chemistry* **2010**, *12*, 1207.

(137) Ettre, L. S.; Sakodynskii, K. I. *Chromatographia* **1993**, *35*, 223.

(138) Ettre, L. S. *J. High. Resolut. Chromatogr.* **1993**, *16*, 258.

(139) Bayer, E.; Chovin, P.; Cremer, E.; Deans, D. R.; Geiss, F.; Guiochon, G.; Halász, I.; Jentzsch, D.; Kaiser, R.; Lebbe, J.; Machata, G.; Munier, R. L.; Oster, H.; Prevot, A.; Rohrschneider, L.; Schay, G.; Schomburg, G.; Stahl, E.; Szepesy, L.; Tranchant, J. *Chromatographia* **1968**, *1*, 153.

(140) Li, Y.; Gu, B.; Dennis Tolley, H.; Lee, M. L. *J. Chromatogr. A* **2009**, *1216*, 5525.

(141) Gu, B.; Li, Y.; Lee, M. L. *Anal. Chem.* **2007**, *79*, 5848.

(142) Moody, H. W. *J. Chem. Educ.* **1982**, *59*, 290.

(143) van Deemter, J. J.; Zuiderweg, F. J.; Klinkenberg, A. *Chem. Eng. Sci.* **1956**, *5*, 271.

(144) Kubin, M.; Spacek, P.; Chromecek, R. *Collect. Czech. Chem. Commun* **1967**, *32*, 3881.

(145) Schnecko, H.; Bieber, O. *Chromatographia* **1971**, *4*, 109.

(146) Hjertén, S.; Liao, J.-L.; Zhang, R. *J. Chromatogr. A* **1989**, *473*, 273.

(147) Svec, F.; Frechet, J. M. J. *Anal. Chem.* **1992**, *64*, 820.

(148) Minakuchi, H.; Nakanishi, K.; Soga, N.; Ishizuka, N.; Tanaka, N. *Anal. Chem.* **1996**, *68*, 3498.

(149) Fields, S. M. *Anal. Chem.* **1996**, *68*, 2709.

(150) Cabrera, K.; Lubda, D.; Eggenweiler, H.-M.; Minakuchi, H.; Nakanishi, K. *J. High. Resolut. Chromatogr.* **2000**, *23*, 93.

(151) Cabrera, K. *J. Sep. Sci.* **2004**, *27*, 843.

(152) Svec, F. *J. Chromatogr. A* **2010**, *1217*, 902.

(153) Svec, F. *J. Sep. Sci.* **2004**, *27*, 1419.

(154) Lee, D.; Svec, F.; Fréchet, J. M. J. *J. Chromatogr. A* **2004**, *1051*, 53.

(155) Yue, Z.; Wen, F.; Gao, S.; Ang, M. Y.; Pallathadka, P. K.; Liu, L.; Yu, H. *Biomaterials* **2010**, *31*, 8141.

(156) Reichelt, S.; Abe, C.; Hainich, S.; Knolle, W.; Decker, U.; Prager, A.; Konieczny, R. *Soft Matter* **2013**, *9*, 2484.

(157) Svec, F.; Frechet, J. M. J. *Chem. Mater.* **1995**, *7*, 707.

(158) Viklund, C.; Svec, F.; Fréchet, J. M. J.; Irgum, K. *Chem. Mater.* **1996**, *8*, 744.

(159) Zhu, G.; Yang, C.; Zhang, L.; Liang, Z.; Zhang, W.; Zhang, Y. *Talanta* **2006**, *70*, 2.

(160) Yao, C.; Qi, L.; Jia, H.; Xin, P.; Yang, G.; Chen, Y. *J. Mater. Chem.* **2009**, *19*, 767.

(161) Wang, Q. C.; Svec, F.; Frechet, J. M. J. *Anal. Chem.* **1995**, *67*, 670.

(162) Langer, J. S. *Reviews of Modern Physics* **1980**, *52*, 1.

(163) Butler, M. F. *Crystal Growth & Design* **2001**, *2*, 59.

(164) Butler, M. F. *Crystal Growth & Design* **2001**, *1*, 213.

(165) Deville, S. *Adv. Eng. Mater.* **2008**, *10*, 155.

(166) Deville, S. *J. Mater. Res.* **2013**, *FirstView* (in print).

(167) Oetjen, G.-W. In *Freeze-Drying, Ullmann's Encyclopedia of Industrial Chemistry.; Wiley-VCH* 2000.

(168) Oetjen, G.-W.; Haseley, P. *Freeze-Drying, Food and Luxury Food.; Wiley-VCH* **2007**.

(169) Staudinger, H. *Ber. Deut. Chem. Ges* **1920**, *53*, 1073.

(170) Mülhaupt, R. *Angew. Chem. Int. Ed.* **2004**, *43*, 1054.

(171) Smith, J. K.; Hounshell, D. A. *Science* **1985**, *229*, 436.

(172) Carothers, W. H. *J. Am. Chem. Soc.* **1929**, *51*, 2548.

(173) Flory, P. J. *Principles of polymer chemistry; Cornell University Press.* **1953**.

(174) Billiet, L.; Fournier, D.; Du Prez, F. *J. Polym. Sci., Part A: Polym. Chem.* **2008**, *46*, 6552.

(175) Mallakpour, S.; Rafiee, Z. *J. Appl. Polym. Sci.* **2007**, *103*, 947.

(176) Spindler, R.; Frechet, J. M. J. *Macromolecules* **1993**, *26*, 4809.

(177) Houmam, A. *Chem. Rev.* **2008**, *108*, 2180.

(178) Henríquez, C.; Bueno, C.; Lissi, E. A.; Encinas, M. V. *Polymer* **2003**, *44*, 5559.

(179) Bahri-Laleh, N.; Abbas-Abadi, M. S.; Haghighi, M. N.; Akbari, Z.; Tavasoli, M. R.; Mirjahanmardi, S. H. *J. Appl. Polym. Sci.* **2010**, *117*, 1780.

(180) Mucci, V.; Vallo, C. *J. Appl. Polym. Sci.* **2012**, *123*, 418.

(181) Fischer, H.; Baer, R.; Hany, R.; Verhoolen, I.; Walbiner, M. *Journal of the Chemical Society, Perkin Transactions 2* **1990**, *0*, 787.

(182) Barner-Kowollik, C.; Vana, P.; Davis, T. P. *J. Polym. Sci., Part A: Polym. Chem.* **2002**, *40*, 675.

(183) Wunsch, J. R. *Polystyrene Synthesis, Production and Applications.; Rapra technology limited* **2000**.

(184) Tunc, D.; Yagci, Y. *Polymer Chemistry* **2011**, *2*, 2557.

(185) Morancho, J.; Cadenato, A.; Fernández-Francos, X.; Salla, J.; Ramis, X. *J. Therm. Anal. Calorim.* **2008**, *92*, 513.

(186) Decker, C.; Moussa, K. *UV-Radiation- and Laser-Induced Polymerization of Acrylic Monomers.; Radiation Curing of Polymeric Materials.; vol 417.; American Chemical Society* **1990**.

(187) Chen, S.; Cook, W. D.; Chen, F. *Polym. Int.* **2007**, *56*, 1423.

(188) Hall, A. W.; Blackwood, K. M.; Milne, P. E. Y.; Goodby, J. W. *Chem. Commun.* **2003**, 2530.

(189) Kirsebom, H.; Rata, G.; Topgaard, D.; Mattiasson, B.; Galaev, I. Y. *Macromolecules* **2009**, *42*, 5208.

(190) Petrov, P.; Petrova, E.; Tsvetanov, C. B. *Polymer* **2009**, *50*, 1118.

(191) Ishizone, T.; Han, S.; Okuyama, S.; Nakahama, S. *Macromolecules* **2002**, *36*, 42.

(192) Sawamoto, M.; Higashimura, T. *Makromolekulare Chemie. Macromolecular Symposia* **1990**, *32*, 131.

(193) Matyjaszewski, K. *Macromolecules* **2012**, *45*, 4015.

(194) Gregory, A.; Stenzel, M. H. *Prog. Polym. Sci.* **2012**, *37*, 38.

(195) Qiu, L.; Bae, Y. *Pharm. Res.* **2006**, *23*, 1.

(196) Dai, S.; Ravi, P.; Tam, K. C. *Soft Matter* **2009**, *5*, 2513.

(197) Gong, C. B.; Lam, M. H. W.; Yu, H. X. *Adv. Funct. Mater.* **2006**, *16*, 1759.

(198) Woodward, R. T.; Olariu, C. I.; Hasan, E. A.; Yiu, H. H. P.; Rosseinsky, M. J.; Weaver, J. V. M. *Soft Matter* **2011**, *7*, 4335.

(199) Schmaljohann, D. *Adv. Drug Delivery Rev.* **2006**, *58*, 1655.

(200) Han, L.-H.; Lai, J. H.; Yu, S.; Yang, F. *Biomaterials* **2013**, *34*, 4251.

(201) Brown, P.; Butts, C. P.; Cheng, J.; Eastoe, J.; Russell, C. A.; Smith, G. N. *Soft Matter* **2012**, *8*, 7545.

(202) Yan, Q.; Hoffman, A. S. *Polymer* **1995**, *36*, 887.

(203) Ni, C.; Zhu, X.-X. *Eur. Polym. J.* **2004**, *40*, 1075.

(204) Varaprasad, K.; Ravindra, S.; Reddy, N. N.; Vimala, K.; Raju, K. M. *J. Appl. Polym. Sci.* **2010**, *116*, 3593.

(205) Yuk, S. H.; Cho, S. H.; Lee, S. H. *Macromolecules* **1997**, *30*, 6856.

(206) Lutz, J.-F.; Weichenhan, K.; Akdemir, Ö.; Hoth, A. *Macromolecules* **2007**, *40*, 2503.

(207) Hu, Z.; Cai, T.; Chi, C. *Soft Matter* **2010**, *6*, 2115.

(208) Lutz, J.-F. *J. Polym. Sci., Part A: Polym. Chem.* **2008**, *46*, 3459.

(209) Lutz, J.-F. *Adv. Mater.* **2011**, *23*, 2237.

(210) Mandal, T. K. *Eur. J. Pharm. Biopharm.* **2000**, *50*, 337.

(211) Patel, V. R.; Amiji, M. M. *Pharm. Res.* **1996**, *13*, 588.

(212) Zhang, Z.; Chen, L.; Deng, M.; Bai, Y.; Chen, X.; Jing, X. *J. Polym. Sci., Part A: Polym. Chem.* **2011**, *49*, 2941.

(213) van de Wetering, P.; Moret, E. E.; Schuurmans-Nieuwenbroek, N. M. E.; van Steenbergen, M. J.; Hennink, W. E. *Bioconjugate Chem.* **1999**, *10*, 589.

(214) Gopishetty, V.; Tokarev, I.; Minko, S. *J. Mater. Chem.* **2012**.

(215) Lee, E.; Kim, B. *Polym. Bull.* **2010**, *67*, 67.

(216) Yanfeng, C.; Min, Y. *Radiat. Phys. Chem.* **2001**, *61*, 65.

(217) Kim, J. H.; Lee, S. B.; Kim, S. J.; Lee, Y. M. *Polymer* **2002**, *43*, 7549.

Chapter 2

Characterization Methods and Equipment

List of Figures

2.1 Scanning Electron Microscopy

The morphology of materials was observed using a Hitachi-S4800 scanning electron microscope. A small piece was cut from the monolith using a blade and then adhered to a stud using Araldite resin. The samples were coated with gold using a sputter-coater (EMITECH K550X) for 2 minutes at 30 mA before SEM imaging. The author or Drs. Haifei Zhang, Neil Grant, Tom McDonald or Marco Giardiello observed samples.

2.1.1 SEM Instrument

Scanning electron microscopy is a technique used to observe the surface morphology of solid materials.[1,2] The microscope produces images by scanning a material with a focused beam of electrons produced from a metal filament such as tungsten wire or lanthanum hexaboride cathode filament.[2] These materials are selected for their excellent mechanical strength and high melting point. The components of an SEM are outlined in Figure 2.1. Typical imaging takes place under vacuum because having a gas atmosphere causes the electron beam to lose it's intensity.[3] The electron beam, which normally has energy ranging from 0.2 keV to 40 keV, is focused by one or

two condenser lenses to a spot about 0.4 - 5 nm in diameter. An aperture is used to control the size of the beam that hits the sample. It is possible to increase resolution by increasing the strength of the condenser lens and reducing the aperture size to obtain a narrow beam. The stigmator, which is a collection of small pieces of electromagnetic coils within the objective lens, corrects any astigmatism caused by the condenser lenses.

The types of signals generated by an SEM include: secondary electrons (SE), back scattered electrons (BSE), transmitted electrons, X-rays and light.[1,2] Signals used for imaging are SE and BSE. SE signals are generated by inelastic electron collisions whereas the BSE are generated by an elastic collision of the nucleus of an atom causing the electrons to back scatter.[2] Samples must be conductive to eradicate electron charging on the surface of the material.[2] Non-conductive samples are typically sputtered with a thin layer of a conductive metal such as gold.

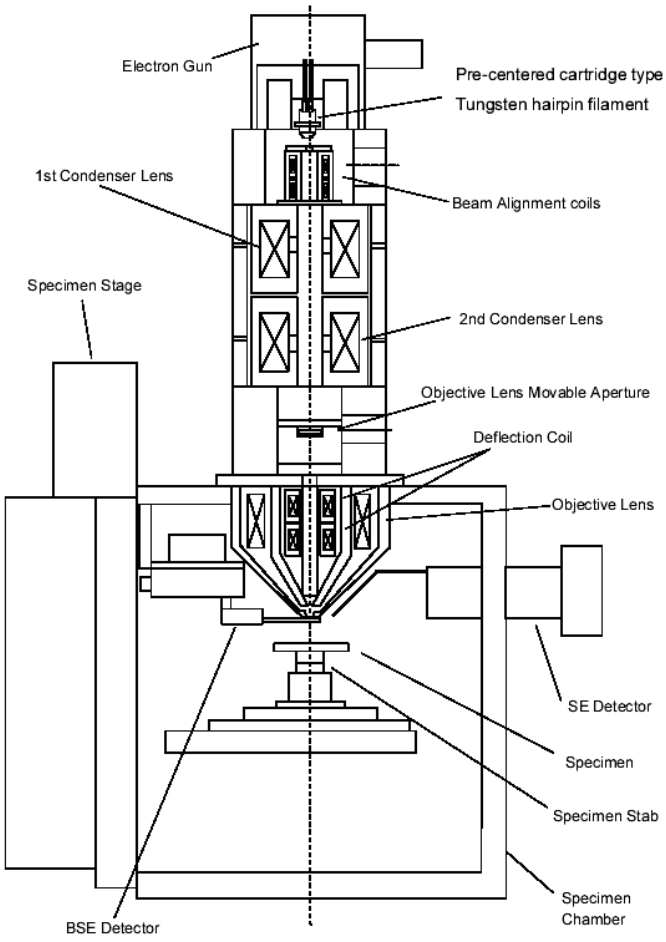

Figure 2.1 Schematic of a scanning electron microscope.[3]

2.2 Mercury Intrusion Porosimetry

Intrusion volume and macropore size distribution were measured using a Micromeritics Autopore IV 9500 porosimeter over a pressure range of 0.10 – 60000 psia. The intrusion volume was calculated by subtracting the intrusion arising from mercury interpenetration in large spaces (> 150 μm) from the total intrusion. Roughly 20 mg was used per sample. The author ran all samples.

2.2.1 Mercury Intrusion Porosimeter

Mercury intrusion porosimetry (Figure 2.2A) is a method used to determine pore size distributions of macroporous materials with pore sizes ranging from 0.003-200 μm. A porous sample is placed into penetrometer and sealed. The penetrometer is placed in the low pressure port where the chamber is evacuated and filled with mercury. It is then placed into the high pressure chamber.

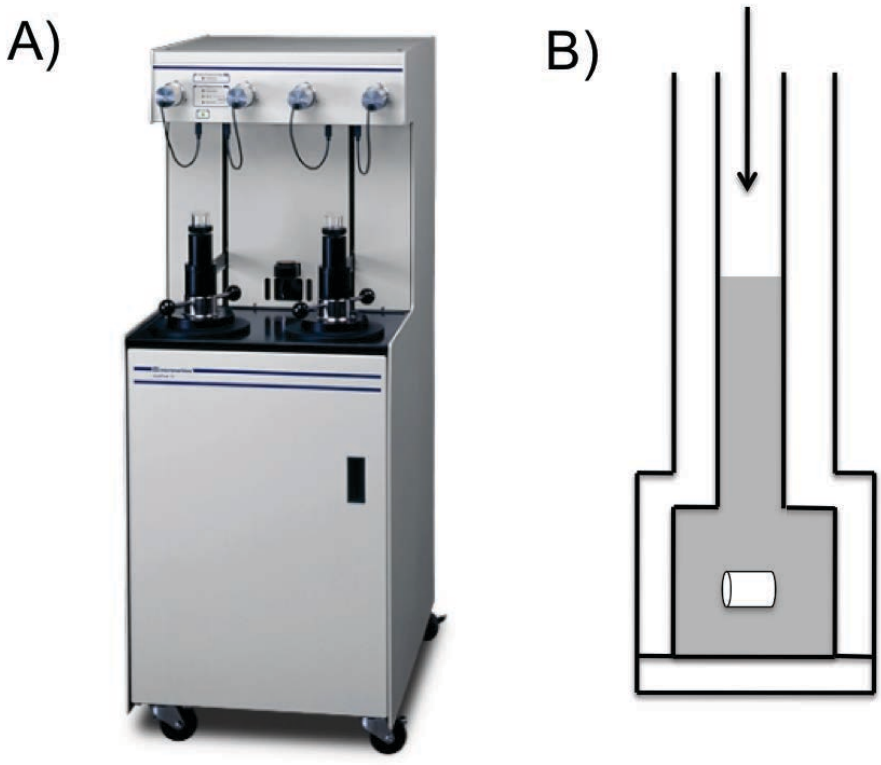

Figure 2.2 A) Photograph of Micromeritics Autopore IV 9500[4] B) Schematic of penetrometer containing a monolithic porous polymer sample surrounded in mercury and pressure being applied downwards.

High pressure is required to force the mercury into the pores because under normal conditions mercury does not enter a porous material by capillary action due to its high surface tension (485.5 mN/m). The pressure is increased in stages from 25-60,000 psia. After a given pressure cycle, mercury is forced into the pores and is detected by a change in the amount of mercury between the penetrometer ends (Figure 2.2B). The Washburn equation states that pressure is inversely proportional to a pore diameter (Equation 2.1).[5-7]

$$D = \frac{-4\gamma\cos\theta}{P} \tag{2.1}$$

D = pore diameter, γ = surface tension of mercury, P = applied pressure, θ = contact angle. This equation is used for pore size distribution calculations, and using volume calibration and masses recorded throughout the analysis it is possible to calculate bulk density total porosity of a sample.[5]

2.3 High Performance Liquid Chromatography (HPLC)

Columns were assessed on a HPLC instrument (Agilent 1200 series), consisting of a vacuum degasser, quaternary pump, ALS auto-sampler, heated column compartment and UV-Vis detector. Data analysis was performed using Agilent Chemstation software, version B.02.01 (Agilent Technologies, USA). Columns were packed and ran by the author, Dr. Adham Ahmed and Dr. Ali Entimimi.

2.3.1 HPLC Instrument

High performance liquid chromatography (HPLC) is a chromatographic technique used in chemistry and biology to separate a mixture of compounds. The method differs from normal liquid chromatography [8] because operational pressures used are much higher (around 50 – 350 bar) giving greater resolution.

A schematic of HPLC setup is shown in Figure 2.3. Solvent containers are attached to a pump which provides pressure for the flow of solvent (mobile phase) through a HPLC column. The pumps are able to mix solvents in the required ratios for efficient

separation. Typical reverse phase solvents include acetonitrile, water and methanol. HPLC columns are normally packed with small spherical sorbent particles (size 2-50 μm) made from silica or polymers known as a stationary phase (SP). The most common type of detector is UV/Vis which can generate signals corresponding to the amount a compound leaving the column.

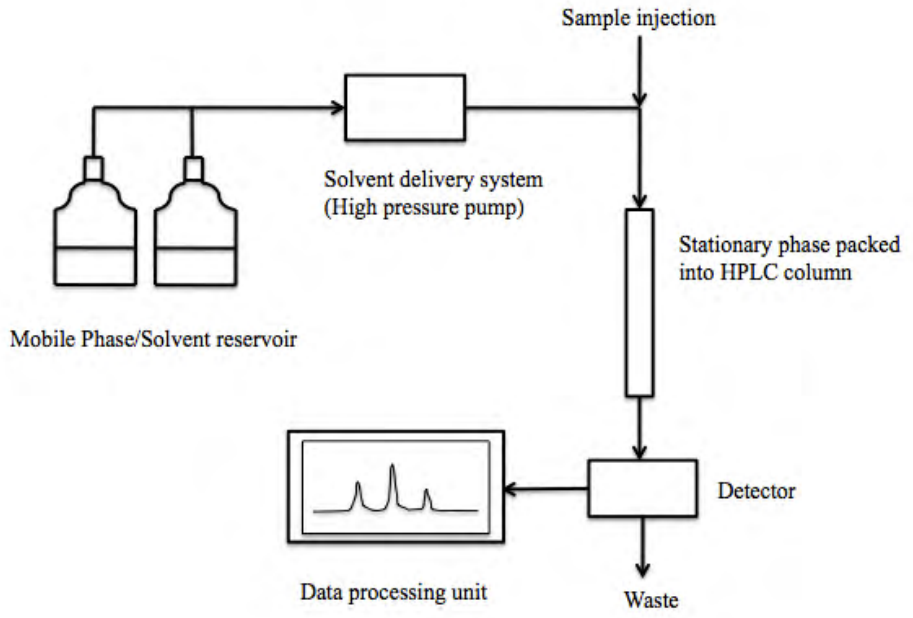

Figure 2.3 Schematic of high performance liquid chromatography.

Separation of a mixture of compounds is achieved via different degrees of interaction for each substituent with the sorbent (stationary phase). Type of interactions include: hydrophobic, dipole-dipole and ionic. HPLC columns are normally prepared with sorbent silica spheres around 2-5 μm. Smaller particles give more resolving power however smaller particles can significantly increase back pressure as shown in Equation 2.2.

$$\Delta P = \frac{\eta F L}{K_0 \pi r^2 d_p{}^2} \tag{2.2}$$

Where P = pressure, η = viscosity, F= flow rate and column length K = specific permeability r = column radius and d_p = particle diameter.[9,10]

Back-pressure is generated because when a pump is working to move air through the whole column system, it must overcome the forces that resist air movement. These can include: resistance from chemical sorbents, filters, viscosity or friction from inside of tubing. Any of the factors in Equation 2.2 can be altered to tune the back-pressure generated. High back-pressures are not favourable because they could be outside the capability range/operating pressures of the pump.[9] This makes it difficult to make results reliable and reproducible. Macroporous monolithic materials are advantageous as stationary phases because they can lower back-pressure and increase rate of transfer, by providing voids for the mobile phase to flow through.

2.4 Gas Chromatography

Gas chromatography (GC) samples were run using an Agilent Technologies 6890 Network GC system, fitted with an Agilent technologies 7683B series injector. The author or Dr. Adham Ahmed ran samples.

2.4.1 GC Instrument

GC is a separation method that works on the basis that a mixture of compounds can be separated via vaporization without decomposing the sample in question. Figure 2.4 outlines the components of a GC machine.

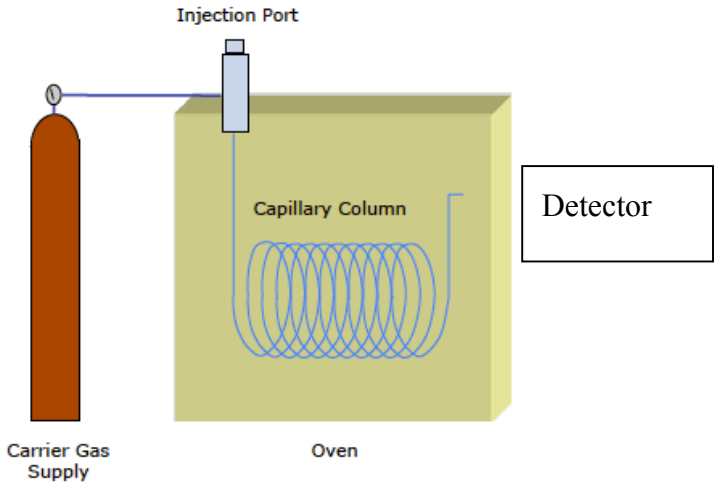

Figure 2.4 Schematic of gas chromatography.

The mobile phase in GC is generally an inert carrier gas such as helium or nitrogen, however hydrogen is also commonly used. The stationary phase is a very long piece of silica or metal tubing with a liquid silicon material fused to the inside of the tubing. Separation and run time depends on factors such as thickness of stationary phase, column diameter and column length. Polarity of a sample must be similar to polarity of the stationary phase of the column to increase resolution and separation.

The separation mixture is injected into the entrance head of a column using a microsyringe. The carrier gas carries the mixture through the column and as it does so its motion is neglected by adsorption of the sample to the stationary phase on the capillary wall. Each compound will have a different degree of adsorption, and the columns are relatively large so samples reach the end of the column at different times. In general compounds are normally eluted in order of boiling point.

2.5 Conductivity Measurements

Front panel resistance measurements were taken via a two-probe method using a Keithley 2600A I-V sourcemeter, sourcing 1 mA current (40 V limit) and measuring the voltage drop between the same probes. This gives a resistance value on the sourcemeter. Conductive silver glue was used to stick the probes to the porous material (Figure 2.5).

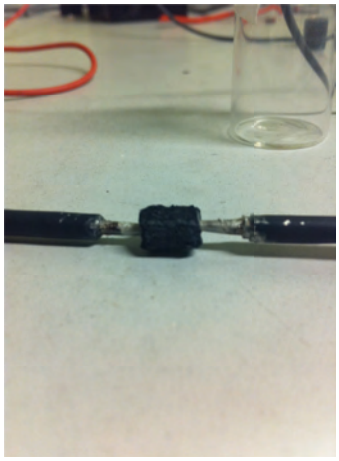

Figure 2.5 Image of voltmeters attached to porous polymer sample by conductive silver adhesive.

Resistivity values for bulk materials are worked out using volume resistivity formula shown in equation 2.3 where ρ = volume resistivity, V = voltage, I = current, A = cross sectional area of sample, L = distance between voltage probes.[11]

$$\rho = \left(\frac{V}{I}\right)\left(\frac{A}{L}\right) \tag{2.3}$$

Resistance (Ω) is defined as voltage over current (Equation 2.4).

$$\Omega = \frac{V}{I} \tag{2.4}$$

Resistivity is the reciprocal of conductivity (Equation 2.5).[11]

$$\rho = \frac{1}{\sigma} \tag{2.5}$$

2.6 Mechanical Stability

Compression tests were taken using an Instron 4204 with a 5kN loading cell and a velocity of compression of 0.5 mm/minute. Polymer samples were sliced into a specific shape (either cylinders or cubes for chapter 3 and chapter 4) for testing. Samples were run by Mr Stephen Pennington.

To evaluate the mechanical stability of each material, compression tests were conducted to determine the Young's modulus (Figure 2.6). This is defined as the stiffness of an elastic material and is calculated by dividing stress/strain from the initial linear part of the stress-strain curve. The initial linear part of a stress-strain curve is used because this is the region where the material is said to be coping with the increasing mechanical load placed upon it. Stress is defined as a measure of internal force acting within a deformable body and has units of pressure (Pascals or

N/m^2). Strain is defined as a normalized measure of deformation of an elastic body in terms of displacement and has no units.

Figure 2.6 Image of porous polymer placed between two loading cells for compression testing.

Therefore Young's modulus values are given in pascals or N/m^2. This is outlined in equation 2.6 where E = Young Modulus, F = force, A = Area, ΔL displacement of sample, L_0 = Initial length of sample.[12]

$$E = \frac{Stress}{Strain} = \frac{F/A}{\Delta L/L_0} \tag{2.6}$$

2.7 Fourier Transform Infrared Spectroscopy (FTIR)

Fourier transform infrared spectroscopy measurements were conducted using a Bruker Tensor 27 spectrometer to show the disappearance of C=C bond. The frozen samples were taken away from the UV lamp at different time intervals, dried under vacuum and sliced in cross sections. The material at the middle was analyzed to show whether the monomers were polymerizing all the way through the sample. To do the analysis, the material was ground up using a pestle and mortar. A KBr pellet was then made by grinding 200 mg KBr in a mortar with 2 mg of the material, which was then compressed into a pellet using 2 tonnes pressure for one minute then at 10 tonnes for a further minute. Each sample was scanned 16 times.

2.8 Gel Permeation Chromatography

Gel permeation chromatography (GPC) measurements were conducted using a Viscotek 270 max triple detection to evaluate molecular weight and polydispersity index for polymers with different polymerization times under UV irradiation. For GPC, samples were directionally frozen and polymerized on dry ice, then removed at different time intervals and freeze-dried for 48 hours. The GPC is equipped with two T6000M columns using a mobile phase of THF at 35ºC and a flow rate of 1.0 ml min^{-1}. Polymer concentrations for GPC measurements were 4 mg ml^{-1}. Samples were run by Ms. Fiona Hatton.

2.9 Surface Area Measurements

Apparent surface area measurements were carried out using a Quantachrome Nova 4200 (Figure 2.7). Approximately 100 mg of sample was used for analysis and degassed for 15 hours under vacuum at 120 °C. Five point measurements were taken between pressures (P/P_0) of 9.5×10^{-2} and 2.98×10^{-1} at 77.3K.

Figure 2.7 Quantachrome Nova 4200 gas sorption analyzer

Samples were run by either Mr. Rob Clowes or Ms. Thanchanok Ratvijitvech.

2.10 X-Ray Diffraction

Powder X-Ray Diffraction (pXRD) analysis was run by Mr Rob Clowes using the panalytical X'Pert PRO HTS X-Ray Diffracometer.

2.11 Thermogravimetric Analysis

Thermogravimetric analysis (TGA) was carried out using a Q5000IR TGA that contains an overhead thermobalance. The samples were heated at a rate of 10 °C per minute to 1000°C under a constant flow of air. Measurements were run by Dr. Adham Ahmed.

2.12 Energy-Dispersive X-Ray Spectroscopy

Energy-dispersive X-Ray spectroscopy is a technique used to analyze the elemental make-up of the surface of a material. The facility is part of the Hitachi-S4800 scanning electron microscope. Samples were run by Mr Rob Clowes.

2.13 Elemental Analysis

Elemental analysis was carried out by Mrs. Jean Ellis in the University of Liverpool chemistry departmental service. Carbon, nitrogen and hydrogen are given as % by mass. It can also be determined if sulfur is present within a material, however the % by mass is unknown.

2.14 UV lamp and Wavelength

Polymerizations were carried out using 40-watt Spectroline ® X-series UV bench and display lamp (wavelength 365 nm). Samples were placed on dry ice or ice and placed directly underneath the UV source (Figure 2.8).

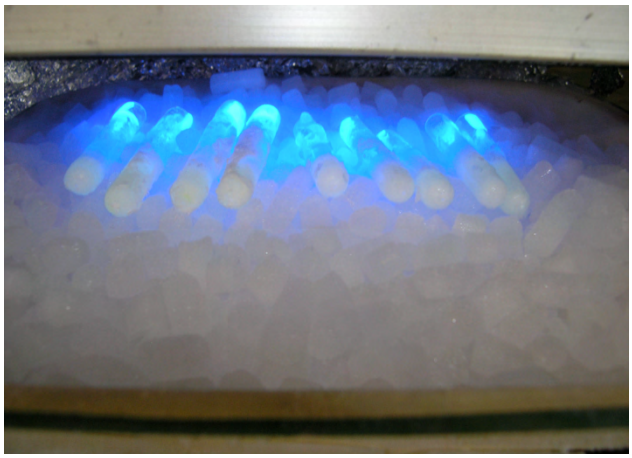

Figure 2.8 Image of frozen polymer samples underneath the UV source on a bed of dry ice (-78 °C).

2.15 Optical Microscope and Freeze Stage Equipment

All optical images were taken with an Olympus 5.1 megapixel C-5060 wide zoom camera. The camera could be fixed directly onto the Olympus CX41 microscope. The freeze stage equipment used was a Linkam PE94 scientific temperature controller where a glass slide was placed between two temperature controlled plates. One plate was set at room temperature the other at -20 °C. The slide was gradually moved across to the colder plate so freezing patterns could be observed.

2.16 Freeze Dryer

For freeze-dried samples in chapter 4 a VIRTIS Advantage Freeze drier was used. Condenser temperature was set at -80 °C and shelf temperature 10 °C.

2.16 References

(1) Cosslett, V. E. *Ann. N.Y. Acad. Sci.* **1962**, *97*, 464.

(2) Goldstein, J.; Newbury, D. E.; Echlin, P.; Joy, D. C.; Lyman, C. E.; Lifshin, E.; Sawyer, L.; Joseph, M. R. *Scanning Electron Microscopy and X-Ray Microanalysis.; Third Ed.; Springer.* **2003**.

(3) *Hitachi_ S-3400N Scanning Electron Microscope manual* http://taltos.stanford.edu/docs/Hitachi_man.pdf.

(4) *Autopore IV Series Micromertrics Instrument Manual* http://www.micromeritics.com/Repository/Files/AutoPore_IV_Series_Mercury_Porosimeters_Brochure.pdf.

(5) Webb, P. A.; Orr, C. *Analytical methods in fine partical technology.; First ed.; Micromeritics.* **1997**.

(6) Pirard, R.; Alié, C.; Pirard, J.-P. *Powder Technol.* **2002**, *128*, 242.

(7) Washburn, E. W. *Proc Natl Acad Sci U.* **1921**, 115.

(8) Chojnowski, J.; Rubinsztajn, S.; Wilczek, L. *Macromolecules* **1987**, *20*, 2345.

(9) MacNair, J. E.; Lewis, K. C.; Jorgenson, J. W. *Anal. Chem.* **1997**, *69*, 983.

(10) Snyder, L. R.; Kirkland, J. J. I. *Introduction to Modern Liquid Chromatography; John Wiley & Sons, Inc.* **1979**.

(11) *Keithley Low Level Mesurements Handbook 6th Editon* http://www.keithley.com/knowledgecenter/knowledgecenter_pdf/LowLevMsHandbk_1.pdf.

(12) *"Young's modulus." The Columbia Encyclopedia, 6th ed.. 2012. Encyclopedia.com.*

Chapter 3

Aligned Porous Structures by Directional Freezing and Frozen UV Initiated Polymerization with Increased Mechanical Stability, Conductivity and as a Stationary Phase for HPLC

List of Figures

List of Schemes

List of Tables

3.1 Introduction

Control of pore morphologies in porous materials is extremely important for targeted applications.[1,2] It is well known that ordered porous structures can be fabricated by surfactant templating or colloidal crystal templating.[3,4] Other types of ordered structures are orientated surface patterns or 3-dimensional (3D) porous materials with parallel microchannels.[5] These type of materials have not been investigated as extensively as ordered porous materials but are highly important for a range of applications such as directing axonal regeneration[6] or flow-through porous electrodes.[7] Aligned surface patterns are commonly fabricated by microfabrication or soft lithography,[8] whilst it is still highly challenging to construct 3D aligned porous structures.

Ice templating is a simple and versatile route to prepare a wide range of porous materials.[9,10] In general, a solution or colloidal suspension is frozen in a cold liquid or environment and the subsequent removal of ice by freeze drying can produce porous structures. Recently, a directional freezing process was employed to orientate the growth of ice crystals and the frozen samples were then freeze dried to generate aligned porous materials which included hydrophilic polymer, hydrophobic polymers and composite materials.[5,11,12] However, the produced structures are fragile and mechanically very weak and they can be dissolved or shrink in the presence of solvents. This significantly limits their applications because most of the applications will involve the use or presence of liquids and require satisfying mechanical stability. Ceramic colloidal suspensions have been processed by freeze-casting and sintering to produce relatively strong porous ceramics.[13] More significantly, the layered porous ceramics are impregnated with organic polymers to mimic structures from nature, resulting in tough composite materials.[14,15] There are two important limitations to these materials: the lack of surface functionality of the porous ceramics and the loss of porosity in the tough composite materials.

Polymers or colloids (organic or ceramic) are frequently used for most of the freeze-drying process to make porous structures.[9,10,12] Monomers have rarely been used for the preparation of porous materials, particularly aligned porous materials. We believe that by controlled freezing of monomer solutions and polymerizing the monomers in the frozen state, it is possible to produce aligned porous crosslinked structures with significantly enhanced mechanical stability. The challenge is the slow polymerization due to the hindered transport of the monomers and free radicals in the solid state & low temperature and the danger of frozen solvent melting during the course of the polymerization. Cryogels have been prepared by 'semi-frozen polymerization' from aqueous solutions, which suggested that the polymerization in the frozen state was possible.[16]

In this chapter we investigate the fabrication of aligned porous crosslinked polymers by frozen polymerization and the subsequent modification to prepare porous conducting composites. The aligned porous polymer monoliths are also assessed as columns for high performance liquid chromatography (HPLC).

3.2 Experimental

3.2.1 Chemicals and Reagents

Tetraethylene glycol dimethacrylate (TEGDMA, assay spec ≥ 90% by GC), ethylene glycol dimethacrylate (EGDMA, 99%), 2,2-dimethoxy-2-phenylacetophenone (DMPA, 99%), 3-(trimethoxylsilyl)propyl methacrylate (TMSPMA, 98%), hydroxyethyl methacrylate (HEMA, ≥99%), poly(3,4-ethylenedioxythiophene)-poly(styrenesulfonate) (PEDOT-PSS, 1% aqueous solution), dioxane, camphene, cyclohexane were purchased from Sigma Aldrich and used as received. Graphite flakes were purchased from Alfa Aeser. The HPLC test mixture was a gift from Thermo Fisher Scientific.

3.2.2 Frozen Polymerization Procedure

Typically 5 ml of solution in a cylindrical glass tube (dimension 75 mm long x 10 mm diameter) was slowly immersed into liquid nitrogen at a rate of around 75 mm/min until it was fully frozen. The frozen sample was then placed on ice or dry ice under a 40-watt Spectroline ® X-series ultra-violet (UV) bench and display lamp (wavelength 365 nm) and polymerized for 2 hours (unless stated otherwise). The samples were turned every 30 minutes during the polymerization to ensure complete polymerization. There was no melting observed. After polymerization, the frozen samples were placed in a vacuum oven overnight at room temperature to remove the solvent and obtain dry porous material.

Dioxane solutions*:* 1:5, 1:10, 1:20 volume to volume (v/v) of TEGDMA/dioxane solutions were prepared with 1 wt% initiator DMPA with respect to amount of monomer. All the frozen dioxane samples were polymerized on ice under UV light.

Cyclohexane solutions*:* 1:5 volume to volume (v/v) of TEGDMA/cyclohexane solutions were prepared with 1 wt% DMPA initiator as before. The frozen samples were polymerized on dry ice.

Camphene solutions*:* 1:5 mass to mass (m/m) (camphene is solid at room temperature (RT)) TEGDMA/ camphene solution was prepared with 1 wt% DMPA

initiator as before. It was heated to 60°C to get a clear solution. This solution was then transferred into a pre-warmed glass tube for directional freezing. The frozen polymerization was carried out on dry ice to ensure no or little camphene was polymerized.

3.2.3 Post Treatment of Porous PTEGDMA

Porous PTEGDMA was soaked in 10 ml 1% aqueous PEDOT-PSS solution for 48 hours and then dried in a vacuum oven. Also, PTEGDMA was soaked in 10 ml 0.4% graphene oxide (GO) suspension for 48 hours then dried under vacuum. The GO suspensions were prepared following a procedure reported before.[17] The dry GO-PTEGDMA was placed in 1 ml hydrazine monohydrate in 100 ml of distilled water at 120°C for 48 hours in order to reduce GO to graphene.[18] PTEGDMA made from 1:20 dioxane solution was washed at least 3 times with dioxane for 24 hours to remove any unreacted monomers, initiator, or oligomers, and then dried in the vacuum oven overnight. The monolith was then washed 3 times with distilled water to remove any hydrazine and vacuum dried before the mass was recorded. The mass increase data for both experiments are shown in the results and discussion section.

3.2.3.1 Preparation of graphene oxide

Graphene oxide was prepared using a modified Hummers method similar to a previously reported method.[17] Concentrated sulfuric acid (50 mL) was added to a mixture of graphite flakes (2 g) and sodium nitrate (1 g), and the mixture was cooled using an ice bath to 0 °C. Potassium permangenate (9.0 g) was added slowly in portions to keep the reaction temperature below 20 °C. The reaction was warmed to 35 °C and stirred for 7 h then added to 200ml of ice cold distilled water and refluxed at 98°C for one week. The reaction mixture was cooled to room temperature and poured onto ice (200 mL) with 30% hydrogen peroxide (2 mL). The mixture was then purified *via* centrifuging and continuously washed with water for 1 week. Then the product was washed with diethyl ether to yield 1.2 g of graphene oxide, which was confirmed by CHN and transmission electron microscopy.

3.2.4 PTEGDMA Columns for HPLC

1 ml TEGDMA + 4.25 g camphene + 1 wt% DMPA were heated to 60 ^{0}C to obtain a transparent solution and stirred. A silanized glass column was filled with the mixture,

directionally frozen, and polymerized on dry ice under UV irradiation for 3 hours. Glass tubes with dimensions 88 mm L x 3.5 mm O.D. x 2.0 mm were silanized with 30% of 3(trimethoxysilyl) propyl methacrylate (TMSPMA) in acetone to provide a vinyl group for anchoring of polymer monoliths following the procedure developed by Gu *et al.*[19] The tubes were washed with ethanol and water then treated with 2 M HCl and heated at 110 °C for 3 h. The tubes were rinsed with ethanol and dried at 110 °C overnight in a vacuum oven. Silanization of the surface-activated tubes were performed at 25 °C overnight with the TMSPMA solution. After silanization, the tubes were rinsed with acetone and dried at 25 °C in a vacuum oven overnight.

3.3 Results and Discussion

3.3.1 Preliminary Experiments

Scheme 3.1 outlines the preparation procedures. A monomer solution is directionally frozen in liquid nitrogen and the monomers are polymerized in the frozen state (on ice or dry ice). Once the polymerization is completed, the frozen sample can be warmed up to room temperature. The solvent can be simply removed under vacuum at room temperature or elevated temperature to produce the aligned porous structure.

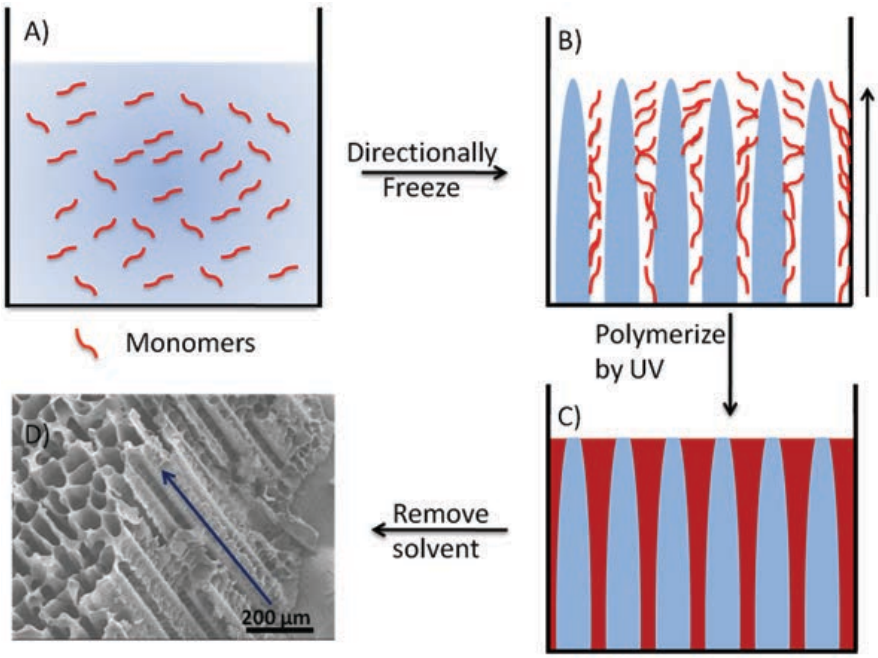

Scheme 3.1 Schematic representation of the preparation of aligned porous materials by directional freezing, frozen polymerization and then the removal of solvent under vacuum at room temperature.

In this study, UV-initiated polymerization was used because thermal polymerization would thaw the frozen sample and destroy the aligned structure. It is also thought that crosslinking monomer solutions could increase the mechanical properties of the resulting material compared to conventional freeze dried polymer monoliths. An advantage of removing the solvent under vacuum at room temperature is that the energy and time intensive freeze drying step is no longer required.

Methacrylate monomers were selected as acrylate monomers are widely used in UV-curable formulations.[20,21] Also methacrylate monomer formulations are currently the standard dental restoration materials for their flexibility and strength.[22] For the frozen polymerization, the use of solvent is critically important. Such solvents should have a relatively high melting point, be able to dissolve methacrylate monomers, and their frozen crystals can be orientated during the freezing process. Camphene (mp 50 ^{0}C and bp 160 ^{0}C) was firstly selected because it is solid at room temperature, can readily melt at 60 ^{o}C, and has been used as a solvent to prepare porous ceramics by a freeze-drying approach.[23,24] Structures of the compounds used in this study are outlined in Scheme 3.2. The photoinitiator used is 2,2-dimethoxy-2-phenylacetophenone (DMPA) which is widely used in UV curing of methacrylate monomers.[25,26]

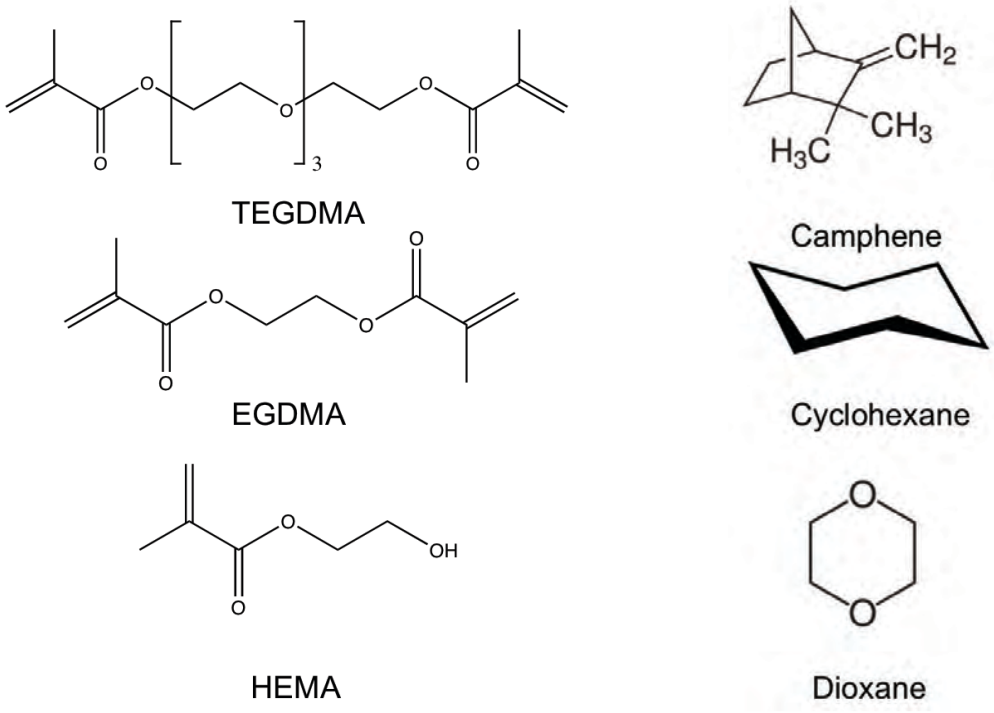

Scheme 3.2 Monomers (left) and solvents (right) used in this study.

To demonstrate if the concept worked, tetraethyleneglycol dimethacrylate (TEGDMA) was mixed with camphene 1:1 (m/m) and heated to 60 ^{o}C. 1% DMPA was added with respect to mass of TEGDMA. The resulting solution was frozen in freezer (-20 ^{0}C) and then polymerized on dry ice under a UV lamp. A randomly porous structure was produced after removing camphene, as observed by SEM (Figure 3.1A).

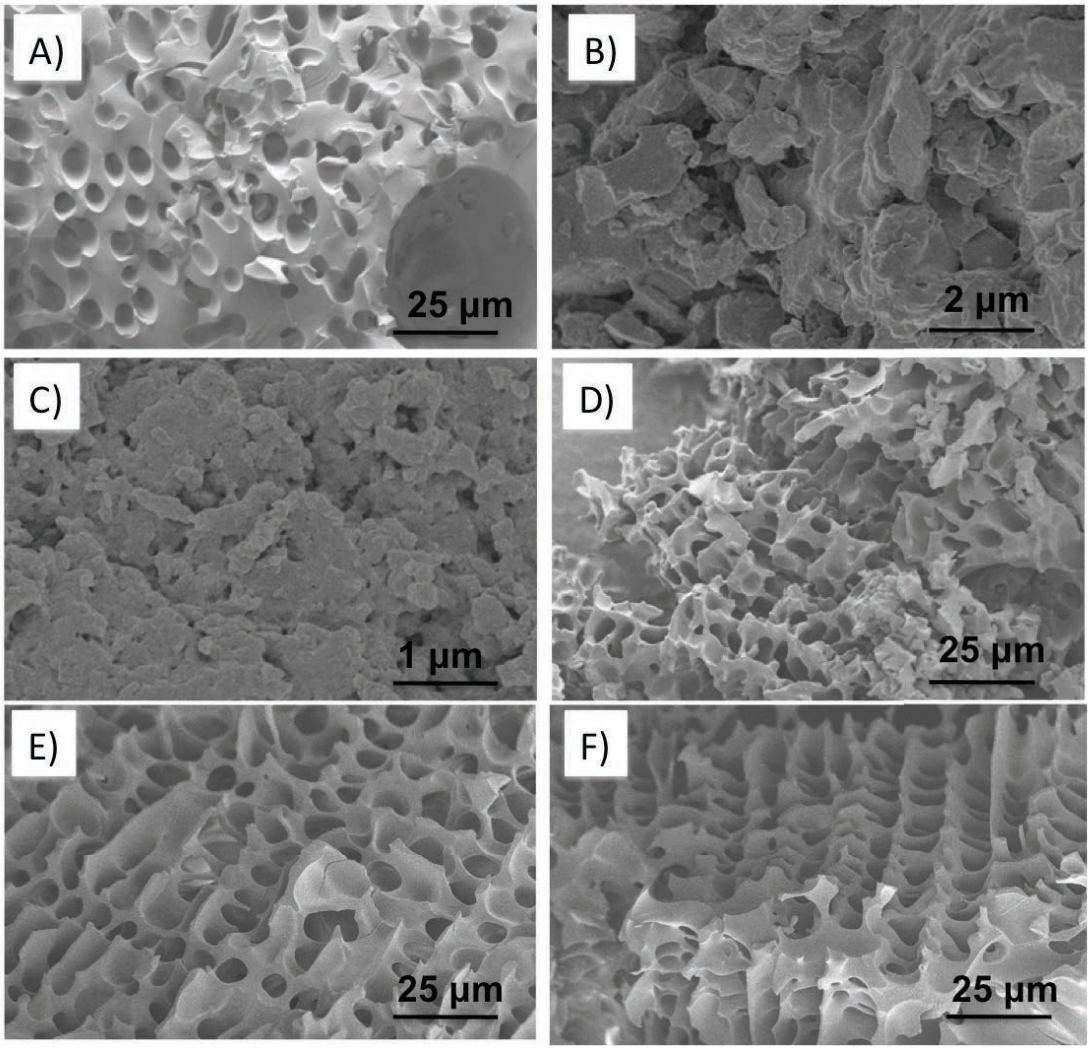

Figure 3.1 A) TEGDMA/camphene 1:1 (m/m) 1% DMPA initiator heated to 60°C until dissolved and randomly frozen in a freezer (-20 ^{0}C), polymerized on dry ice for 2 hours. B) Same procedure as in (A), but after freezing the cold sample was allowed to warm up and polymerized at room temperature. C) Same procedure as in (A) but the cold sample was warmed up and polymerized at 60 ^{0}C. D) Same monomer mixture was heated to 60 ^{0}C, directionally frozen in liquid nitrogen, polymerized on dry ice and placed in vacuum oven at room temperature to remove solvent. E) & F) 1:3 TEGDMA/camphene heated to 60 °C with 1% initiator, directionally frozen and polymerized on dry ice.

However, when the frozen solution was warmed up and polymerized at room temperature or 60 ^{0}C, the pore structure was destroyed (Figure 3.1B & C). This showed the importance of polymerizing at low temperature. When the monomer solution was directionally frozen in liquid nitrogen and polymerized on dry ice, an aligned porous structure was observed after removing camphene in vacuum at room temperature (Figure 3.1D). This structure was also observed when a 1:3 TEGDMA/camphene (m/m) solution was polymerized in the same manner (Figure 3.1E & F).

Another method used to verify that the concept was viable was observing directional freezing patterns of the solutions under an optical microscope (Figure 3.2).

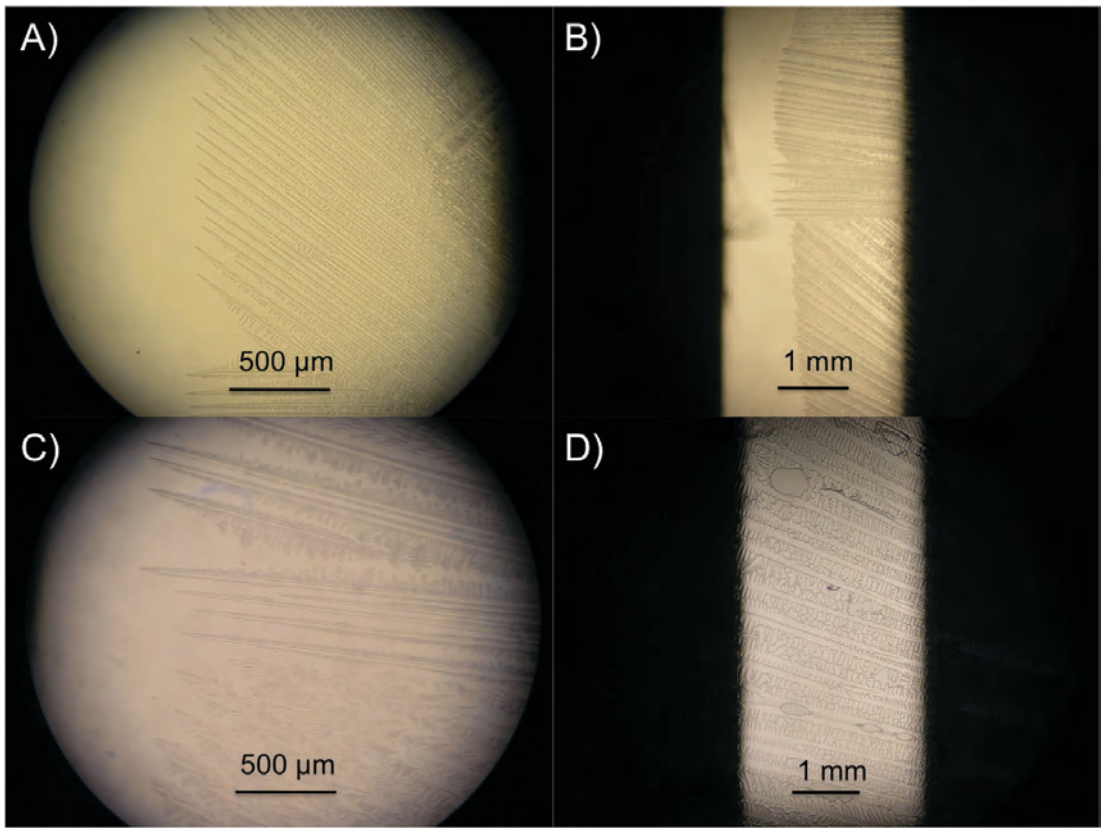

Figure 3.2 Optical microscope images showing freezing patterns of TEGDMA/dioxane solutions of different concentrations A) 1:2 TEGDMA/dioxane (v/v) B) & C) 1:5 TEGDMA/dioxane (v/v) D) 1:10 TEGDMA/dioxane (v/v).

This was achieved by preparing TEGDMA/dioxane solutions of varying concentrations with 1% DMPA initiator with respect to amount of monomer. One drop of the solution was placed on a glass slide, which was placed between two

temperature controlled plates. One plate was kept at room temperature whilst the other was cooled to -20 °C. Gradually the slide was moved towards the cold plate making it possible to observe the freezing stage under the microscope. The images in Figure 3.2 show that there is a clear phase separation between the monomers and solvent. TEGDMA/dioxane solutions of different concentration ratios (1:2, 1:5 and 1:10 (v/v)) were observed, showing phase separation for all solutions.

Using this evidence to suggest that a directional freezing and frozen UV polymerization method was possible, TEGDMA samples were then prepared using camphene, dioxane and cyclohexane as solvents and UV polymerized whilst keeping the samples frozen. The amount of initiator was maintained at 1% with respect to mass of monomers, as this amount appeared to work for samples prepared in Figure 3.1.

3.3.2 Aligned Porosity

Figure 3.3A shows the pore structure prepared from a 1:5 (v/v) TEGDMA/camphene solution. The aligned pore structure is observed across the whole sample. The orientated channels are highly interconnected (Figure 3.3B), which is a replica of orientated dendritic camphene crystals prepared previously using directional freezing.[23] Even though an aligned porous structure is observed, camphene contains a C=C bond, meaning it could be possible that camphene is copolymerized with the monomers during the polymerization. The use of other solvents was therefore investigated. Cyclohexane has a high melting point (~ 6 ^{0}C) with low toxicity, and was used to prepare porous structures and organic nanoparticles by freeze-drying in our group's previous study.[27] TEGDMA and the DMPA UV initiator could be readily dissolved in cyclohexane. Following the procedure described in Scheme 3.1 (frozen polymerization on dry ice), an aligned porous structure was produced with the aligned microchannels perpendicular to the substrate and across the whole sample (Figure 3.3C). Another organic solvent, dioxane, was also investigated. Dioxane is slightly more polar than cyclohexane and may dissolve a wider range of monomers. Aligned porous polyTEGDMA was produced with the same preparation procedure (Fig. 3.3D). Due to its relatively high melting point (~ 12 ^{0}C), the frozen dioxane solution could be polymerized on ice.

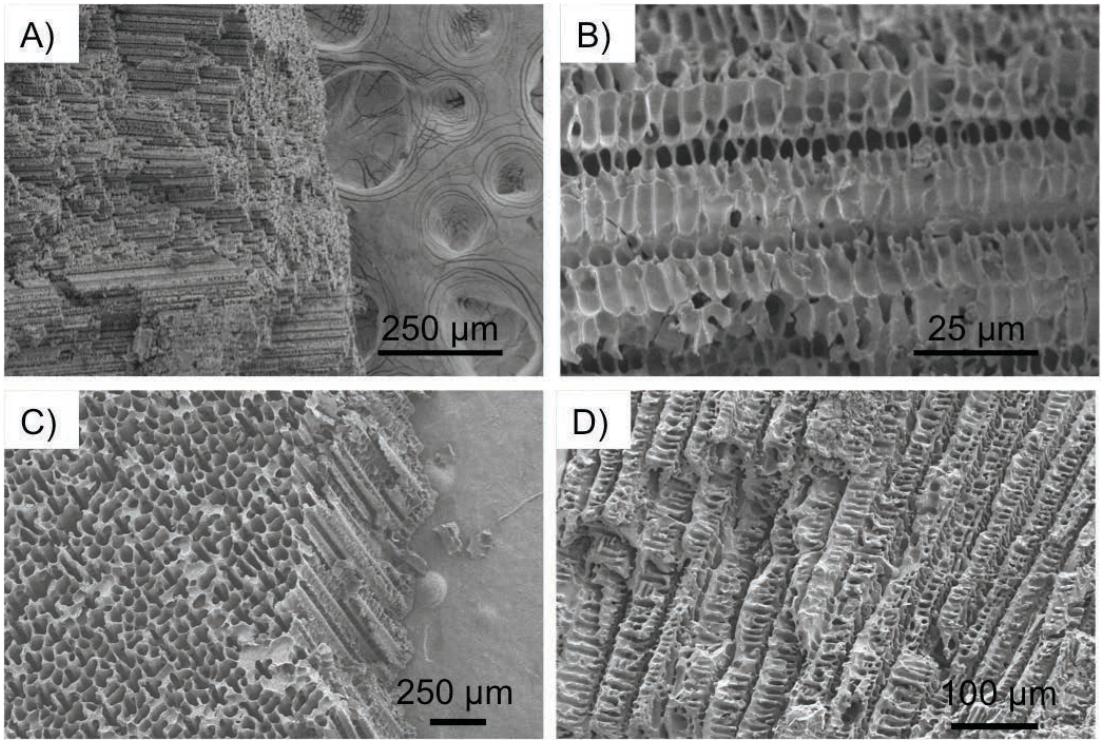

Figure 3.3 A & B) SEM images for materials made from solutions of 1:5 TEGDMA/camphene (m/m) at different magnification. C) 1:5 TEGDMA/cyclohexane (v/v) D) 1:5 TEGDMA/dioxane. (v/v).

These aligned porous materials exhibited high pore volumes and double macropore size distributions (Figure 3.4A) measured by mercury porosimetry. The double macropore peaks suggest that the materials contain smaller interconnected pores in the range of 1-10 µm in diameter. Although the materials have roughly the same overall porosity (5.54, 5.04 and 4.02 ml/g with respect to camphene, cyclohexane and dioxane) due to the concentration of the corresponding monomer solutions, they all have different pore size distributions. This is because the primary structure of the materials depends upon the shape and size of the solvent crystals formed upon freezing.

An advantage of the directional freezing and frozen UV polymerizations method is the facile tuning of pore volume or porosity of the materials simply by varying the monomer concentration. TEGDMA/dioxane solutions with the volume ratio of 1:10 and 1:20 were also processed with the procedure described in Scheme 1. In both cases, aligned porous polyTEGDMA structures were successfully produced. The pore volumes increased from 4.02 ml/g (1:5 dioxane) to 9.06 ml/g (1:10 dioxane) and 10.61 ml/g (1:20 dioxane), as characterized by Hg intrusion porosimetry. The

macropore size distribution is shown in Figure 3.4B. The incremental intrusion in the range of pore size range of 1 – 10 μm increases significantly, suggesting that the pore interconnectivity increases considerably.

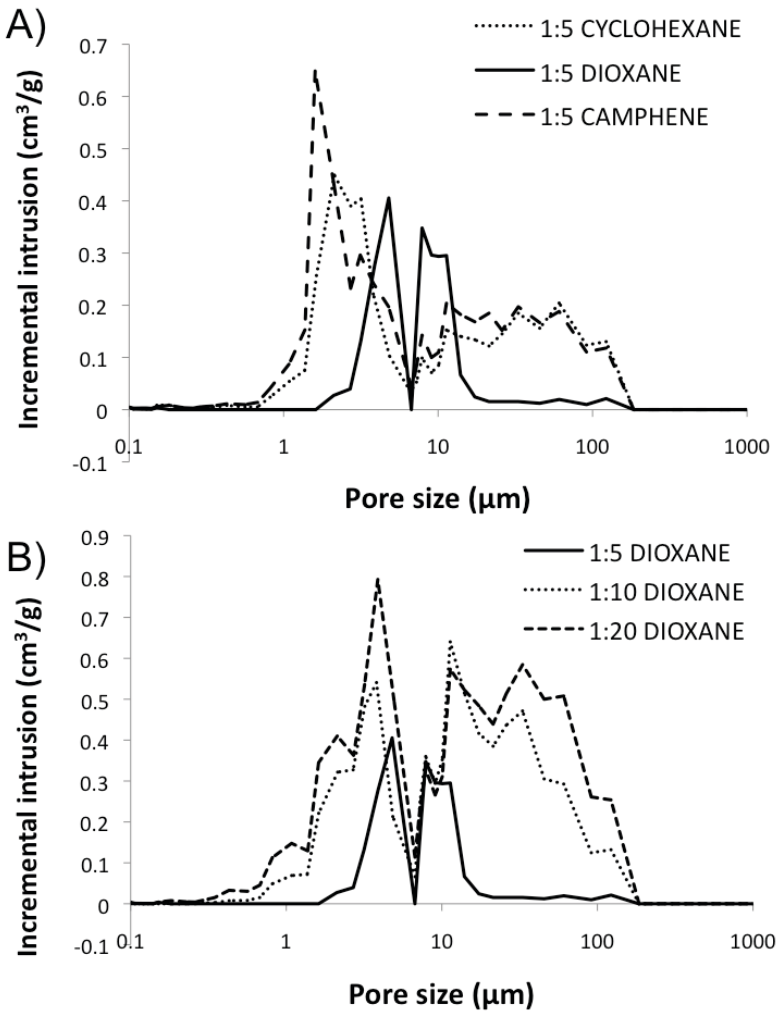

Figure 3.4 A) Macropore size distributions measured by Hg intrusion porosimetry for samples prepared from camphene cyclohexane and dioxane systems shown in Figure 3.3. Pore volumes are 5.54, 5.04 and 4.02 ml/g B) Pore size distribution of PTEGDMA prepared from 1:5, 1:10, and 1:20 dioxane solutions. The pore intrusion volumes are 4.02, 9.06, 10.61 ml/g, respectively.

When the porosity is increased it is important to show that the aligned porous nature of the material is retained. Figure 3.5 shows that as the porosity is increased from 1:5 to 1:20 (v/v) in dioxane sample the aligned porous morphology is retained throughout the whole material.

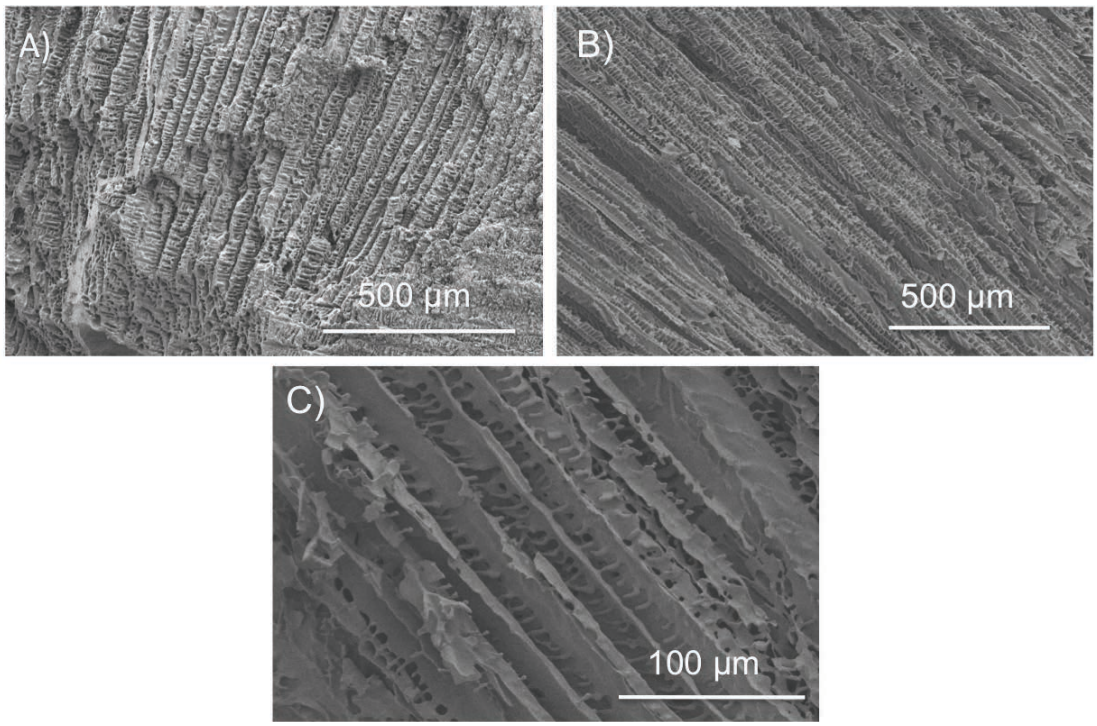

Figure 3.5 SEM images of aligned porosity in materials prepared from solutions of A) 1:5 TEGDMA/dioxane (v/v) B) 1:10 TEGDMA/dioxane (v/v) C) 1:20 TEGDMA/dioxane (v/v).

3.3.3 Mechanical Stability

The main target of this study is to produce crosslinked aligned structures with enhanced mechanical stability. This study was then focused on the porous structures made from dioxane solutions, because it is thought that polymerizations on ice can produce material with more mechanical stability. TEGDMA is a bifunctional crosslinker that contains two C=C double bonds and after frozen polymerization, polyTEGDMA is a highly crosslinked material and becomes insoluble in any common solvents. Compression tests were performed on cylindrical polyTEGDMA monoliths and the results are shown in Figure 3.6.

The initial linear part of the stress-strain curve is used to calculate the Young modulus. The Young's modulus increases considerably with the decrease of porosity: 290 kPa for the structure made from 1:20 dioxane solutions, and 750 kPa and 9 MPa for the structures made from 1:10 and 1:5 dioxane solutions. Typically, for porous poly(vinyl alcohol) scaffolds prepared by freeze drying, the compression moduli are in the range of 0.003 – 0.0175 MPa.[28] Therefore, the mechanical stability has been improved significantly for the porous structures made by frozen polymerization. The aligned porous crosslinked polyTEGDMA structures are flexible.

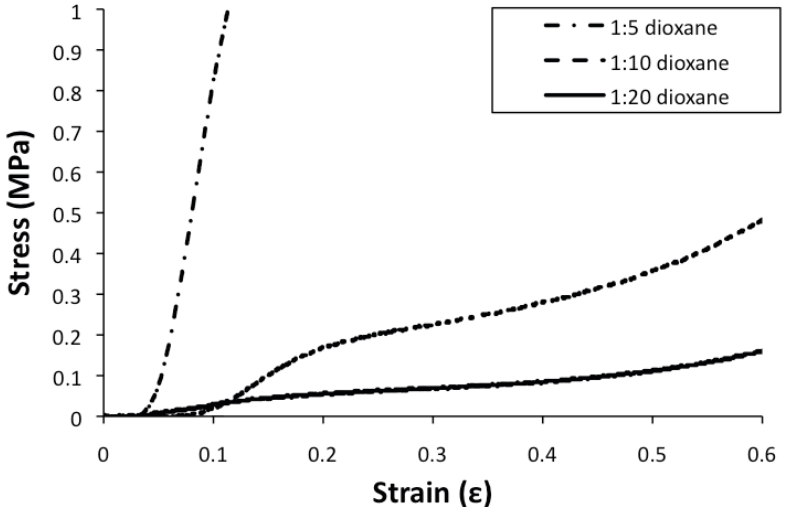

Figure 3.6 Stress/strain curves for samples prepared from 1:5 1:10 and 1:20 TEGDMA/dioxane solutions (v/v).

The materials appeared to cope with the increase of strain and compression failure was not observed, unlike porous ceramics or bioglass scaffolds.[29] From the full compression test plots (Table 3.3 & Figure 3.12), the maximum stresses observed were 1.5 MPa, 3.5 MPa, and 25 MPa at large strain values for the porous polyTEGDMA prepared from 1:20, 1:10 and 1:5 dioxane solutions, respectively. Figure 3.7 shows stress/strain curves for polyTEGDMA samples prepared using different solvents of similar concentration.

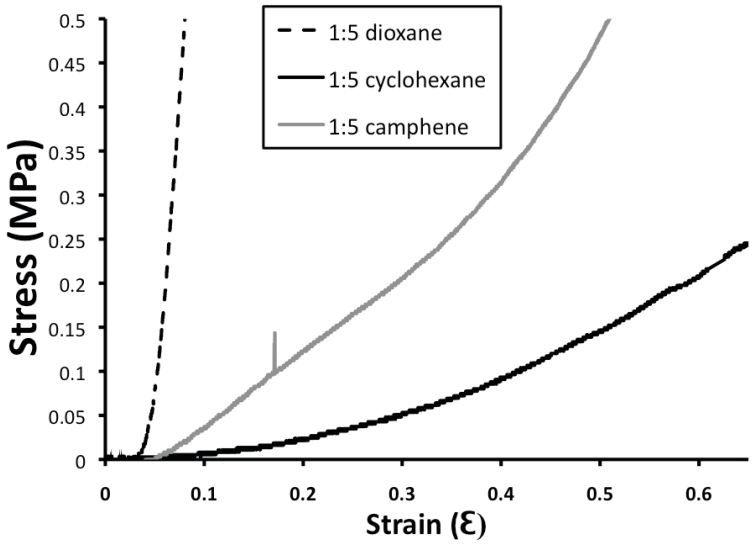

Figure 3.7 Stress/strain curves for samples of similar concentration using different solvents.

The 1:5 dioxane (v/v) sample had a Young's Modulus of 9 MPa compared to 540 kPa and 230 kPa for 1:5 camphene (m/m) and cyclohexane (v/v). The big difference

in compression strength between the dioxane sample and the others could be due to the fact dioxane samples can be polymerized on ice, resulting in a higher degree of polymerization.

3.3.4 Conductive Samples

Porous polyTEGDMA made from dioxane solutions was further modified to generate conductivity. This was achieved by depositing a layer of conducting polymer poly(3,4-ethylenedioxythiophene)-poly(styrenesulfonate) (PEDOT-PSS) or graphene sheets by a soaking method. SEM images for these composites are shown in Figure 3.8 and macropore size distributions in Figure 3.9.

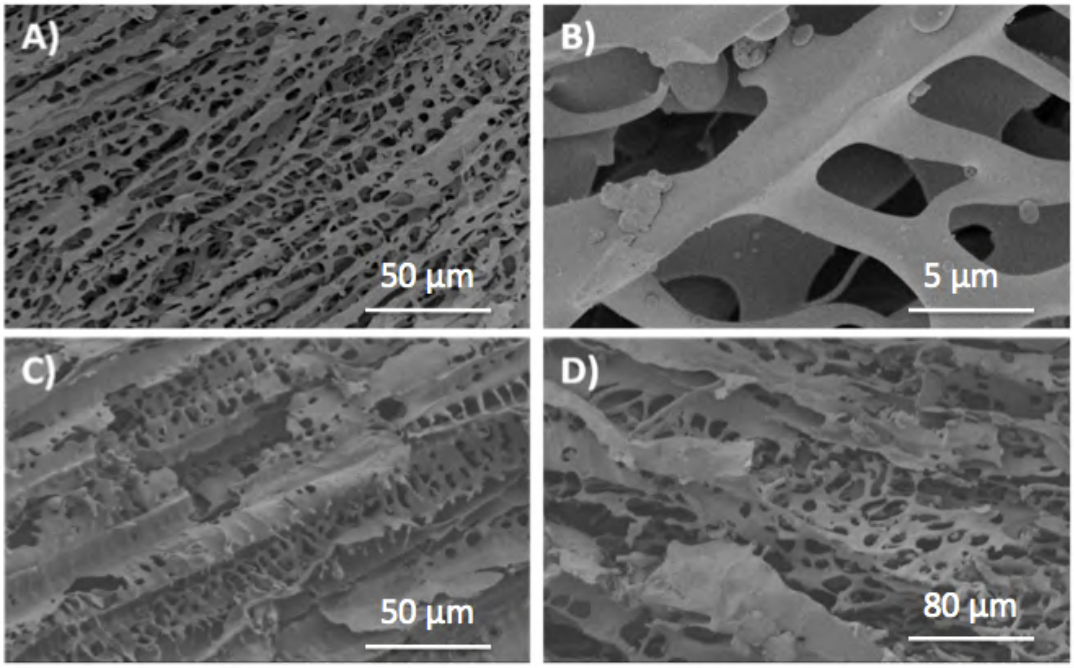

Figure 3.8 A & B) SEM images at different magnifications for aligned porous PTEGDMA made from 1:20 with dioxane. C) Aligned porous PTEGDMA loaded with graphene. D) Aligned porous structure loaded with PEDOT-PSS.

PolyTEGDMA prepared from a 1:20 dioxane (v/v) solution was used due to its highly interconnected porosity (Figure 3.8A &B). The resulting polyTEGDMA was soaked in 10 ml of a 0.4 wt% graphene oxide suspension and then dried. The dry sample was then reduced with hydrazine following a method used previously.[18] A mass increase of 4.84% compared to polyTEGDMA was achieved, and overall porosity decreased from 10.61 ml/g to 7.30 ml/g (Figure 3.9). polyTEGDMA was soaked in 1 wt% aqueous PEDOT-PSS solution and a mass increase of 4.62 % was

recorded. As a result of the loading, the pore volume decreased from 10.61 ml/g to 8.12 ml/g and pore size decreased accordingly (Figure 3.9). Even though some pores are covered up in both composites, an aligned porous structure is still observed throughout (Figure 3.8C & D). This could be crucial for potential applications. The mass changes for the samples are recorded in Table 3.1.

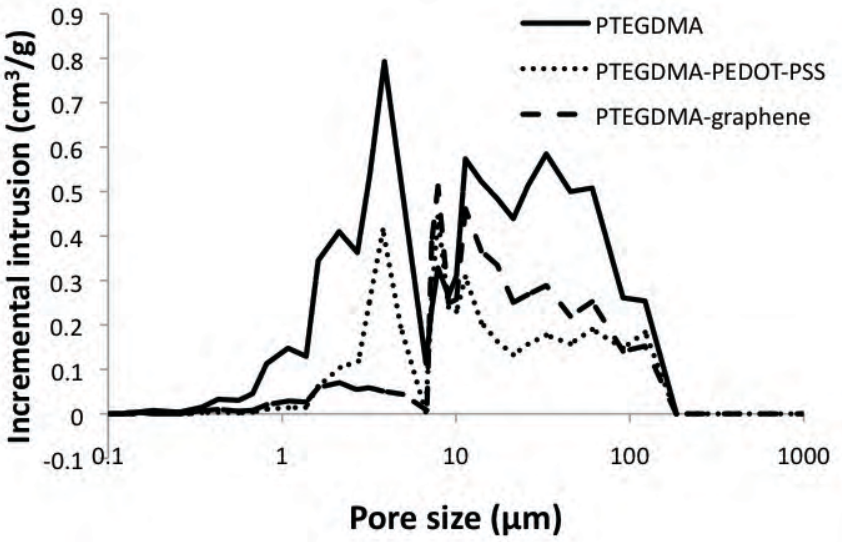

Figure 3.9 Macropore size distributions of polyTEGDMA and its composites as measured by Hg intrusion porosimetry. The intrusion pore volumes are 10.61, 8.12 and 7.30 ml/g for porous polyTEGDMA, polyTEGDMA-PEDOT-PSS and polyTEGDMA-graphene, respectively.

Table 3.1 Mass and surface area after loading 1:20 sample with graphene and PEDOT-PSS

Sample	Concentration of soaking solution	Mass of PTEGDMA	Mass increase after	% Mass increase	Porosity (ml/g)	Surface area (m^2/g)
PTEGDMA	n/a	n/a	n/a	n/a	10.61	11.96
PTEGDMA-PEDOT-	1 % (10 mg/ml)	0.0476 g	0.0022 g	4.62%	8.12	29.37
PTEGDMA-Graphene	0.4 % (4mg/ml)	0.0372 g	0.0018 g	4.84%	7.30	24.47

The overall porosity is decreased upon loading but interestingly, surface area of the monoliths is increased slightly upon loading. The atomic-thick graphene oxide sheets were prepared before treatment of polyTEGDMA using a modified Hummer's method and showed an area dimension in the size of micrometres, as observed by transmission electron microscopy (Figure 3.10). The results of front panel resistance measurements are shown in Table 3.2. When the polyTEGDMA was tested for conductivity before the soaking procedure, no conductivity value was recorded. This is because the highly crosslinked polymer is an electrical insulator and its resistance value was out of the measurement range of the sourcemeter. For the PEDOT-PSS covered monolith the conductivity measured by a two-probe method was 5.2 x 10^{-6} S/cm. This was consistent with the conductivity measured for PEDOT-PSS monolith by other researchers,[30] suggesting that a complete layer of PEDOT-PSS was covering the pore surface of PTEGDMA. For the graphene loaded sample, the conductivity was measured to be 1.91 x 10^{-4} S/cm, which was consistent with the PS/graphene composite reported before.[31]

Table 3.2 Results of front panel resistance measurements.

Sample	Length and diameter	Resistance	Resistivity	Conductivity
1:20 PTEGDMA PEDOT-PSS	L - 1 cm D - 0.7 cm	500 kΩ	192000 Ωcm	5.2 x 10^{-6} S/cm
1:20 PTEGDMA Graphene	L – 1 cm D – 0.7 cm	3.43 kΩ	1320 Ωcm	1.91 x 10^{-4} S/cm

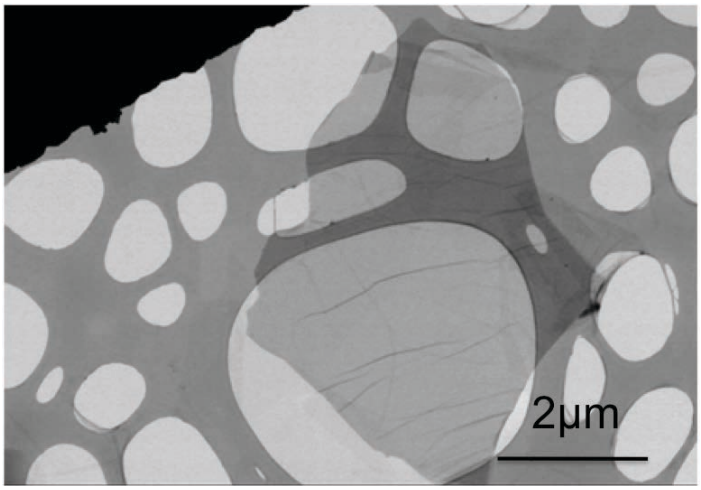

Figure 3.10 Transmission electron microscope image of single graphene oxide sheet.

Before soaking, the polyTEGDMA monolith was white and the pore surface was smooth (Figure 3.11A). The composite monoliths turned a dark blue after loading with PEDOT-PSS and brown after loading with graphene oxide. Upon reduction the graphene composite turned black. In the case of PEDOT-PSS, the surface became rough but a layer of PEDOT-PSS could not be observed (Figure 3.11B). This was understandable because the PEDOT-PSS molecules were deposited on the pore surface during the soaking and drying procedure. Layers of graphene were observed on the pore surface (Figure 3.11C) in the dry composite material after reduction of the graphene oxide sheets.

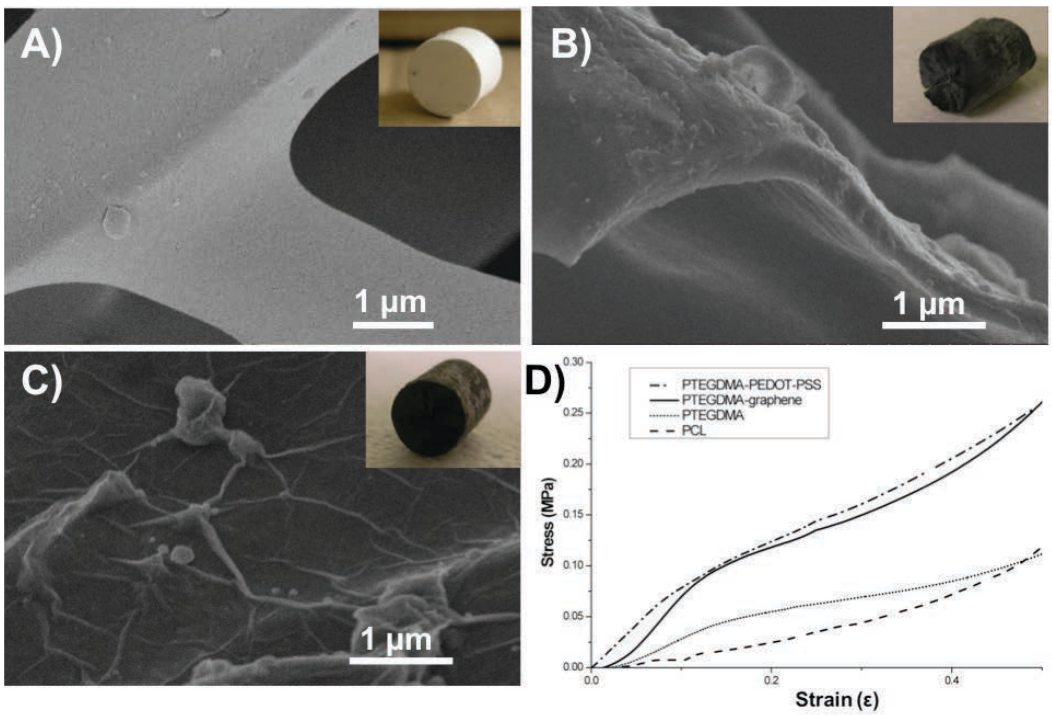

Figure 3.11 A) SEM image showing the pore surface of polyTEGDMA made from 1:20 dioxane solution. B) The PTEGDMA was uploaded with PEDOT-PSS. C) PolyTEGDMA was uploaded with graphene. The insets in A-C show the photos of the relevant monoliths. Scale bar: 7 mm. D) Plot of the mechanical stability test for the three samples and the control PCL sample.

Compression tests were conducted on these materials. As a reference sample, aligned porous polycaprolactone (PCL) was prepared by directional freezing and freeze drying of a 1:20 PCL/dioxane (v/v) solution. PCL is a biodegradable polymer used in tissue engineering that has previously been used to prepare aligned porous structures by freeze drying.[5] The stress-strain plots are shown in Figure 3.11D. The Young's moduli calculated from the initial linear part of the curves are 95 kPa, 290 kPa, 700 kPa, and 850 kPa for aligned porous PCL, polyTEGDMA, PTEGDMA-graphene,

and PTEGDMA-PEDOT-PSS, respectively. (Full elastic curves and young's moduli values for all samples are shown below in Figure 3.12 and Table 3.3)

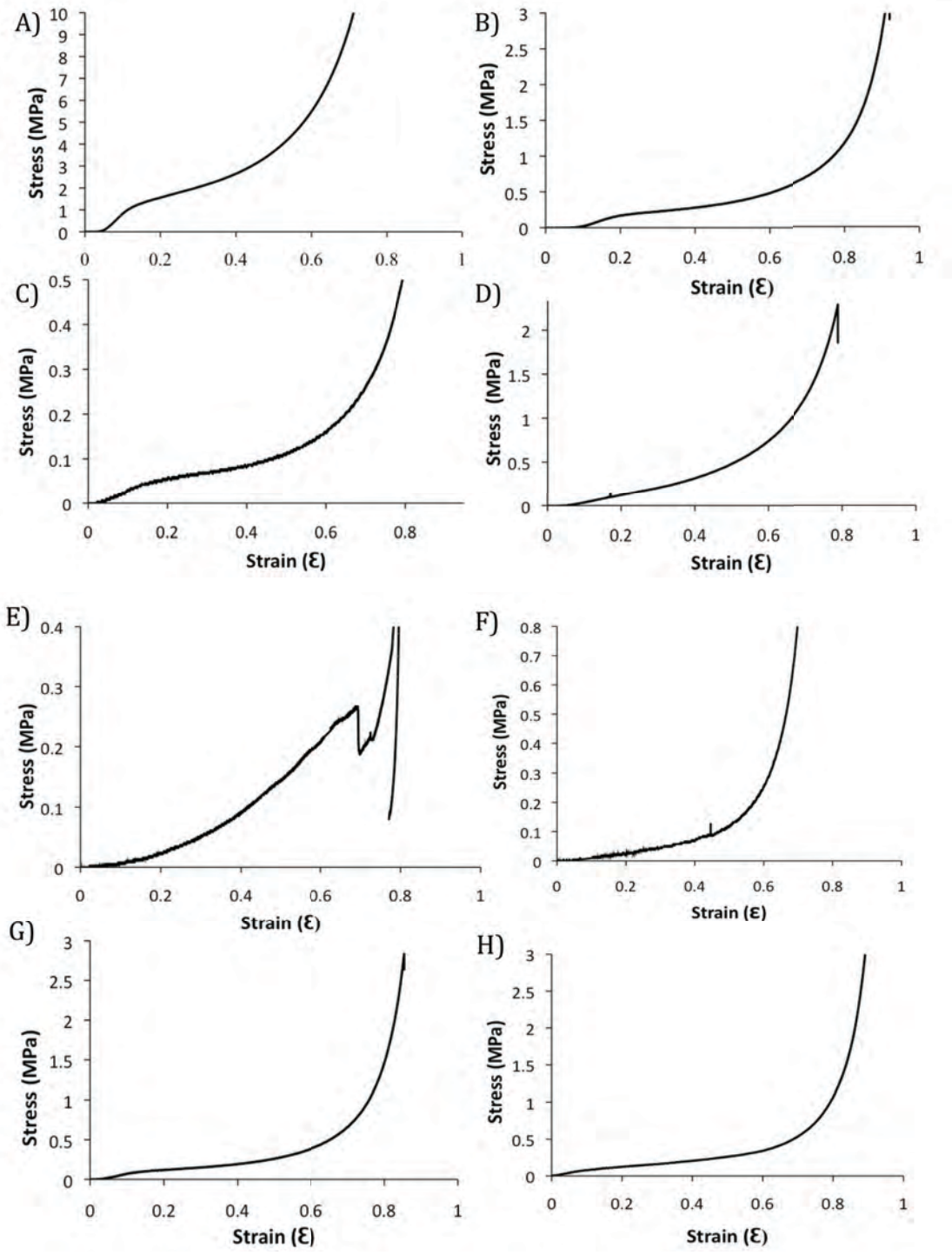

Figure 3.12 Full elastic stress/strain curves for all materials tested A) 1:5 TEGDMA/dioxane (v/v) B) 1:10 TEGDMA/dioxane (v/v) C) 1:20 TEGDMA/dioxane D) 1:5 TEGDMA/camphene (m/m) E) 1:5 TEGDMA/cyclohexane (v/v) F) 1:20 PCL (v/v) G) 1:20 TEGDMA/dioxane (graphene) H) 1:20 TEGDMA/dioxane (PEDOT-PSS).

Table 3.3 Table of Young's Modulus values recorded for all samples

Sample	Young's Modulus
1:5 TEGDMA/cyclohexane	230 kPa
1:5 TEGDMA/camphene	540 kPa
1:5 TEGDMA/dioxane	9 MPa
1:10 TEGDMA/dioxane	750 kPa
1:20 TEGDMA/dioxane	290 kPa
1:20 TEGDMA/dioxane (PEDOT-PSS)	700 kPa
1:20 TEGDMA/dioxane (graphene)	850 kPa
1:20 PCL/dioxane	95 kPa

In addition to the conductivity, the mechanical stability is also improved after modifying polyTEGDMA with graphene and PEDOT-PSS because of the increase in sample density. Comparing Young's Modulus of 1:20 polyTEGDMA with 1:20 PCL also shows that material prepared from the frozen polymerization is about three times stronger in terms of elastic stiffness. The Young's modulus values for all samples prepared are listed in Table 3.3 and full elastic curves are shown in Figure 3.12.

3.3.5 Frozen Polymerization

Free radical polymerization requires sufficient monomers and mobility to facilitate the reactions. When the polymerization is carried out in the solid state, extremely poor reaction kinetics and low double bond conversion is usually expected. A cyclic acetal-functionalized urethane acrylate monomer was polymerized in a crystalline solid state without the polymerization kinetics being deleteriously affected. It was argued that templating of the acrylic double bonds in the crystalline state facilitated rapid, minimally activated propagation.[32] However, such templating effect was not available for the TEGDMA system. Oxygen is known as the scavenger for free radicals and its solubility in a monomer solution decreases with temperature.[33] However, in the frozen state, the solubility of oxygen is reduced to a minimum which could be beneficial for a free radical polymerization. In our study, the fact that the frozen crosslinking polymerization was successfully performed was highly likely due

to the low solubility of oxygen and a highly concentrated semi-frozen state in the monomers-rich region.[16]

Other types of methacrylate monomers were also used to demonstrate the versatility of this method. Monomer hydroxyethyl methacrylate (HEMA) and crosslinker ethylene glycol dimethacrylate (EGDMA) (9:1 (v/v)) were mixed with camphene (1:5 and 1:10 in mass) and heated to 60 ^{0}C. As before 1% initiator was added with respect to amount of monomer. After frozen UV initiated polymerization and removal of camphene, uniformly aligned porous structures were produced (Figure 3.13). In all cases, aligned porous structures were produced with a higher crosslinker amount likely producing a more robust aligned structure.

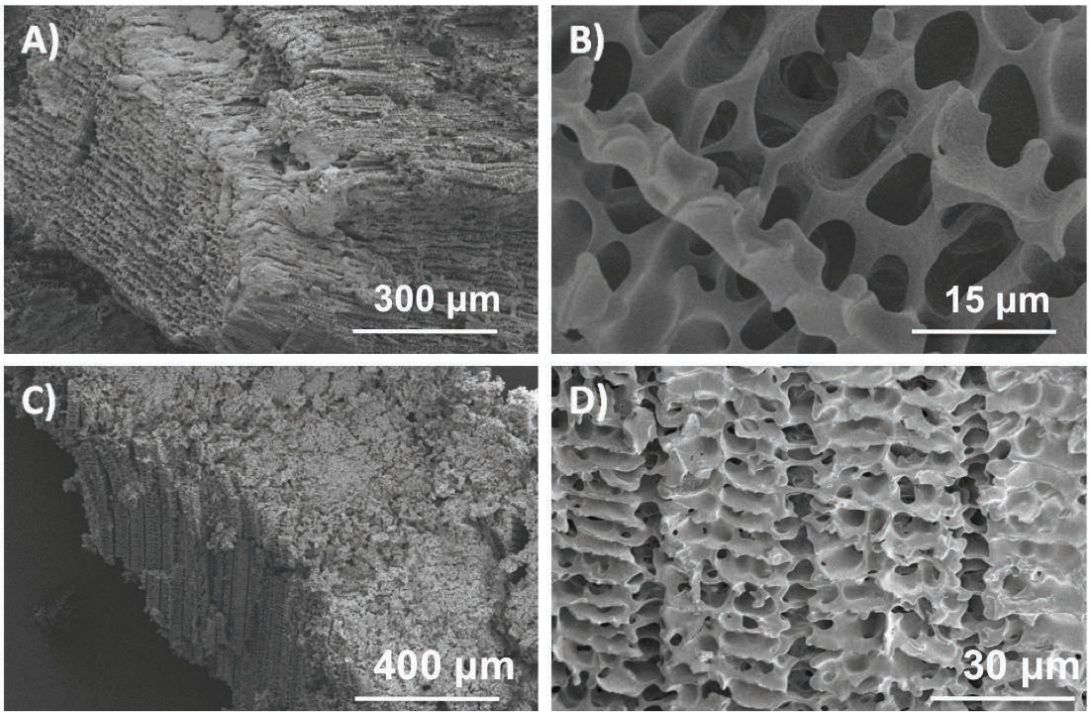

Figure 3.13 A&B) 1:5 (m/m) of (HEMA/EGDMA (9:1 v/v)) to camphene heated to 60°C with 1 wt% DMPA added and 1ml of sample was frozen in liquid nitrogen and polymerized on dry ice. C&D) 1:10 (m/m) (HEMA/EGDMA 9:1 mix)/camphene, other conditions are same.

To evaluate the frozen polymerization, reactions were monitored by FTIR with time on the reduction and disappearance of the C=C peak at ca. 1637 cm^{-1}. Due to the weak signal from the polyTEGDMA system, a 1:1 EGDMA/dioxane solution was polymerized and characterized at different reaction time. It was observed that with frozen polymerization time 20, 40, 60 minutes, the absorbance intensity of C=C

bonds decreased continuously (Figure 3.14A). In the 1:10 (HEMA+EGDMA 9:1 (v/v)) mixture/camphene system, after frozen polymerization on dry ice for 2 hours, the absorbance from double bonds disappeared, suggesting a moderate conversion of double bonds (Figure 3.14B). All the frozen polymerizations were performed for 2 hours or longer to ensure conversion of monomers.

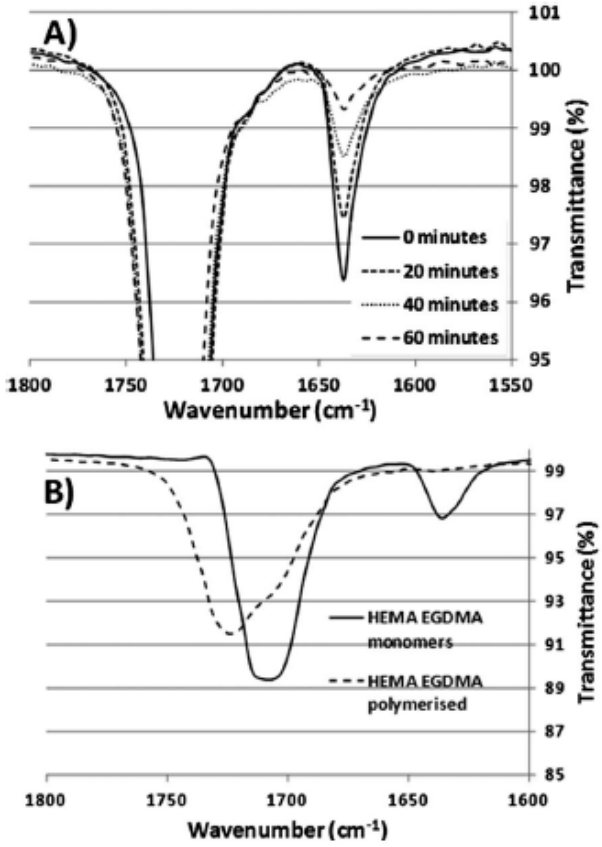

Figure 3.14 A) 1:1 EGDMA/dioxane (v/v) solution was directionally frozen and polymerized on dry ice under UV light (365 nm) with different time, monitored by FTIR. B) 1:10 (HEMA EGDMA 9:1 mix)/camphene heated to 60°C and 1ml of sample was frozen in liquid nitrogen and polymerized on dry ice for 2 hours.

Another concern was whether camphene was copolymerized with the monomers. While aligned porous structures were produced when polymerizing on dry ice (Figure 3.1A), camphene participated in the polymerization at room temperature with the pore structure destroyed (Figure 3.1B & C). This was also observed when polymerizing camphene solutions on ice. A controlled experiment was carried out, polymerizing a mixture of DMPA and camphene on dry ice.

The resulting material was placed in vacuum at room temperature and all the material was removed, suggesting that camphene did not polymerize at dry ice temperature (-78 °C). When the same experiment was carried out on ice, at RT and at 60 °C solid material was obtained. This suggests that the DMPA initiator could polymerize camphene at these temperatures under UV.

Therefore for future studies, materials will be produced with dioxane as the dioxane solutions can be polymerized on both ice and dry ice, and when the solvent is removed or under vacuum or by washing it is almost certain that only crosslinked methacrylate polymer will remain.

A controlled study was undertaken to understand more about the frozen UV polymerization technique. Two 2 ml 1:5 TEGDMA/dioxane (v/v) solutions were directionally frozen and UV polymerized on dry ice, however one was covered in black masking tape. This study was used to show that it is in fact the UV irradiation that initiates the polymerization of TEGDMA and not a thermal initiation upon warming the samples in a vacuum oven. Figure 3.15A shows the frozen samples on a bed of dry ice before polymerization. After two hours under the UV lamp the samples were placed in a vacuum oven to remove the solvent. Upon removing the black tape from the covered sample (Figure 3.15B & C) it was revealed a small amount of liquid at the bottom tube suggesting that no or very little polymerization had taken place.

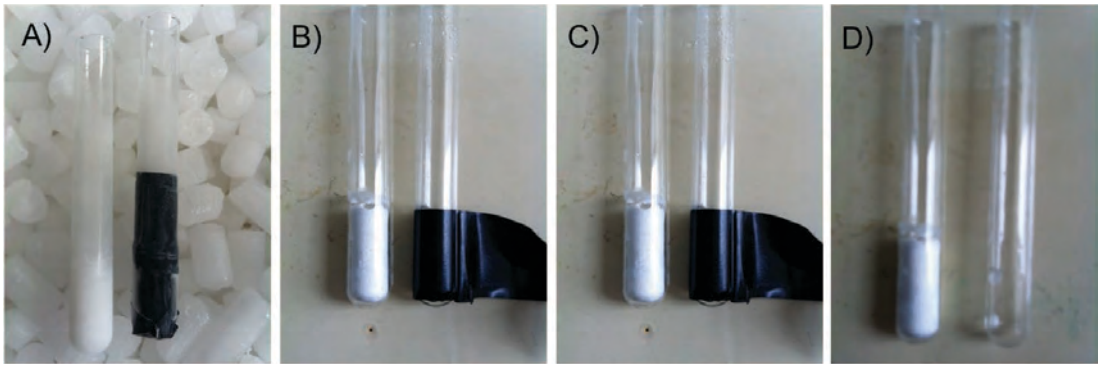

Figure 3.15 1:5 TEGDMA/dioxane (v/v) solutions directionally frozen, A) frozen samples before polymerization (left) uncovered (right) covered with black tape. B) C) Samples after polymerization and solvent removal. D) (left) dry porous material (right) black tape is removed to reveal a small amount of liquid in the bottom of the tube. Sample diameter - 7mm.

To further this study two more samples of 2 ml 1:5 TEGDMA/dioxane (v/v) solutions were polymerized in the same manner. After polymerization, one was placed in the vacuum oven as before, the other was washed in methanol cooled in dry ice (-78 °C) for 12 hours then taken out and dried in a vacuum oven overnight. This was to confirm that even though UV radiation initiates the polymerization, most of the polymerization was completed in the frozen state and not upon warming in the vacuum oven. Any soluble monomers, oligomers should be removed upon solvent exchange with methanol at (-78 °C). After both samples were taken out of the vacuum oven the masses of the dry materials were recorded (Table 3.4). The difference in mass between the two samples is very small (10 mg which equates to about 4%), suggesting that most of the polymerization takes place when the samples are frozen.

Table 3.4 Recorded mass after different methods of solvent removal.

Sample	Mass after drying
1:5 TEGDMA/dioxane (v/v) vacuum dried	0.3103 g
1:5 TEGDMA/dioxane (v/v) washed in dry ice in methanol then dried	0.2968 g

3.3.6 Aligned Porous Monoliths for HPLC

Porous monoliths (including polymer and silica) have been widely used as columns for HPLC, with the advantage of fast analysis and low back pressure.[34] So far, interconnected cellular porous monoliths have been used.[34,35] To the best of our knowledge, there are no reports for the use of aligned porous monoliths as HPLC columns.[34,35] In chromatography, peak height and peak broadening are governed by kinetic processes in the column. According to the van Deemter equation, the three processes (eddy diffusion, longitudinal diffusion and resistance against mass transfer) can contribute to peak broadening.[34,35] Eddy diffusion is the most important factor, where analyte molecules follow different flow paths, which causes dispersion. Some molecules travel more slowly and thus lag behind the peak. In principle, the

aligned pores may provide through flow paths to keep the back-pressure low and reduce the eddy diffusion. In this study, an aligned porous monolith was explored as a stationary phase column for HPLC separation. Aligned porous polyTEGDMA was prepared in a glass column (88 mm L x 3.5 mm O.D. x 2.0 mm I.D.) (Figure 3.16) and was directly connected to the HPLC instrument and assessed with the standard test mixture.

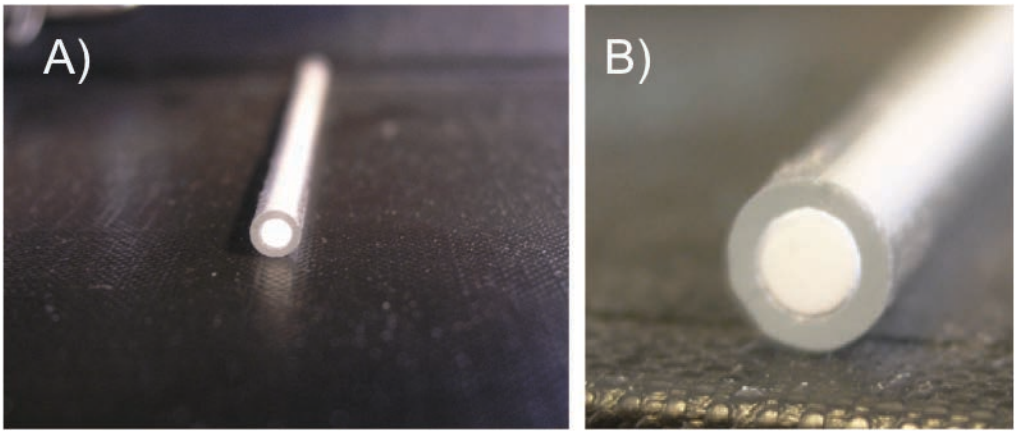

Figure 3.16 Align porous PTEGDMA in a glass column (88 mm L x 3.5 mm O.D. x 2.0 mm I.D.) optical images of A) whole column B) image diameter of column.

Four well-resolved peaks are observed with the shoulder of the second peak indicating phenol. The overlapping of phenol and caffeine peaks could be due to the absence of residual hydroxyl groups on the polymer column.[36] This reduces the exchange kinetics of the solutes between different interaction sites (*i.e.,* hydrophobic and hydroxyl groups) and the surface acidity, which has been a complex problem for silica columns.[36,37]

As observed from Figure 3.17, the polyTEGDMA monolith shows excellent hydrophobic properties and the hydrocarbon molecules are efficiently separated at low back-pressure of 59 bar. Although certain peak broadening was observed, this test demonstrated the potential use of aligned porous polymer monolith for a faster mass transfer kinetic with low back pressure, which is particularly important for the separation of large biomacromolecules and natural products.

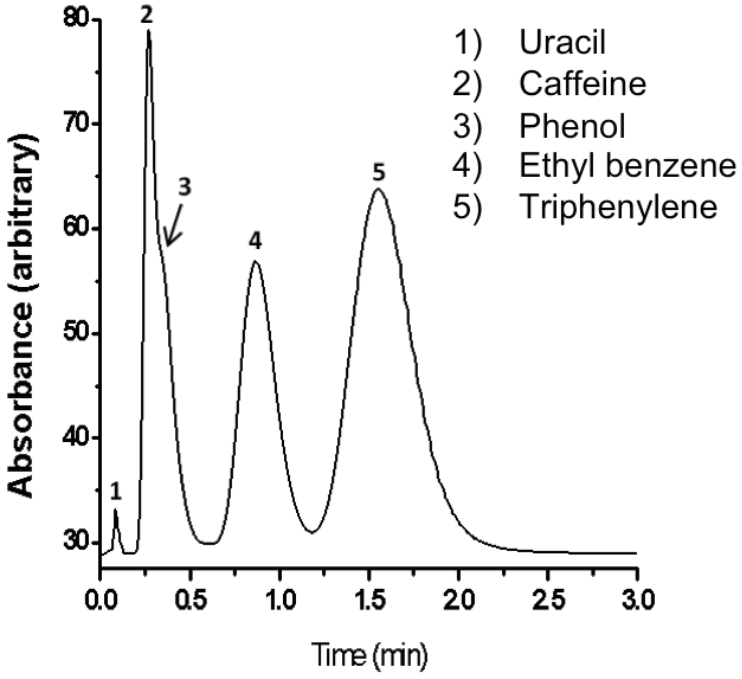

Figure 3.17 Chromatogram of the text mixture containing uracil, caffeine, phenol, ethylbenzene, phyenylene with the PTEGDMA column. Mobile phase: 50/50 v/v acetonitrile/water; flow rate: 1 ml/min; injection volume: 7 µ; back pressure: 59 bar; UV detection: 254 nm.

3.4 Conclusions

A new directional freezing and frozen polymerization method was developed to produce aligned porous materials. Using this method, dimethacrylate monomer solutions were used to fabricate crosslinked aligned porous structures with significantly improved mechanical stability. As a result of frozen polymerization, the frozen sample could be warmed up to remove the solvent under vacuum at room temperature, avoiding the use of freeze-drying procedure but maintaining the aligned structures. The aligned porous polymer could be further treated with graphene and PEDOT-PSS to produce conductive porous structures. The aligned porous polymer monolith was also assessed for HPLC, demonstrating the separation of the test mixture with well-resolved peaks. This highlights the potential of this material as a stationary phase in reverse phase chromatography. It is possible to produce a range of functional aligned porous materials for applications in chromatography or porous electrodes. The method was expanded to produce aligned porous structures using different methacrylates such as polyHEMA. In the following chapters, we attempt to

extend this method to polymerize various methacrylates in the frozen state to produce aligned porous materials with different functionality and surface properties.

3.5 References

(1) Hahn, M. S.; Miller, J. S.; West, J. L. *Adv. Mater.* **2006**, *18*, 2679.

(2) Choi, S.-W.; Xie, J.; Xia, Y. *Adv. Mater.* **2009**, *21*, 2997.

(3) Kresge, C. T.; Leonowicz, M. E.; Roth, W. J.; Vartuli, J. C.; Beck, J. S. *Nature* **1992**, *359*, 710.

(4) Stein, A.; Li, F.; Denny, N. R. *Chem. Mater.* **2007**, *20*, 649.

(5) Zhang, H.; Hussain, I.; Brust, M.; Butler, M. F.; Rannard, S. P.; Cooper, A. I. *Nat Mater* **2005**, *4*, 787.

(6) Yao, L.; de Ruiter, G. C. W.; Wang, H.; Knight, A. M.; Spinner, R. J.; Yaszemski, M. J.; Windebank, A. J.; Pandit, A. *Biomaterials* **2010**, *31*, 5789.

(7) Katuri, K.; Ferrer, M. L.; Gutiérrez, M. C.; Jiménez, R.; del Monte, F.; Leech, D. *Energy Environ. Sci.* **2011**, *4*, 4201.

(8) Qin, D.; Xia, Y.; Whitesides, G. M. *Nat. Prot.* **2010**, *5*, 491.

(9) Gutiérrez, M. C.; Ferrer, M. L.; del Monte, F. *Chem. Mater.* **2008**, *20*, 634.

(10) Qian, L.; Zhang, H. *J. Chem. Tech. & Biotechnol.* **2011**, *86*, 172.

(11) Zhang, H.; Long, J.; Cooper, A. I. *J. Am. Chem. Soc.* **2005**, *127*, 13482.

(12) Zhang, H.; Cooper, A. I. *Adv. Mater.* **2007**, *19*, 1529.

(13) Deville, S. *Adv. Eng. Mater.* **2008**, *10*, 155.

(14) Deville, S.; Saiz, E.; Nalla, R. K.; Tomsia, A. P. *Science* **2006**, *311*, 515.

(15) Munch, E.; Launey, M. E.; Alsem, D. H.; Saiz, E.; Tomsia, A. P.; Ritchie, R. O. *Science* **2008**, *322*, 1516.

(16) Plieva, F. M.; Galaev, I. Y.; Mattiasson, B. *J. Sep. Sci.* **2007**, *30*, 1657.

(17) Marcano, D. C.; Kosynkin, D. V.; Berlin, J. M.; Sinitskii, A.; Sun, Z.; Slesarev, A.; Alemany, L. B.; Lu, W.; Tour, J. M. *ACS Nano* **2010**, *4*, 4806.

(18) Stankovich, S.; Dikin, D. A.; Piner, R. D.; Kohlhaas, K. A.; Kleinhammes, A.; Jia, Y.; Wu, Y.; Nguyen, S. T.; Ruoff, R. S. *Carbon* **2007**, *45*, 1558.

(19) Gu, B.; Li, Y.; Lee, M. L. *Anal. Chem.* **2007**, *79*, 5848.

(20) Decker, C. *Macromol. Rapid Commun.* **2002**, *23*, 1067.

(21) Wozniak, M.; de Hazan, Y.; Graule, T.; Kata, D. *J. Eur. Ceram. Soc.* **2011**, *31*, 2221.

(22) Cramer, N. B.; Stansbury, J. W.; Bowman, C. N. *J. Dent. Res.* **2010**, *90*, 402.

(23) Han, J.; Hong, C.; Zhang, X.; Du, J.; Zhang, W. *J. Eur. Ceram. Soc.* **2010**, *30*, 53.

(24) Yoon, B.-H.; Lee, E.-J.; Kim, H.-E.; Koh, Y.-H. *J. Am. Ceram. Soc.* **2007**, *90*, 1753.

(25) Stauch, O.; Uhlmann, T.; Fröhlich, M.; Thomann, R.; El-Badry, M.; Kim, Y.-K.; Schubert, R. *Biomacromolecules* **2002**, *3*, 324.

(26) Mucci, V.; Vallo, C. *J. Appl. Polym. Sci.* **2012**, *123*, 418.

(27) Zhang, H.; Wang, D.; Butler, R.; Campbell, N. L.; Long, J.; Tan, B.; Duncalf, D. J.; Foster, A. J.; Hopkinson, A.; Taylor, D.; Angus, D.; Cooper, A. I.; Rannard, S. P. *Nat. Nanotechn.* **2008**, *3*, 506.

(28) Vickery, J. L.; Patil, A. J.; Mann, S. *Adv. Mater.* **2009**, *21*, 2180.

(29) Fu, Q.; Saiz, E.; Rahaman, M. N.; Tomsia, A. P. *Materials Science and Engineering: C* **2011**, *31*, 1245.

(30) Zhang, X.; Li, C.; Luo, Y. *Langmuir* **2011**, *27*, 1915.

(31) Stankovich, S.; Dikin, D. A.; Dommett, G. H. B.; Kohlhaas, K. M.; Zimney, E. J.; Stach, E. A.; Piner, R. D.; Nguyen, S. T.; Ruoff, R. S. *Nature* **2006**, *442*, 282.

(32) Berchtold, K. A.; Hacioglu, B.; Nie, J.; Cramer, N. B.; Stansbury, J. W.; Bowman, C. N. *Macromolecules* **2009**, *42*, 2433.

(33) Scherzer, T.; Langguth, H. *Macromol. Chem. Phys.* **2005**, *206*, 240.

(34) Svec, F. *J. Chromatogr. A* **2010**, *1217*, 902.

(35) Lesellier, E.; West, C. *J. Chromatogr. A* **2007**, *1158*, 329.

(36) Layne, J. *J. Chromatogr. A* **2002**, *957*, 149.

(37) Svec, F. *J. Sep. Sci.* **2004**, *27*, 1419.

Chapter 4

Aligned Porous Stimuli-Responsive Hydrogels *via* Directional Freezing and Frozen UV Initiated Polymerization

List of Figures

List of Schemes

List of Tables

4.1 Introduction

Hydrogels are hydrophilic three dimensional polymer networks that contain large amounts of water. Due to their rapid swelling properties,[1] macroporous hydrogels have a wide range of applications including drug delivery,[2] tissue engineering,[3] chromatography[4] and water treatment.[5] These materials can be fabricated using various techniques such as cryopolymerization,[6,7] emulsion templating,[8,9] CO_2 technology or gas foaming[10-12] and freeze-drying.[13,14]

Significant interest has been shown in porous hydrogel systems that have the ability to change their swelling behaviour in response to external stimuli in aqueous conditions.[15-17] Particularly, biodegradable materials that can be applied *in vitro* and respond to body temperature or pH have been extensively investigated.[18-21]

For potential applications, control of pore morphology is of high importance.[22,23] When applied as scaffolds in tissue engineering, aligned porous structures show unique characteristics as they can mimic properties of some natural tissues, increase perfusion, and direct cell growth.[24-26] As mentioned before, directional freezing is a simple method for preparing aligned porous materials.[27-29] The method involves lowering a polymer solution into a cold liquid bath (*e.g.,* liquid nitrogen) at a controlled rate, thus orienting the growth direction of solvent crystals. The solvent is generally removed by freeze drying to obtain aligned porous materials. The disadvantages associated with the freeze-dried materials are that they are mechanically very weak and can dissolve or shrink when exposed to a solvent.

In general, to make porous polymeric material by the freeze-drying approach, a polymer is dissolved in a suitable solvent and the resulting solution is then frozen and freeze dried. Alternatively, one can consider dissolving monomers in a solvent, freeze the resulting solution, and polymerizing the monomers whilst in the frozen state. The solvent can be removed by freeze-drying or under vacuum at ambient temperature. This approach can avoid the energy-consuming step. More importantly, the produced crosslinked porous polymer may be more stable mechanically and insoluble in common solvents. The challenge is how to polymerize the monomers

without affecting the freezing structure. By employing a solvent with high melting point in a slurry of alumina particles, a freeze-gel casting method was used to prepare porous ceramics. During thermal treatment after freezing, monomer gelation and solvent removal take place simultaneously.[30] However, most of the solvents used in the freeze-drying approach have rather low melting points. The thermal treatment of a frozen body is not widely viable. To decouple the freezing step and the thermal treatment step, de Hazan developed a freeze-photocuring-casting process to make porous ceramic, polymer, and composites. Polyethylene glycol diacrylate was used as monomer and polymerized in the absence and presence of ceramic colloids under UV irradiation.[31]

Cryopolymerization is a technique where a monomer solution in a frozen or semi-frozen state is polymerized at subzero temperature to produce macroporous gels. The polymerization often occurs in a freezer (or alternative cold environment) or by UV initiated polymerization.[32] Highly interconnecting and randomly macroporous structures are usually formed. Directional freezing and cryopolymerization have been used to prepare aligned porous organogels based on polyisobutane.[33] Aligned porous hydrogels have also been prepared by pre-forming gelatin and agarose gels and then directionally freezing to introduce aligned porosity.[34,35] Very recently, by combining directional freezing and cryopolymerisation, aligned porous hydrogels from poly(ethylene glycol)-water system (polymerized in freezer – 15 ^{o}C for 12 h) and urethane diacrylate-dioxane system (UV polymerization) have been produced.[6,36] We have produced crosslinked aligned porous materials by directional freezing and UV frozen polymerization of dimethacrylate monomers with different organic solvents.[37] These materials exhibited enhanced mechanical stability and were further modified to give good conductivity. More importantly, the aligned porous structure was assessed as a stationary phase for high performance liquid chromatography (HPLC) showing fast mass transfer kinetics with low back pressure.

Although poly(*N*-isopropylacrylamide) was incorporated into aligned crosslinked poly(ethylene glycol) to demonstrate the temperature-responsive anisotropic swelling,[38] to the best of our knowledge, stimuli-responsive aligned porous hydrogels have not been directly produced. In this paper, we describe the preparation of temperature and pH-responsive hydrogels via directional freezing and frozen UV

initiated polymerization. We investigate further how porosity and crosslinking percentage affect the swelling properties and compare diffusion behavior with randomly frozen hydrogels.

4.2 Experimental

4.2.1 Chemicals and Reagents

Di(ethylene glycol) methyl ether methacrylate ($OEGMA_{175}$, Mw 175), poly(ethylene glycol) methyl ether methacrylate ($OEGMA_{475}$, Mw 475), 2-(dimethylamino) ethyl methacrylate (DMAEMA, Mw 157.2), ethylene glycol dimethacrylate (99% EGDMA), 2,2-dimethoxy-2-phenylacetophenone (DMPA 99%) and 1,4-dioxane were purchased from Sigma Aldrich and used as received. Distilled water was used for all swelling tests. Rhodamine B was purchased from Acros Organics.

4.2.2 Preparation of Responsive Aligned Porous Polymer

For the temperature responsive polymer, EGDMA (at the molar ratio of 3, 5, 10 %) was added to a mixture of $OEGMA_{175}$ and $OEGMA_{475}$ (9:1 molar ratio). The obtained solution was then diluted to 1:5 and 1:10 (v/v) with dioxane. 1 wt% DMPA initiator was added with respect to the mass of the monomer. For the pH responsive polymer, the OEGMA monomers were simply replaced with DMAEMA.

Typically, 2 cm^3 monomer solution in dioxane was placed in a cylindrical glass tube (75 mm length x 10 mm diameter) and directionally frozen by dipping the tube into liquid nitrogen at an approximate rate of 75 mm min^{-1}. The frozen sample was then placed on dry ice (-78 °C) and polymerized for 7 hours using a 40 watt Spectroline® X-series UV lamp (wavelength 365 nm). The sample was turned every 30 minutes to ensure complete polymerization. The samples were freeze dried for 48 hours using a VIRTIS advantage freeze dryer (condenser -84 °C shelf temp 10 °C) to produce dry aligned porous materials for further tests.

4.2.3 Swelling Measurement

To quantify the swelling/deswelling properties, swelling of the hydrogels in water was assessed by mass change. The dry samples with similar mass (≈ 0.1 g) and in

cylindrical shape were soaked in water for 2 hours. Before weighing the soaked samples, the water on the surface was wiped off with greaseproof paper. The swelling ratio was calculated using the equation:

Swelling ratio = M_s/M_d

where M_s is the soaked mass and M_d is the dry mass. For each sample, three soaking experiments were carried out and the average swelling ratios were used for the plots. Generally, the standard deviations over the 3 measurements were around 6%.

4.3 Results and Discussion

4.3.1 Aligned Porous Stimuli Responsive Hydrogels

Scheme 4.1 outlines the preparation procedures. A monomer solution is directionally frozen and polymerized in the frozen state under UV irradiation. After polymerization is complete the solvent is removed to obtain aligned porous material. Sublimation by freeze-drying was used to remove the solvent in order to produce dry aligned porous material. Because the monomers have already been crosslinked, it is possible to generate dry porous materials by vacuum drying at ambient temperature. Such approach has been used for ceramic composites or porous polymers prepared from only diacrylate monomers.[31,36,37]

In this study, if the samples are warmed to room temperature after UV frozen polymerization, a very soft gel is formed. The molar crosslinker (EGDMA) ratios are 3, 5, 10%, with respect to amount of moles of monomer. Like common hydrogels, the pore structure can collapse if the solvent is removed at room temperature. Therefore, the gels were freeze dried to produce dry porous materials which were then used for further tests.

It is already well known that polyOEGMA material responds to temperature in water whilst polyDMAEMA material is sensitive to pH. Lutz *et al*. have shown that polymers fabricated from OEGMA monomers (Scheme 4.2A) exhibit interesting responsive properties in water.[39,40] Factors such as nature of polymerization group,

end groups, and number of ethylene units can alter the responsive properties of the resulting polymer. For example, using a 9:1 molar mixture of monomers $OEGMA_{175}$ and $OEGMA_{475}$ resulted in polymers exhibiting lower critical solution temperature (LCST) around 39-40°C. Adding small amounts of EGDMA (Scheme 4.2C) produces crosslinked hydrogels that exhibit LCST behaviour similar to that of the single chain polymers.[41] Crosslinked hydrogels that respond to pH have previously been produced using DMAEMA monomer[42,43] (Scheme 4.2B).

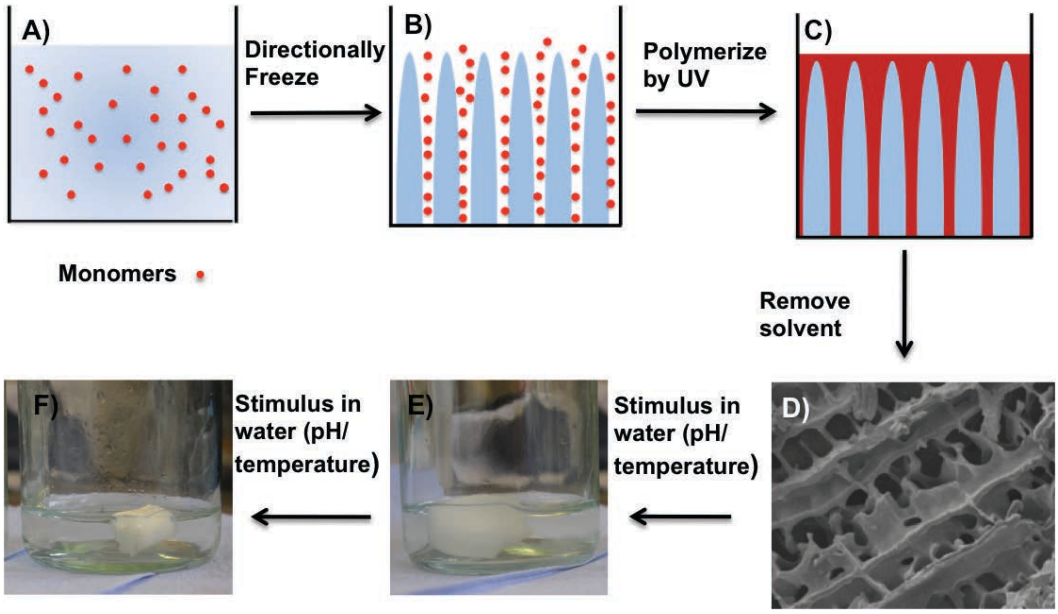

Scheme 4.1 Preparation of aligned porous stimuli responsive hydrogels from a monomer solution followed by stimuli responsive behaviour in aqueous conditions.

These hydrogels are cationic, because when the pH of the surrounding solution is below the pKa of the ionizing group of DMAEMA (7-7.5),[44-46] the tertiary amine group is protonated and becomes more hydrophilic causing the material to swell. In basic conditions the tertiary amine group in a mostly neutral state and is said to be less hydrophilic. These monomers were therefore used here to produce aligned porous responsive hydrogels.

Figure 4.1A & B show aligned porous structures obtained from 1:5 OEGMA-dioxane (v/v) solutions. This structure is also observed for the material prepared from DMAEMA solution (Figure 4.1C & D). Highly interconnected and oriented channels are observed across the whole sample.

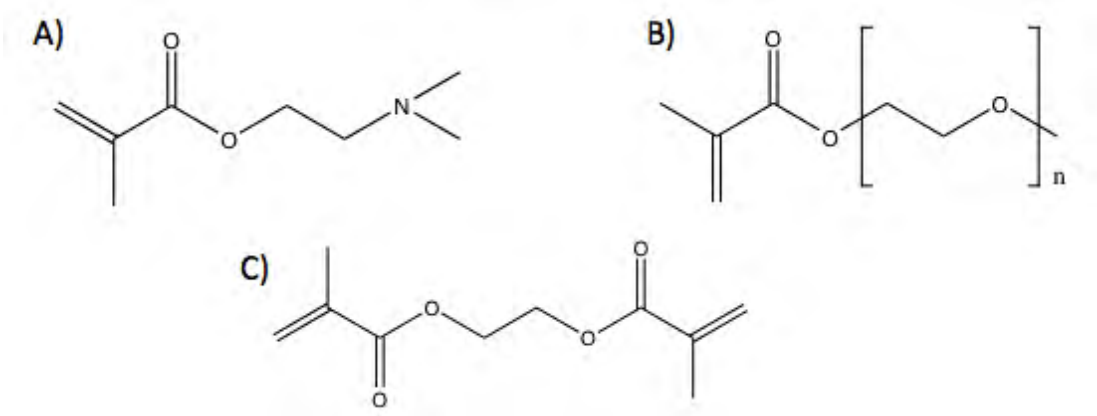

Scheme 4.2 Monomers used in the synthesis. A) 2-(dimethylamino) ethyl methacrylate (DMAEMA) B) Oligo (ethylene glycol) methacrylate (OEGMA). C) Ethylene glycol dimethacrylate (EGDMA).

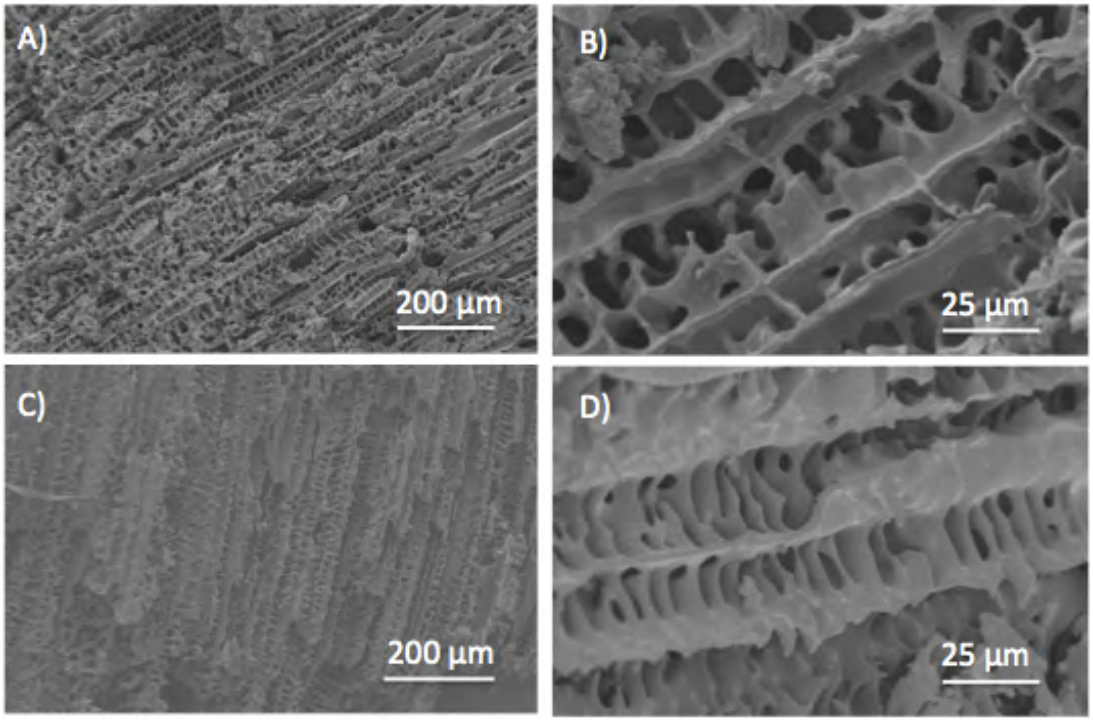

Figure 4.1 SEM images showing aligned porous structures made from A & B) 1:5 OEGMA/dioxane (v/v) (5% EGDMA), C & D) 1:5 DMAEMA/dioxane (v/v) (5% EGDMA).

The porosity can be easily tuned by altering the monomer-solvent concentration of the initial solution, whilst retaining an aligned porous structure (Figure 4.2). For example, the materials prepared from 1:5 and 1:10 DMAEMA-dioxane (v/v) (10% EGDMA) solutions were fairly rigid allowing the use of mercury intrusion. The total

intrusion volumes obtained were 4.25 cm^3 g^{-1} and 8.74 cm^3 g^{-1} respectively, with the 1:10 sample showing smaller interconnecting pores (Figure 4.3).

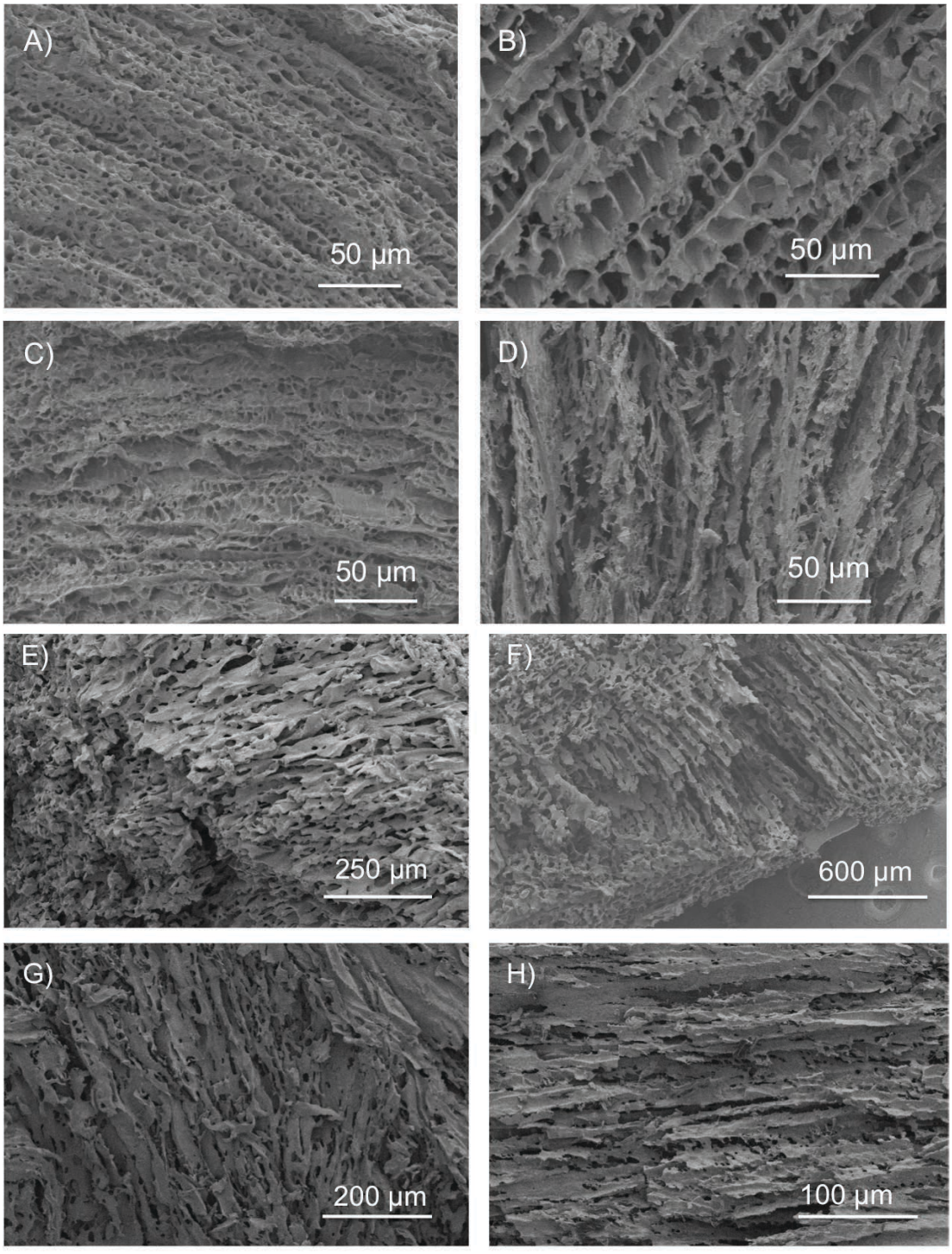

Figure 4.2 SEM images showing aligned porous structures made from solutions of: A) 1:5 OEGMA/dioxane (v/v) (3% EGDMA) B) 1:5 OEGMA/dioxane (v/v) (10% EGDMA). C) 1:10 OEGMA/dioxane (v/v) (3% EGDMA) D) 1:10 OEGMA/dioxane (v/v) (10% EGDMA) E) 1:5 DMAEMA/dioxane (v/v) (3% EGDMA) F) 1:5 DMAEMA/dioxane (v/v) (10% EGDMA) G) 1:10 DMAEMA/dioxane (v/v) (3% EGDMA) H) 1:10 DMAEMA/dioxane (v/v) (10% EGDMA).

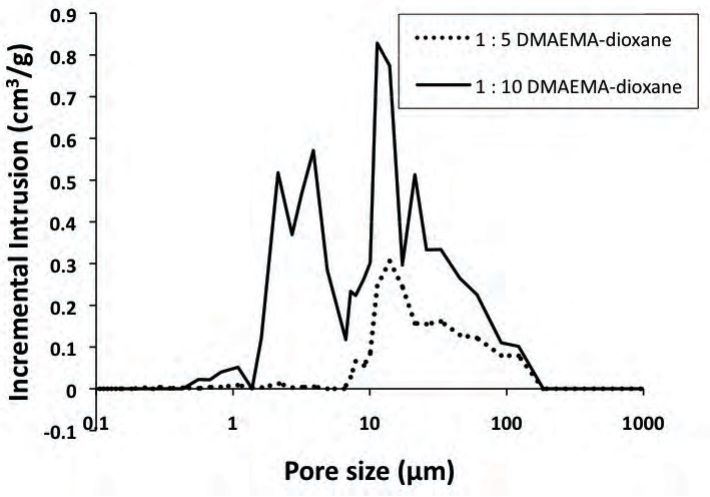

Figure 4.3 Pore size distributions of the samples prepared from 1:5 and 1:10 DMAEMA-dioxane (v/v) (10% EGDMA) by Hg intrusion porosimetry.

4.3.2 Frozen Polymerization

Characterization of crosslinked material is often challenging due to their insolubility in common solvents. However, FTIR measurements can be used to show the disappearance of C=C bonds in the polymerization system. FTIR spectra of both OEGMA (Figure 4.4A) and DMAEMA (Figure 4.4B) monomer mixtures containing 10% EGDMA were recorded. These were compared with materials obtained after 1:5 monomer/dioxane (v/v) solutions containing 3 and 10% EGDMA were directionally frozen and UV polymerized on dry ice for 7 hours, before freeze drying. For both systems, strong C=C peaks (≈ 1640 cm^{-1}) are observed for the monomers. After the UV polymerization, the C=C peaks are reduced significantly (Figure 4.4A and Figure 4.4B). Due to the highly limited mass transport in solid or frozen crosslinking polymerization, achieving 100% conversion is extremely difficult. Indeed, the degree of polymerization in frozen polymerization systems has been rarely reported. From the FTIR data in Figure 4.4, it is clear that the majority of monomers and crosslinkers have been polymerized. This is also obvious when solid material is obtained after freeze-drying. It appears that higher percentage of crosslinker (EGDMA) in the reaction can result in higher conversion of monomers to polymer.

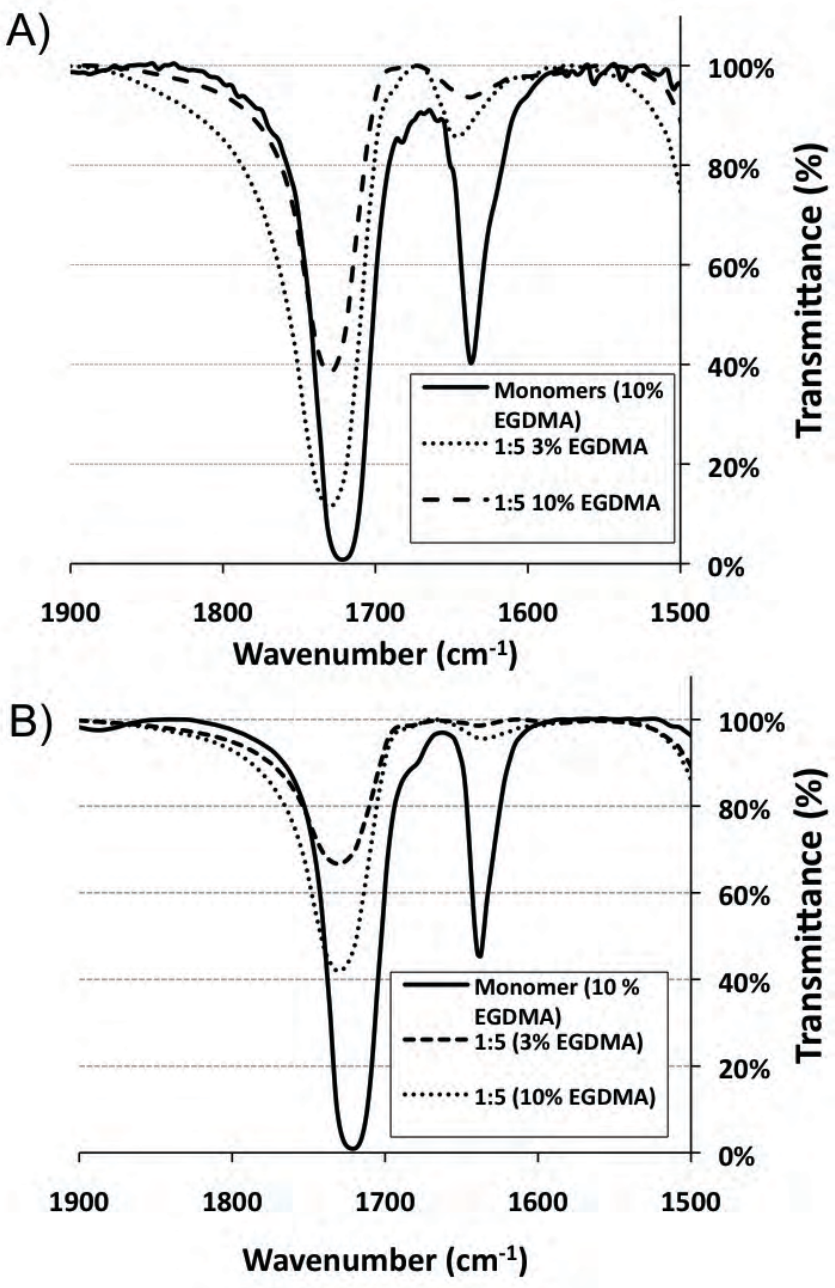

Figure 4.4 FTIR spectra of the monomer + crosslinker (EGDMA) mixtures and the frozen UV polymerized samples: A) polyOEGMA and B) polyDMAEMA.

To understand more about the frozen UV polymerization process, 1:5 monomer-dioxane solutions were polymerized with no EGDMA. With no crosslinker present, change in molecular weight over time could be measured by GPC. Samples were directionally frozen and polymerized on dry ice, then removed at different time intervals and freeze-dried for 48 hours. PolyDMAEMA showed a steady increase in molecular weight with time and polydispersity index (PDI) between 2-2.7 (Figure

4.5A). A full list of polydispersity indexes, number average and weight average molecular weights are given in Table 4.1. The samples taken off dry ice after 2 and 4 hours were viscous gels however the sample taken off after 6 and 8 hours resembled porous white solids. All polyOEGMA samples resembled viscous gels and the polydispersity index (PDI) and degree of polymerization were inconsistent (Figure 4.5B).

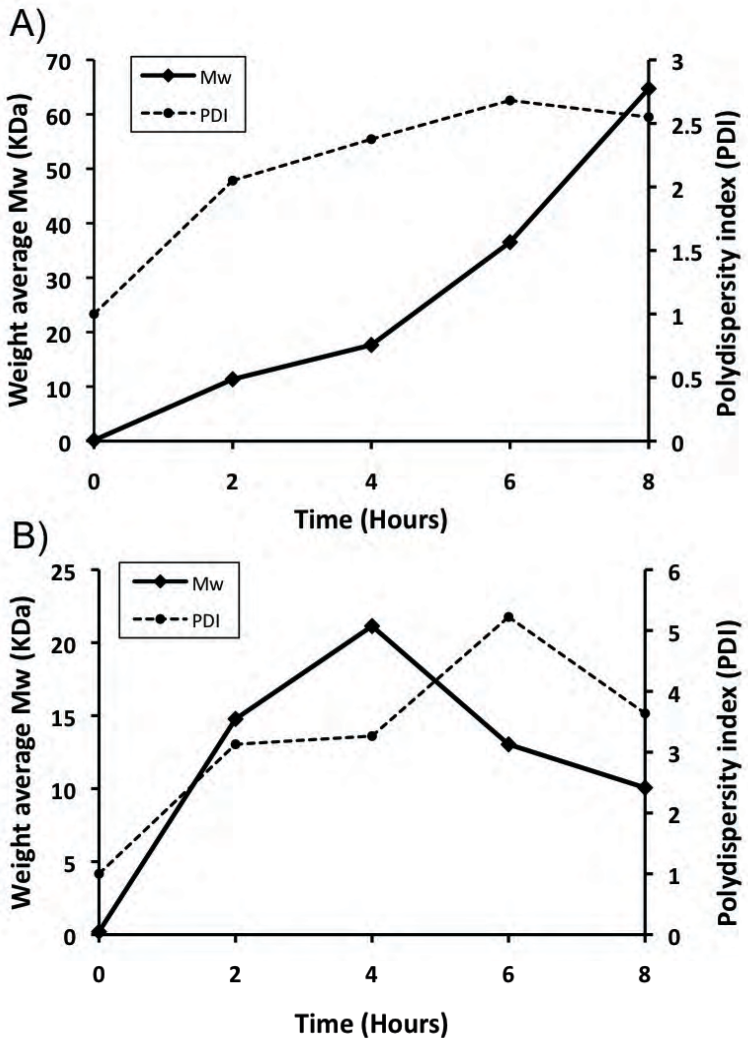

Figure 4.5 Relationship of weight average Mw and polydispersity index with polymerization time for A) 1:5 DMAEMA to dioxane system with no crosslinker EGDMA B) 1:5 OEGMA to dioxane system with no crosslinker EGDMA.

This is expected when applying free-radical polymerization to co-monomer solutions as the two monomers do not necessarily have the same polymerization kinetics. The resulting polymer may contain chain-to chain deviations, hence irregular molecular

weight with reaction time.[40] The presence of crosslinker (EGDMA) facilitates the formation of solid porous materials after freeze drying. This is particularly obvious for polyOEGMA.

Table 4.1 Gel permeation chromatography (GPC) results for the 1:5 monomer(s)-dioxane solutions polymerized with no crosslinker.

OEGMA				DMAEMA			
Time (Hours)	Mn	Mw	PDI	Time (Hours)	Mn	Mw	PDI
0		≈ 200		0		157.2	
2	4724	14777	3.13	2	5294	11349	2.05
4	6475	21141	3.265	4	7469	17644	2.376
6	2495	13035	5.224	6	13623	36526	2.681
8	2767	10064	3.637	8	25303	64716	2.55

4.3.3 Responsive Properties

To demonstrate that the crosslinked materials were responsive to external stimuli, dimension measurement and mass change before and after soaking were recorded. All dry samples were sliced to the same cylindrical dimensions (10 mm length x 7 mm diameter) before placing into different aqueous conditions. The dimensions of these samples after soaking for 2 hours were given in Table 4.2. In general, polyOEGMA samples swelled slightly at 4 °C, then deswelled when the solution was heated to 50 °C. Optical images for pH responsive samples are shown in Figure 4.6.

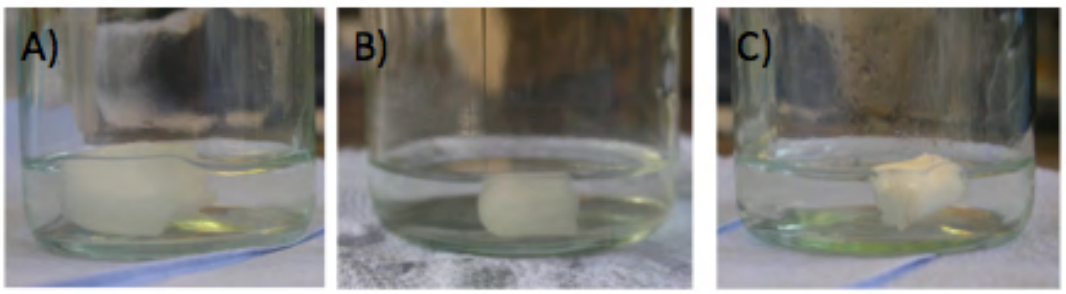

Figure 4.6 Images of polyDMAEMA (1:5 DMAEMA to dioxane (v/v), 3% EGDMA) placed in A) 1 M HCl aqueous solution, B) distilled water and C) 1 M NaOH aqueous solution.

Table 4.2 Dimensions of hydrogels after soaking for 2 hours in different aqueous conditions. All the test samples are cylindrical in shape (10 mm length x 7 mm diameter).

SAMPLE	Dimensions in 4 °C water (length x diameter mm)	Dimensions in 50 °C water (length x diameter mm)
1:5 OEGMA/dioxane (v/v) (3% EGDMA)	13 x 9	10 x 7
1:5 OEGMA/dioxane (v/v) (5% EGDMA)	13 x 9	10 x 7
1:5 OEGMA/dioxane (v/v) (10% EGDMA)	13 x 9	10 x 7
1:10 OEGMA/dioxane (v/v) (3% EGDMA)	13 x 9	11 x 8
1:10 OEGMA/dioxane (v/v) (5% EGDMA)	13 x 9	11 x 8
1:10 OEGMA/dioxane (v/v) (10% EGDMA)	13 x 9	11 x 8
SAMPLE	**Dimensions in 1 M HCl (length x diameter mm)**	**Dimensions in 1 M NaOH (length x diameter mm)**
1:5 DMAEMA/dioxane (v/v) (3% EGDMA)	20 x 15	12 x 8
1:5 DMAEMA/dioxane (v/v) (5% EGDMA)	18 x 14	12 x 8
1:5 DMAEMA/dioxane (v/v) (10% EGDMA)	12 x 11	12 x 8
1:10 DMAEMA/dioxane (v/v) (3% EGDMA)	18 x 15	11 x 8
1:10 DMAEMA/dioxane (v/v) (5% EGDMA)	16 x 12	11 x 8
1:10 DMAEMA/dioxane (v/v) (10% EGDMA)	12x 10	11 x 8

When polyDMAEMA samples were placed into 1 M HCl (pH 0), rapid swelling was observed. Samples with 3% EGDMA roughly doubled in size. The same sample was placed in 1 M NaOH (pH 14) for 2 hours showing gradual deswelling.

Both the temperature and pH responsive hydrogels with different crosslinker ratios (3%, 5%, and 10% EGDMA) and differing porosity were further evaluated. The results shown in Figure 4.7 give clear indication of stimuli-responsive swelling/deswelling behaviour. Samples prepared using 1:5 OEGMA-dioxane (Figure 4.7A) have a swelling ratio around 7 at 4 °C, which drops to between 4-5 when the solutions are heated to 50 °C.

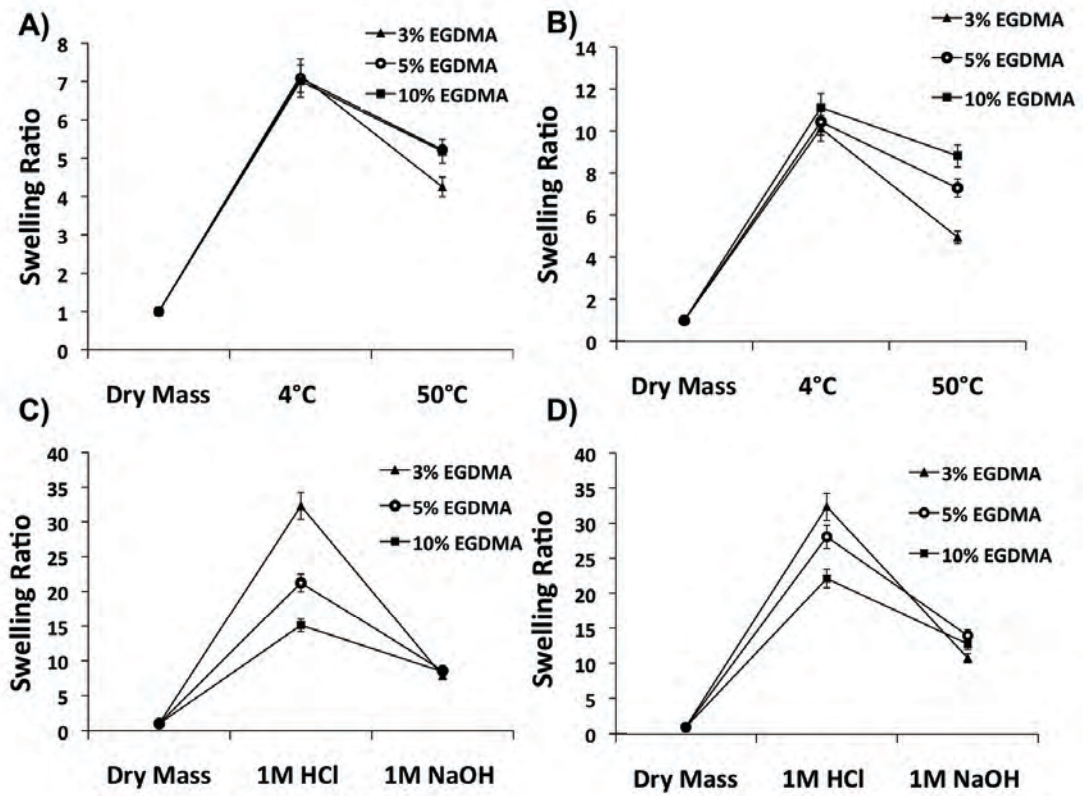

Figure 4.7 Swelling ratios of hydrogels by mass change under different aqueous conditions, with varying ratios of EGDMA. For polyOEGMA, A) 1:5 OEGMA/dioxane (v/v) and B) 1:10 OEGMA/dioxane (v/v); for polyDMAEMA, C) 1:5 DMAEMA/dioxane (v/v) and D) 1:10 DMAEMA/dioxane (v/v).

The hydrogel with 3% EGDMA shrinks more than the hydrogels of 5% and 10% EGDMA. For the polyOEGMA hydrogels prepared from 1:10 dioxane solutions, the swelling ratios in water at 4 ^{o}C are around 10 compared to the initial dry materials (Figure 4.7B). It suggests that when the water phase is heated to 50 ^{o}C, the higher the crosslinking ratio, the lower the shrinking capacity. Figure 4.7A and B show similar swelling ratios for porous polyOEGMA irrespective of crosslinker ratios (3-10%). PolyOEGMA samples do not swell as much because 90% of the monomer mixture contains OEGMA175, for which the side chain only contains two ethylene units so

the resulting polymer is not as hydrophilic as other PEG polymers. This suggests that the crosslinker ratio may have limited influence in the hydrogel swelling. However, the samples deswelling ratios differ because it is thought the sample containing 3% crosslinker is more flexible, so it can contract. Samples with more crosslinker are more rigid and would contract less at high temperature. For polyDMAEMA hydrogels pH responsive behaviour was observed (Figure 4.7C & B). Compared to the polyOEGMA hydrogels, the polyDMAEMA hydrogels took up significantly more water, with the swelling ratio for the hydrogels with 3% EGDMA around 32 in 1M HCl solution. The swelling ratio changes consistently with the change of crosslinking ratio. For the hydrogels prepared from both 1:5 and 1:10 dioxane solutions, the swelling ratio increases with the decrease of the crosslinker (EGDMA) ratio (Figure 4.7C & D). One interesting observation is that when the swollen hydrogels are placed in 1M NaOH solution the hydrogels shrink to a similar point. The average percentage error was calculated at ± 6 % based on three measurements. To examine the LCST behaviour of polyOEGMA material more carefully, swelling ratios were recorded at temperatures between 4 °C and 70 °C. The solution surrounding the material was heated (or cooled) to the chosen temperature and left for 10 minutes before the swelling ratio was recorded. Material prepared from 1:5 OEGMA-dioxane solutions exhibit similar LCST behaviour (Figure 4.8), contracting between 30 °C and 45 °C.

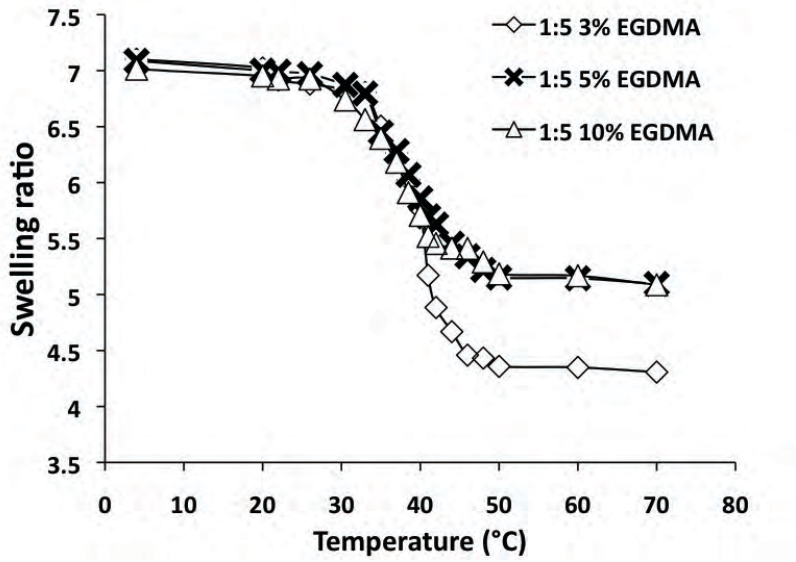

Figure 4.8 LCST behaviour of the polyOEGMA hydrogels with containing different amounts of EGDMA crosslinker.

This broad responsive temperature range is believed to be due to polymer chain-to-chain deviations brought about by free radical polymerization of co-monomer solutions. At 40 °C polyOEGMA samples are mostly in a deswelled state. The material can be swollen again by simply cooling the solution below 30 °C.

4.3.4 Anisotropic Properties

Compression tests were performed to determine gel strength with respect to freezing direction. The dry materials were swollen in distilled water at room temperature and cut into 15 mm cubes. Samples were then crushed parallel and perpendicular to the direction of freezing. Figure 4.9 shows the stress-strain for porous hydrogels prepared from a 1:5 DMAEMA/dioxane (v/v) (10% EGDMA) solution.

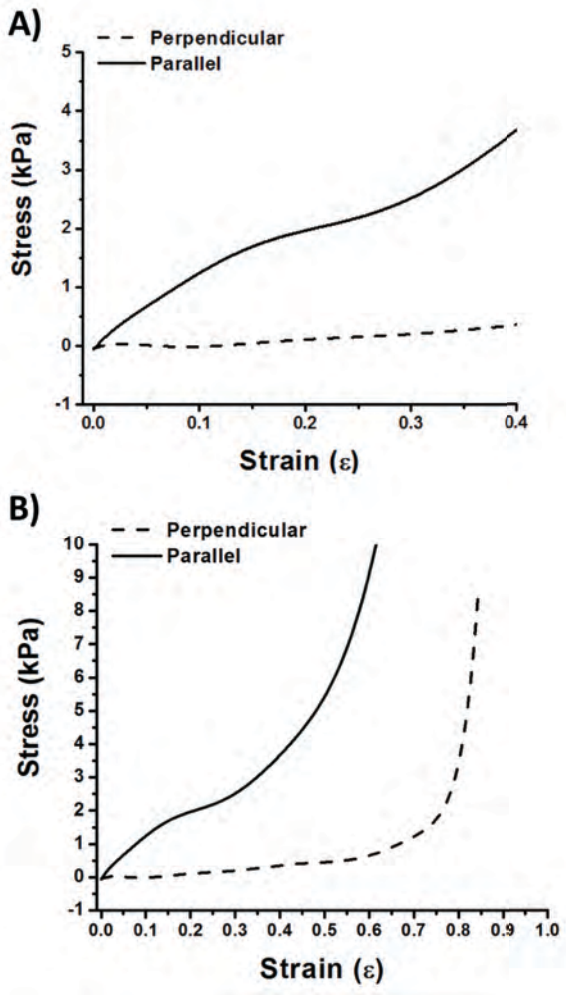

Figure 4.9 Stress-strain curves by compressing tests for sample made from 1:5 DMAEMA/dioxane (v/v) (10% EGDMA). A) Initial linear displacement. B) Overall displacement of the sample.

The initial linear gradient of the curve is used to calculate the Young's modulus (Figure 4.9A), as this is when the material is assumed to be coping with the increasing load placed upon it. The sample crushed parallel to the freezing direction has a Young modulus of 10 kPa and the perpendicular sample has a Young modulus of 0.9 kPa. The initial loading for perpendicular samples is an order of magnitude lower due to the microtubule pores being pressed together and is further evidence of an aligned porous structure throughout the sample. The parallel sample was compressed to 20% strain before being permanently distorted whereas the perpendicular sample was compressed up to 70 % strain (Figure 4.9B).

To demonstrate the diffusion properties of the aligned pores, a randomly porous hydrogel (Figure 4.10) was prepared by freezing in a -20 ^{o}C freezer to compare with an aligned porous hydrogel prepared by directional freezing in liquid nitrogen.

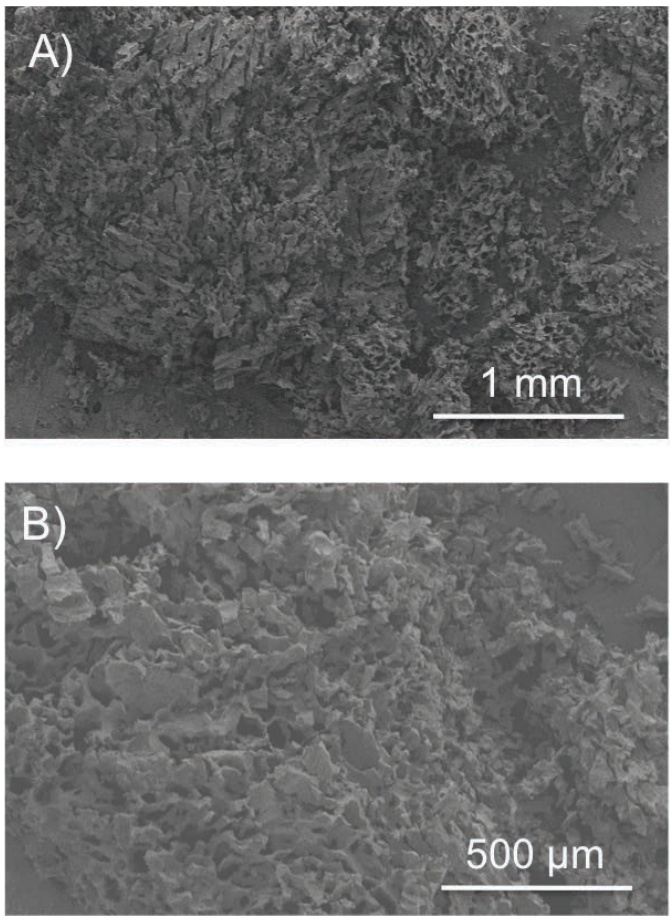

Figure 4.10 Randomly frozen porous hydrogel prepared from 1:5 OEGMA/dioxane (v/v) (5% EGDMA) solution.

Both gels were prepared in cylinder shapes and swollen in distilled water. They were sliced into cross sections, then one drop of Rhodamine B stained water solution (1 mg/ml) was dropped on top of the gels and allowed to diffuse. After about 60 seconds optical images were taken (Figure 4.11). Diffusion of Rhodamine B solution through the aligned porous hydrogel follows a more one-dimensional pathway, diffusing fast parallel to the direction of freezing. Conversely, diffusion through the randomly porous hydrogel is more isotropic.

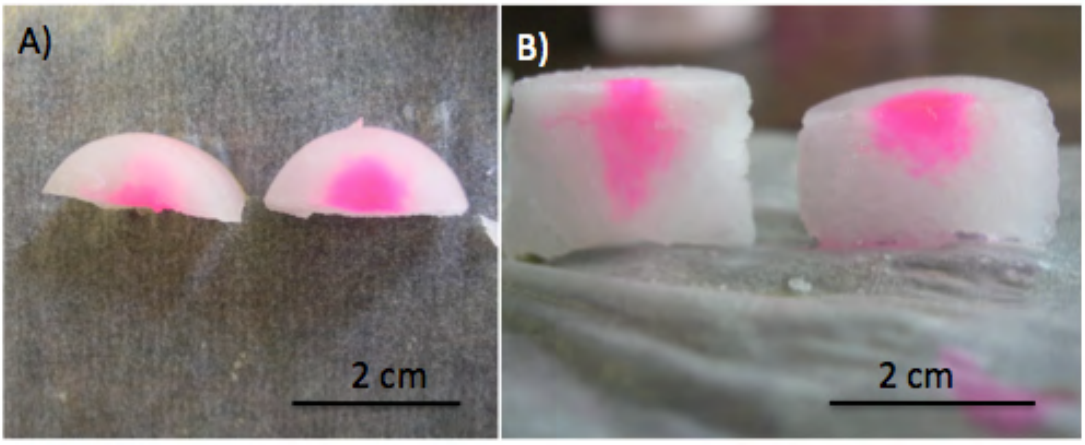

Figure 4.11 Diffusion of Rhodamine B stained water through aligned porous hydrogel (left) and randomly macroporous hydrogel (right) at room temperature: A) Birds-eye view, B) Cross-sectional view. Both samples prepared from 1:5 OEGMA/dioxane (v/v) (5% EGDMA) solution.

4.4 Conclusions

Directional freezing and frozen UV initiated polymerization were used to produce aligned porous temperature- and pH-responsive polymeric materials. The swelling properties of these materials acting as hydrogels could be manipulated by changing crosslinker ratio and porosity, both of which can be achieved simply by changing the compositions of the monomer solutions. Anisotropic compressive strength and diffusion behaviour were observed with respect to the direction of freezing. The anisotropic properties of these materials may be particularly useful for guiding cell growth or targeted delivery. Further studies could be focused on the biocompatibility of the hydrogels and also finely tuning the sensitivity and critical points of the stimuli, (e.g., around body temperature and biological pH range) for potential biological applications.

4.5 References

(1) Yan, Q.; Hoffman, A. S. *Polymer* **1995**, *36*, 887.

(2) Grant, N. C.; Cooper, A. I.; Zhang, H. *ACS Appl. Mater. Interfaces* **2010**, *2*, 1400.

(3) Studenovská, H.; Šlouf, M.; Rypáček, F. *J. Mater. Sci. - Mater. Med.* **2008**, *19*, 615.

(4) Plieva, F. M.; Galaev, I. Y.; Mattiasson, B. *J. Sep. Sci.* **2007**, *30*, 1657.

(5) Savina, I. N.; English, C. J.; Whitby, R. L. D.; Zheng, Y.; Leistner, A.; Mikhalovsky, S. V.; Cundy, A. B. *J. Hazard. Mater.* **2011**, *192*, 1002.

(6) Wu, J.; Zhao, Q.; Sun, J.; Zhou, Q. *Soft Matter* **2012**, *8*, 3620.

(7) Kirsebom, H.; Rata, G.; Topgaard, D.; Mattiasson, B.; Galaev, I. Y. *Macromolecules* **2009**, *42*, 5208.

(8) Zhang, H.; Cooper, A. I. *Soft Matter* **2005**, *1*, 107.

(9) Kimmins, S. D.; Cameron, N. R. *Adv. Funct. Mater.* **2011**, *21*, 211.

(10) Barbetta, A.; Rizzitelli, G.; Bedini, R.; Pecci, R.; Dentini, M. *Soft Matter* **2010**, *6*, 1785.

(11) Chen, K.; Grant, N.; Liang, L.; Zhang, H.; Tan, B. *Macromolecules* **2010**, *43*, 9355.

(12) Tayton, E.; Purcell, M.; Aarvold, A.; Smith, J. O.; Kalra, S.; Briscoe, A.; Shakesheff, K.; Howdle, S. M.; Dunlop, D. G.; Oreffo, R. O. C. *Acta Biomaterialia* **2012**, *8*, 1918.

(13) Guziewicz, N.; Best, A.; Perez-Ramirez, B.; Kaplan, D. L. *Biomaterials* **2011,** *32*, 2642.

(14) Ma, C.; Prabhu, S. *Int. J. Drug Del.* **2011,** *3*, 55.

(15) Gopishetty, V.; Tokarev, I.; Minko, S. *J. Mater. Chem.* **2012**, *22*, 19482.

(16) Kim, J. H.; Lee, S. B.; Kim, S. J.; Lee, Y. M. *Polymer* **2002**, *43*, 7549.

(17) Varaprasad, K.; Ravindra, S.; Reddy, N. N.; Vimala, K.; Raju, K. M. *J. Appl. Polym. Sci.* **2010**, *116*, 3593.

(18) Patel, V. R.; Amiji, M. M. *Pharm. Res.* **1996**, *13*, 588.

(19) Schmaljohann, D. *Adv. Drug Delivery Rev.* **2006**, *58*, 1655.

(20) Mandal, T. K. *Eur. J. Pharm. Biopharm.* **2000**, *50*, 337.

(21) Zhang, Z.; Chen, L.; Deng, M.; Bai, Y.; Chen, X.; Jing, X. *J. Polym. Sci., Part A: Polym. Chem.* **2011**, *49*, 2941.

(22) Choi, S.-W.; Xie, J.; Xia, Y. *Adv. Mater.* **2009**, *21*, 2997.

(23) Choi, S.-W.; Zhang, Y.; Yeh, Y.-C.; Lake Wooten, A.; Xia, Y. *J. Mater. Chem.* **2012**, *22*, 11442.

(24) Hu, X.; Shen, H.; Yang, F.; Bei, J.; Wang, S. *Biomaterials* **2008**, *29*, 3128.

(25) Deville, S.; Saiz, E.; Tomsia, A. P. *Biomaterials* **2006**, *27*, 5480.

(26) Riblett, B. W.; Francis, N. L.; Wheatley, M. A.; Wegst, U. G. K. *Adv. Funct. Mater.* **2012**, *22*, 4920

(27) Zhang, H.; Hussain, I.; Brust, M.; Butler, M. F.; Rannard, S. P.; Cooper, A. I. *Nat Mater* **2005**, *4*, 787.

(28) Zhang, H.; Cooper, A. I. *Adv. Mater.* **2007**, *19*, 1529.

(29) Gutiérrez, M. C.; Ferrer, M. L.; del Monte, F. *Chem. Mater.* **2008**, *20*, 634.

(30) Chen, R.; Wang, C.-A.; Huang, Y.; Ma, L.; Lin, W. *J. Am. Ceram. Soc.* **2007**, *90*, 3478.

(31) de Hazan, Y. *J. Am. Ceram. Soc.* **2012**, *95*, 177.

(32) Petrov, P.; Petrova, E.; Tsvetanov, C. B. *Polymer* **2009**, *50*, 1118.

(33) Dogu, S.; Okay, O. *Polymer* **2008**, *49*, 4626.

(34) Wu, X.; Liu, Y.; Li, X.; Wen, P.; Zhang, Y.; Long, Y.; Wang, X.; Guo, Y.; Xing, F.; Gao, J. *Acta Biomaterialia* **2010**, *6*, 1167.

(35) Yokoyama, F.; Achife, E. C.; Momoda, J.; Shimamura, K.; Monobe, K. *Colloid. Polym. Sci.* **1990**, *268*, 552.

(36) Okaji, R.; Taki, K.; Nagamine, S.; Ohshima, M. *J. Appl. Polym. Sci.* **2012**, *125*, 2874.

(37) Barrow, M.; Eltmimi, A.; Ahmed, A.; Myers, P.; Zhang, H. *J. Mater. Chem.* **2012**, *22*, 11615.

(38) Wu, J.; Lin, Y.; Sun, J. *J. Mater. Chem.* **2012**, *22*, 17449.

(39) Lutz, J.-F.; Akdemir, Ö.; Hoth, A. *J. Am. Chem. Soc.* **2006**, *128*, 13046.

(40) Lutz, J.-F. *J. Polym. Sci., Part A: Polym. Chem.* **2008**, *46*, 3459.

(41) Lutz, J.-F.; Weichenhan, K.; Akdemir, Ö.; Hoth, A. *Macromolecules* **2007**, *40*, 2503.

(42) Yanfeng, C.; Min, Y. *Radiat. Phys. Chem.* **2001**, *61*, 65.

(43) Yıldız, B.; Işık, B.; Kış, M.; Birgül, Ö. *J. Appl. Polym. Sci.* **2003**, *88*, 2028.

(44) Fielding, L. A.; Edmondson, S.; Armes, S. P. *J. Mater. Chem.* **2011**, *21*, 11773.

(45) Kusumo, A.; Bombalski, L.; Lin, Q.; Matyjaszewski, K.; Schneider, J. W.; Tilton, R. D. *Langmuir* **2007**, *23*, 4448.

(46) van de Wetering, P.; Moret, E. E.; Schuurmans-Nieuwenbroek, N. M. E.; van Steenbergen, M. J.; Hennink, W. E. *Bioconjugate Chem.* **1999**, *10*, 589.

Chapter 5

Aligned Porous Composites

List of Figures

List of Schemes

List of Tables

5.1 Introduction

Composite materials are defined as materials made up from two or more materials with different physical or chemical properties. When they are combined they produce a material with characteristics that are different from each individual component. Engineering materials such as concrete, cements and ceramics are good examples of this.[1,2] Naturally occurring composites such as bone and nacre[3] achieve toughness through a hierarchical organic-inorganic system. This hybrid structure can be mimicked using directional freezing of inorganic slurries and filling the pores with a polymer phase to obtain tough materials for biological applications.[4,5] Directional freezing has been used to prepare composites such as aligned porous chitosan/CNT materials used for tissue engineering[6,7] and as anodes in direct methanol fuel cells.[8,9] Our group have prepared composites by first preparing an aligned porous scaffold, then modifying the surface via a soaking method to obtain conductive material with increased mechanical stability.[10] Aligned porous silver composites were prepared in the same manner using solutions of PVA containing silver nanowires.[11] The resulting composite was electrically conductive and showed anisotropic arrangement of the silver nanowires. Other macroporous silver composites have been shown to have interesting catalytic[12] and antimicrobial properties.[13]

Metal organic frameworks (MOFs) are microporous crystalline structures made up of metal ions and organic ligands. Due to their well-defined microporous structures MOFs have functions such as gas storage,[14,15] catalysis[16] and molecular separations.[17-20] Functional groups within MOFs can lead to various host-guest

interactions including π-π stacking, hydrogen bonding and coordination to metal sites, which make them ideal candidates for separations. MOF crystals are normally quite irregular in shape and size so efficient packing into a HPLC column is not easy and high back-pressures are normally observed.[21] Normally, for HPLC applications, uniform microspheres and packing procedure are paramount for column efficiency. Therefore studies have arisen where silica particle/MOF composites are produced to achieve a fast separation of organic compounds that wouldn't be possible with the silica particles or MOF crystals individually,[22-24] and in some cases lowered the back-pressure generated by the stationary phase.

As mentioned in previous chapters macroporous monolithic columns can significantly lower operational back-pressures.[25] So far, there have been no reports of macroporous/MOF composites being used as a stationary phase for liquid chromatography. However, more studies are emerging involving hierarchically porous micro/macroporous MOF composites.[26,27] Mechanical stirring of a macroporous polyHIPE/HKUST-1 composite was shown to displace some MOF crystals from the external surface of the macroporous composite however the crystals inside the support did not change shape or size.[26] When HKUST-1 was stirred alone in solution the crystals were shown to change size and it becomes more difficult to recover all of the material. Essentially, this means that inside of a porous support the MOF crystals are protected.[26] This is a desirable property for heterogeneous catalysis and other flow through reaction systems. Dual porosity can provide further advantages as microporous materials can have low transport kinetics due to their smaller pores. Microporous materials within a macroporous scaffold could improve diffusion of analytes or reaction precursors. Porous HKUST-1/silica composites have been shown to increase catalytic activity when used as a scaffold for flow through catalysis.[28]

The aim of this chapter is to make aligned porous composites. The first part of the synthesis involves directional freezing and frozen UV polymerization, a method developed by our group. The next part of the synthesis involves manipulation of the surface of the scaffolds to produce aligned porous composites. The material is hyper-crosslinked and insoluble in common organic solvents, meaning the surface can be functionalized using solution methods. The aligned porous composites could be ideal

candidates for catalytic reactions, separations or for any flow through methods due to faster mass transport kinetics.

Both thiol and primary amine functionality was introduced to the monoliths to make aligned porous silver composites and aligned porous HKUST-1 MOF composites respectively. The conductivity of the silver coated material was assessed, and the aligned porous MOF composites were assessed as stationary phases for separation of organic compounds.

5.2 Experimental

5.2.1 Chemicals and Reagents

Copper nitrate trihydrate, trimesic acid, silver nitrate, tetraethylene glycol dimethacrylate (TEGDMA, assay spec ≥ 90% by GC), ethylene glycol dimethacrylate (EGDMA, 99%), 2,2-dimethoxy-2-phenylacetophenone (DMPA, 99%), 3-(trimethoxylsilyl)propyl methacrylate (TMSPMA, 98%), Styrene (≥99%), Ethyl benzene (anhydrous 99.8%) 3-aminopropyl trimethoxysilane (APTES), 3-mercaptopropyl trimethoxysilanne (MPTMS) and 1,4-dioxane were purchased from Sigma Aldrich and used as received. Toluene, heptane (HPLC grade), methanol (GPR grade), dimethylsulfoxide (DMSO) were purchased from Fisher Scientific. Distilled water was used for the preparation of all silver nitrate solutions.

5.2.2 Preparation of Aligned Porous Scaffolds

For silver composites, a monomer mixture consisting of 9:1 TMSPMA/EGDMA (v/v) was prepared with 1 % DMPA initiator with respect to mass of monomers. This was then directionally frozen in liquid and polymerized for 7 hours on dry ice and dried in a vacuum oven overnight. 1:5 1:10 and 1:20 (v/v) monomer in dioxane solutions were prepared.

For aligned porous HKUST-1 MOF composites a 1:1 TMSPMA/EGDMA (v/v) monomer mixture was used with 1 % DMPA initiator with respect to mass of monomers. This was then directionally frozen in liquid nitrogen and polymerized for

7 hours on dry ice. 1:5 1:10 and 1:20 (v/v) monomer in dioxane solutions were prepared.

Also 1:5, 1:10, 1:20 TEGDMA/dioxane (v/v) samples were polymerized as per chapter 3, to compare them as scaffolds with respect to the amine functionalized material.

5.2.3 Post Functionalization of Aligned Porous Scaffolds

The surfaces of all silica containing monoliths were hydrolyzed by soaking in 1 M hydrochloric acid (HCl) for 40 °C for 12 hours then dried under vacuum. Each sample was then placed in a solution of toluene (10 ml per gram of scaffold) and 5 mmol per gram 3-mercaptopropyl trimethoxysilanne (MPTMS) (for silver material) 3-aminopropyl trimethoxysilane (APTES) (for MOF material) and refluxed at 110 °C for 24 hours. The monoliths were vacuum dried and then washed in toluene for 24 hours at room temperature to remove any APTES or MPTMS that was not attached to the surface. They were then dried under vacuum at 50 °C overnight.

5.2.4 Preparation of Aligned Porous Silver Composites

The thiolated materials were soaked in aqueous solutions of silver nitrate of different concentrations for 24 hours before being hydrothermally reduced in a Teflon lined autoclave at 120°C for a specified amount of time, and then dried under vacuum at room temperature (RT) overnight.

5.2.5 Synthesis of HKUST-1 on Scaffolds

5.2.5.1 Ethanol/water Samples

Copper nitrate trihydrate $Cu(NO_3)_2.3H_2O$ (146 mg, 0.6 mmol) and BTC (trimesic acid) (280 mg, 1.3 mmol) were mixed together in a 1:1 water/ethanol volume to volume (v/v) solution (10 ml). Monoliths were placed in the solution and left to soak for 24 hours. Samples were placed in Teflon lined autoclaves and placed in an oven at 120 °C for 16 hours. Once cooled the materials were washed in ethanol for 24 hours then vacuum dried overnight at RT.

5.2.5.2 Dimethylsulfoxide (DMSO) HKUST-1 Samples

Stock solutions of $Cu(NO_3)_2 \cdot 3H_2O$ (1.22 g, 5.00 mmol) in BTC (0.58 g, 2.76 mmol) in 10 ml DMSO were used to soak both NH_2 functionalized and polyTEGDMA materials for 24 hours. Samples were placed in a Teflon lined autoclave and placed in an oven at 120 °C for 16 hours. Once cooled the materials were washed in ethanol for 24 hours then vacuum dried over night. For multiple loadings of HKUST-1, the procedure was simply repeated.

5.2.6 Experimental Procedure for Separations

The aligned porous HKUST-1 composite scaffolds were prepared inside a pipette tip. A 1:5 (v/v) monomer to solvent ratio was used using a 1:1 TMSPMA/EGDMA monomer mixture with 1 % DMPA initiator with respect to mass of monomers. The material was functionalized with APTES and loaded 3 times with HKUST-1 MOF using the DMSO method. The bottom of the pipette was plugged with glass wool and the dry monolith was glued back into the pipette end using a small amount of an insoluble adhesive. A 1:1 (v/v) mixture of ethyl benzene and styrene was pipetted on to the top of the monolith (varying between 5-50 μl). A small amount of sand was then placed on top of the monolith and heptane was passed through using gentle pressure from the pipette to separate the mixture.

5.3 Results and Discussion

5.3.1 Preparation of Aligned Porous Monolith and Surface Treatment

The directional freezing and frozen UV polymerization technique used in chapters 3 and 4 was again employed.[10,29] Monomer solutions were polymerized by UV irradiation in the frozen state to produce aligned porous monoliths. TMSPMA was selected as a monomer because our previous studies have shown that methacrylate monomers can be polymerized using this method. The monomer contains a trimethoxysilane group, which could be surface-functionalized with siloxy molecules after production of the aligned porous monolith (Scheme 1). TMSPMA was mixed with EGDMA (Scheme 1) on 1:1 and 9:1 (v/v) ratios.

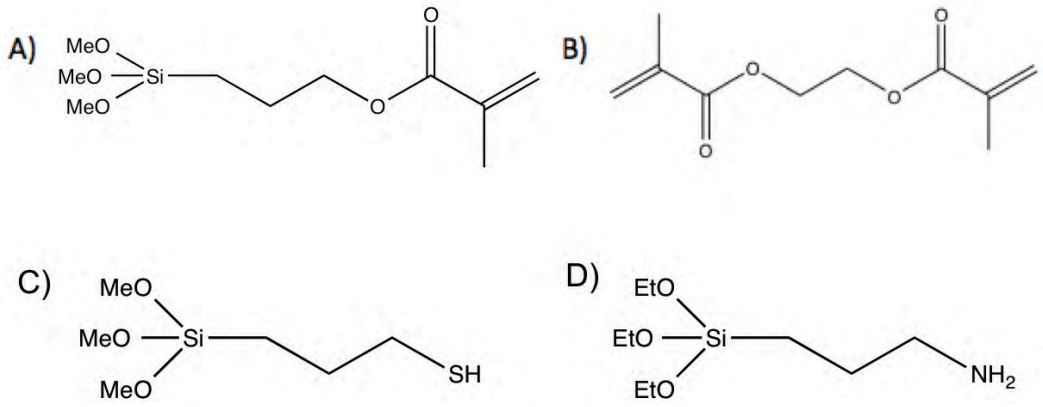

Scheme 5.1 A) TMSPMA monomer B) EGDMA crosslinker C) MPTMS D) APTES.

Monomer solutions with 1:5, 1:10 and 1:20 (v/v) monomer to dioxane ratios were investigated. The monomer solutions were directionally frozen and UV polymerized on dry ice for 7 hours. All samples prepared from 1:5, 1:10 (v/v) monomer to dioxane solutions produced materials with aligned porosity throughout (Figures 1A, B, D, & E). These materials appeared to be rigid and monolithic in nature. When the solutions were diluted to 1:20 (v/v), the resulting material contained some aligned features, however the structures exhibited a more fibrous nature (Figures 1C & F). These materials could not be reproduced as monoliths as they were very fragile and sometimes crumbled after the solvent removal step.

Scheme 5.2 shows the reaction scheme for functionalizing the surface of these materials. The monoliths were placed in 1 M HCL for 24 hours at 40 °C to hydrolyze the trimethoxysilane groups to silane triol groups. Normally, acid or base treatment can be used for the hydrolysis step to form silanol groups.[30,31] Silanol groups can self-condense in solution with other silanol and alkoxysilane molecules to form silica-based gels.[32-34] Polycondensation of tetraethyl orthosilcate (TEOS) is a good example of this.[31,35] However the self-condensation reaction is less likely to happen as the O-H bond is part of the aligned porous scaffolds and there is very low mobility for molecules to react. The hydrolyzed scaffolds underwent condensation reactions via solution treatment with alkoxysilane molecules MPTMS and APTES to anchor thiol and primary amine functionality to the surface of the scaffolds.

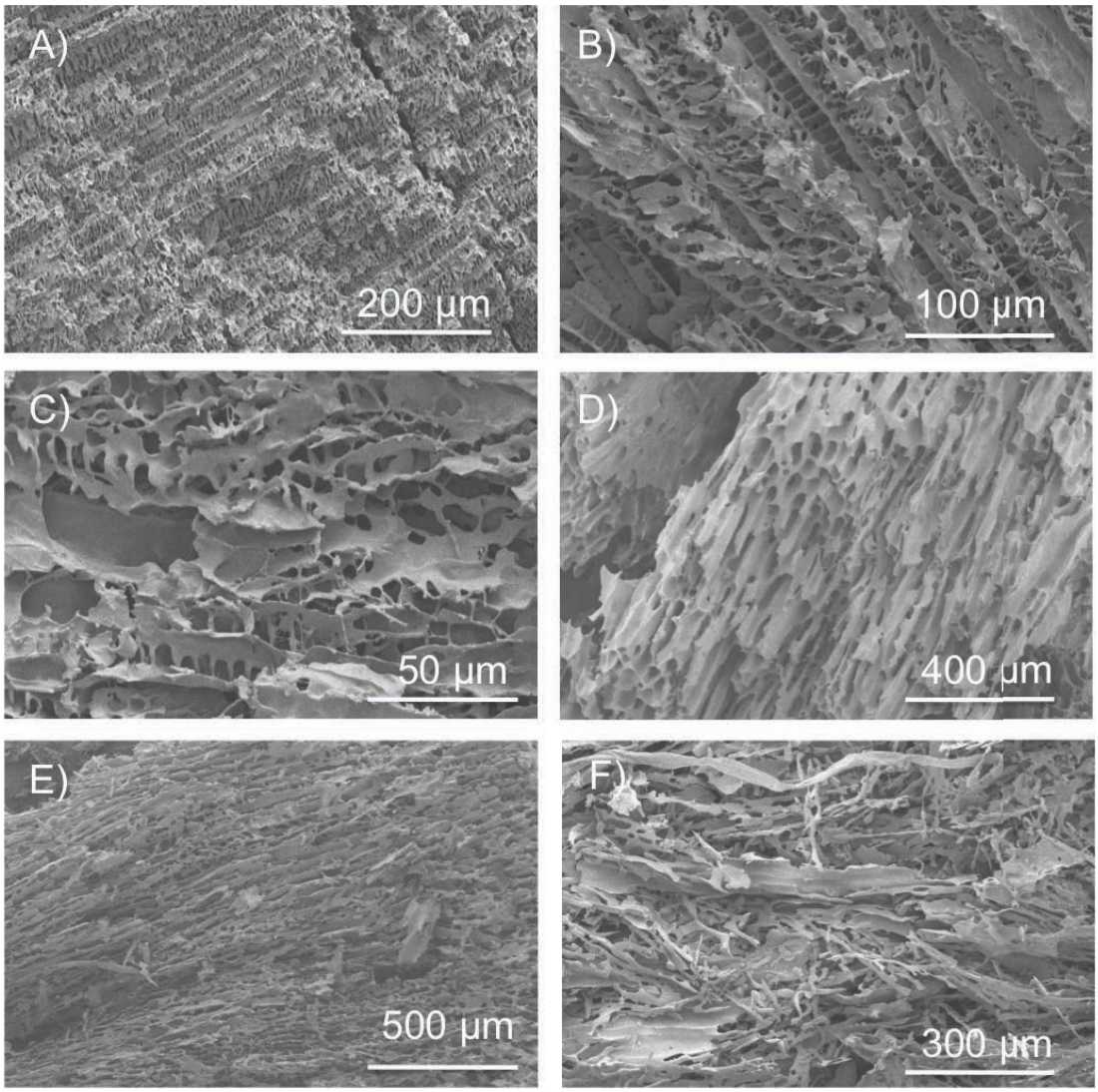

Figure 5.1 Pore morphologies of materials obtained from directional freezing and UV polymerization of solutions of 9:1 TMSPMA/EGDMA (v/v) monomer mixture in dioxane A) 1:5 (v/v) B) 1:10 (v/v) C) 1:20 (v/v) and 1:1 TMSPMA/EGDMA (v/v) monomer mixture in dioxane D) 1:5 (v/v) E) 1:10 (v/v) F) 1:20 (v/v).

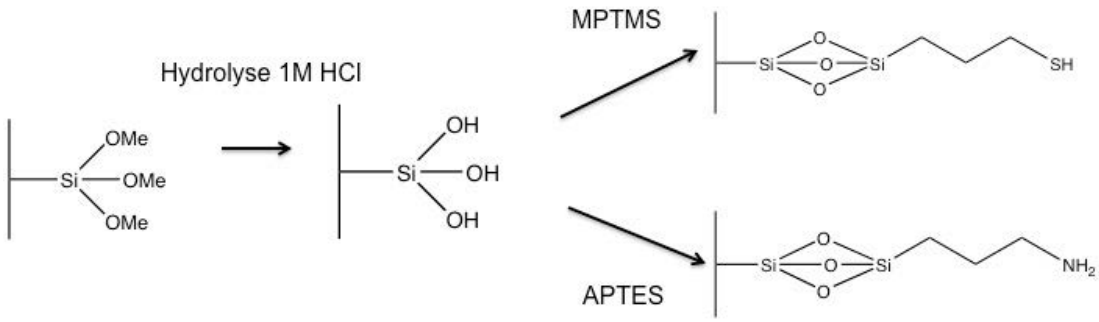

Scheme 5.2 Reaction scheme for functionalizing the surface of the aligned porous silica monoliths using MPTMS and APTES.

MPTMS was chosen to make aligned porous silver composites because it contains a thiol group which has a high affinity for metal ions such as silver or gold.[36,37] For the MOF composites, the material was functionalized with APTES which contains a primary amine group. HKUST-1 was selected as the MOF component of the composite as previous studies have suggested that HKUST-1 can grow from a surface via covalent interaction containing N-H and COOH groups,[26] although the mechanism for this interaction is not fully understood. Also, HKUST-1 composites have recently been used as a component in silica composites for separation purposes.[22] A monomer mixture containing 9:1 TMSPMA/EGDMA (v/v) mixture was used for preparing silver coated materials, as the polymeric structures will contain more methoxysilane groups than the 1:1 TMSPMA/EGDMA (v/v) mixture and could result in a higher loading of silver on the surface of the materials. A 1:1 TMSPMA/EGDMA (v/v) monomer mixture was used to make HKUST-1 MOF composite materials. This is because stationary phases for HPLC need to be rigid enough to cope with high pressures and as the monomer mixture contains 50 % (by volume) of EGDMA, the resulting materials should be rigid. More crosslinker makes the porous structure more rigid by increasing the amount of knitting together of polymer chains. After solution treatment of all the materials it was important to show that both the functionalization process had worked, and the aligned porous morphology was retained. Figure 5.2 shows that after solution treatment with both MPTMS and APTES the scaffolds prepared from both 1:5 and 1:10 (v/v) monomer/dioxane solutions retained the aligned porous morphology. More importantly, the samples did not crumble and stayed in the form of a monolith.

To determine whether the functionalization process had worked, the dry monoliths were washed continuously for 24 hours with toluene so any unreacted APTES or MPTMS was washed away from the surface of the scaffold. After the monoliths were dried FTIR measurements were taken to check for specific functional groups. Figure 3 shows FTIR spectra for materials produced from 1:10 monomer to dioxane (monomer solution contains 9:1 TMSPMA/EGDMA (v/v)) where the blue line represents the unfunctionalized material, the red line represents hydrolyzed material and the purple line represents this material after treatment with MPTMS. The green line represents APTES functionalized material which is made up from monomer

solutions of 1:10 monomer/dioxane, however the monomer concentration in this case consisted of 1:1 TMSPMA/EGDMA (v/v).

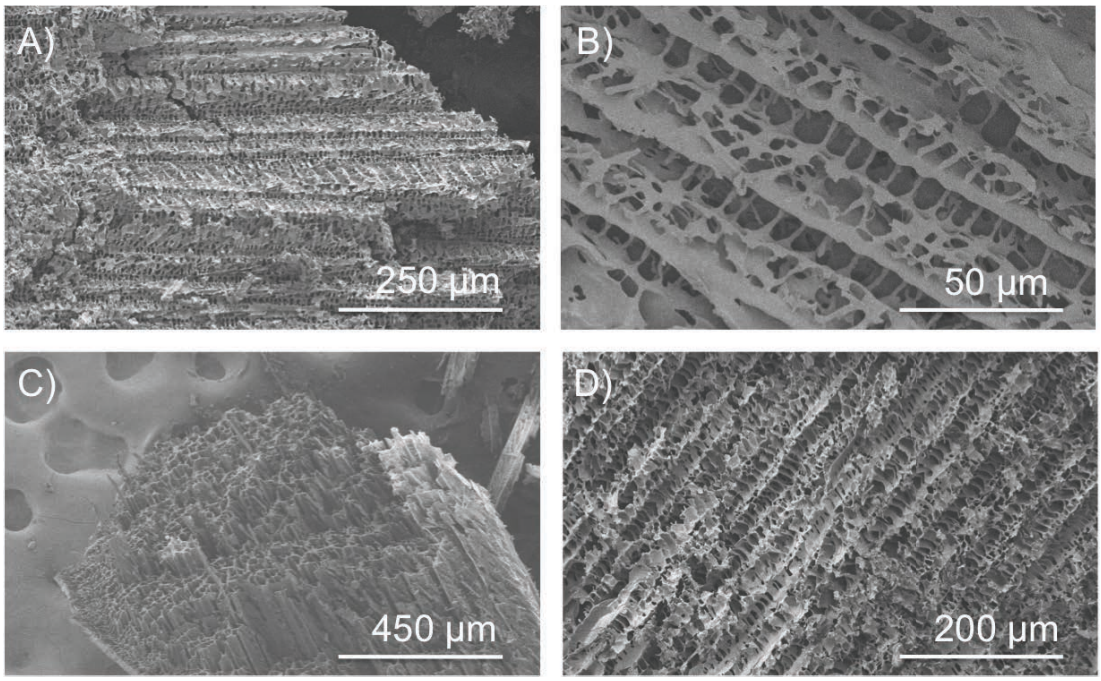

Figure 5.2 Aligned porous materials after surface modification with MPTMS A) 1:5 monomer/dioxane (v/v) B) 1:10 monomer dioxane (v/v) (monomer mixture 9:1 TMSPMA/EGDMA) and APTES C) 1:5 monomer/dioxane (v/v) D) 1:10 monomer dioxane (v/v) (monomer mixture 1:1 TMSPMA/EGDMA).

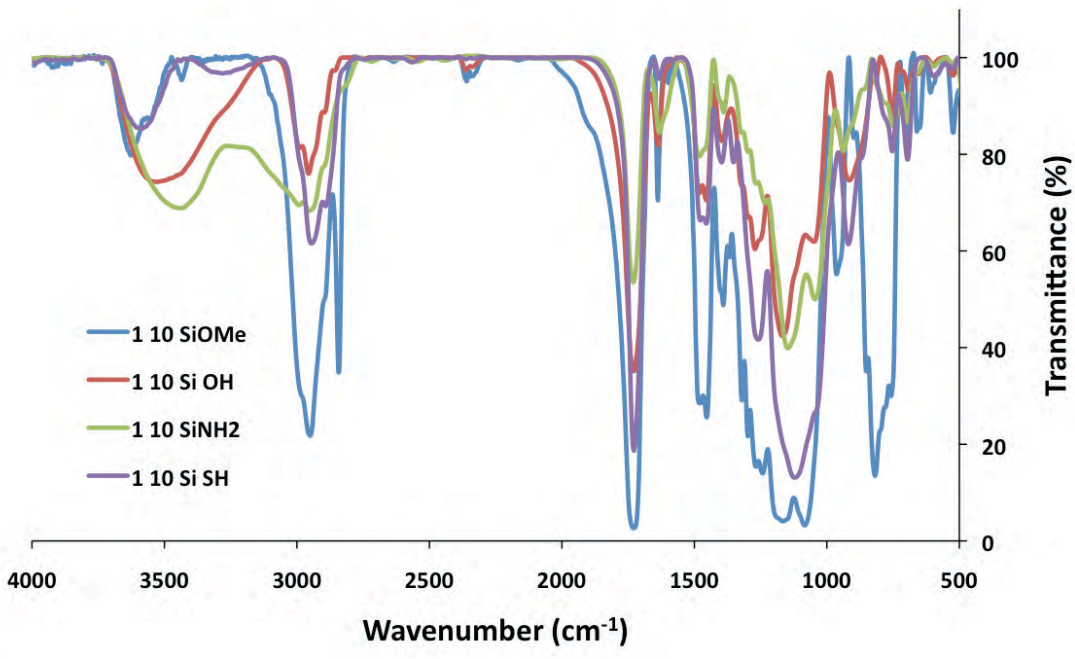

Figure 5.3 FTIR spectra of samples before and after functionalization.

From the IR spectra alone it is unclear whether the functionalization process has worked. Typically thiol peaks are observed between 2550 and 2600 cm^{-1} and N-H bonds are observed at 3600 cm^{-1}. For the material treated with MPTMS no peak is observed for the thiol group. This could be because the material is made up of mostly crosslinked TMSPMA and EGDMA so the broad peaks in the observed at 2900 cm^{-1} (C-H), 1700 cm^{-1} (C=O) and 1100 cm^{-1} (Si-O-Si) reflect this. The thiol group could be too dilute in comparison to other functional groups to appear on the spectra. Also, for the material treated with APTES, it is difficult to predict whether the peak observed at 3500 cm^{-1} is due to N-H functionality or an O-H group obtained after the hydrolysis step. Therefore the same samples were submitted for elemental analysis (CHN) which can give the percentage by mass of carbon, hydrogen and nitrogen within a material. It can also provide a yes or no answer for the presence of sulfur but not the percentage by mass. The results are shown in Table 5.1.

Table 5.1 Elemental content of samples.

Sample	C %	H %	N %	S
1:10 $Si(OMe)_3$	53.56	7.19	0	✗
1:10 $Si(OH)_3$	52.81	6.63	0	✗
1:10 SH (treated with MPTMS)	45.38	6.54	0	✓
1:10 NH_2 (treated with APTES)	42.94	6.45	2.74	✗

The $Si(OMe)_3$ refers to the unfunctionalized material after polymerization. The percentage by mass of carbon is lowered from 53.56 to 52.81% after the hydrolysis step. This could be due to the $Si(OMe)_3$ groups on the surface of the scaffold being replaced with $Si(OH)_3$ groups. The material treated with MPTMS is shown to contain sulfur although the amount is still unknown, and the percentage carbon is reduced further. Material treated with APTES was shown to contain 2.74% nitrogen. The small percentage by mass of nitrogen is expected as each APTES molecule only contains 1 atom of nitrogen. This result indicated that the functionalization step was successful and further surface treatments could be attempted.

5.3.2 Aligned Porous Silver Composites

The scaffolds that were treated with MPTMS to anchor thiol groups on the surface were further treated to covalently attach silver and produce aligned porous conductive monoliths. This was achieved by soaking the thiolated material in a solution of silver nitrate for 24 hours. Hydrothermal reduction in an autoclave was used to reduce the silver ions in the presence of the monolith. Varying scaffold porosity, concentration and reaction time was investigated to optimise the loading of silver and produce conductive material.

5.3.2.1 Scaffolds Prepared from 1:5 Monomer to Dioxane (v/v) Solutions

For scaffolds prepared from 1:5 monomer/dioxane solutions (v/v), a controlled experiment was conducted to see if varying the synthesis time would alter % upload of silver onto the monolith. Three samples of similar mass were used and all soaked in 2 grams silver nitrate overnight in 10 ml water. They were then placed in an autoclave and hydrothermally reduced for different times. The mass increase for different synthesis times (2, 5, and 24 hours at 120 °C) is shown in Table 5.2 and SEM images of the surface morphology are shown in Figure 5.4. As expected when the reaction time was longer, more of the silver nitrate was reduced on to the surface of the monolith. When left for 24 hours the mass of the monolith increased by 340%. The aligned porous structures are maintained throughout for all samples and the pore walls appear to be smooth. After loading with silver there was distinct change in appearance, and the monolith changed from a white colour to silver throughout (Figure 5.5). When the silver samples were tested for conductivity they had very high resistance values which were out of the range of the sourcemeter. This is consistent with the scaffolds prior to loading, and could suggest that the silver on the surface could be made up of small aggregates that are not in contact with each other.

Table 5.2 Mass increase with different reaction times.

Sample (time)	Mass before loading (g)	Mass after loading (g)	% Increase of mass
1 (2 hours)	0.0772	0.2017	261%
2 (5 hours)	0.0857	0.2400	280 %
3 (24 hours)	0.0700	0.2381	340 %

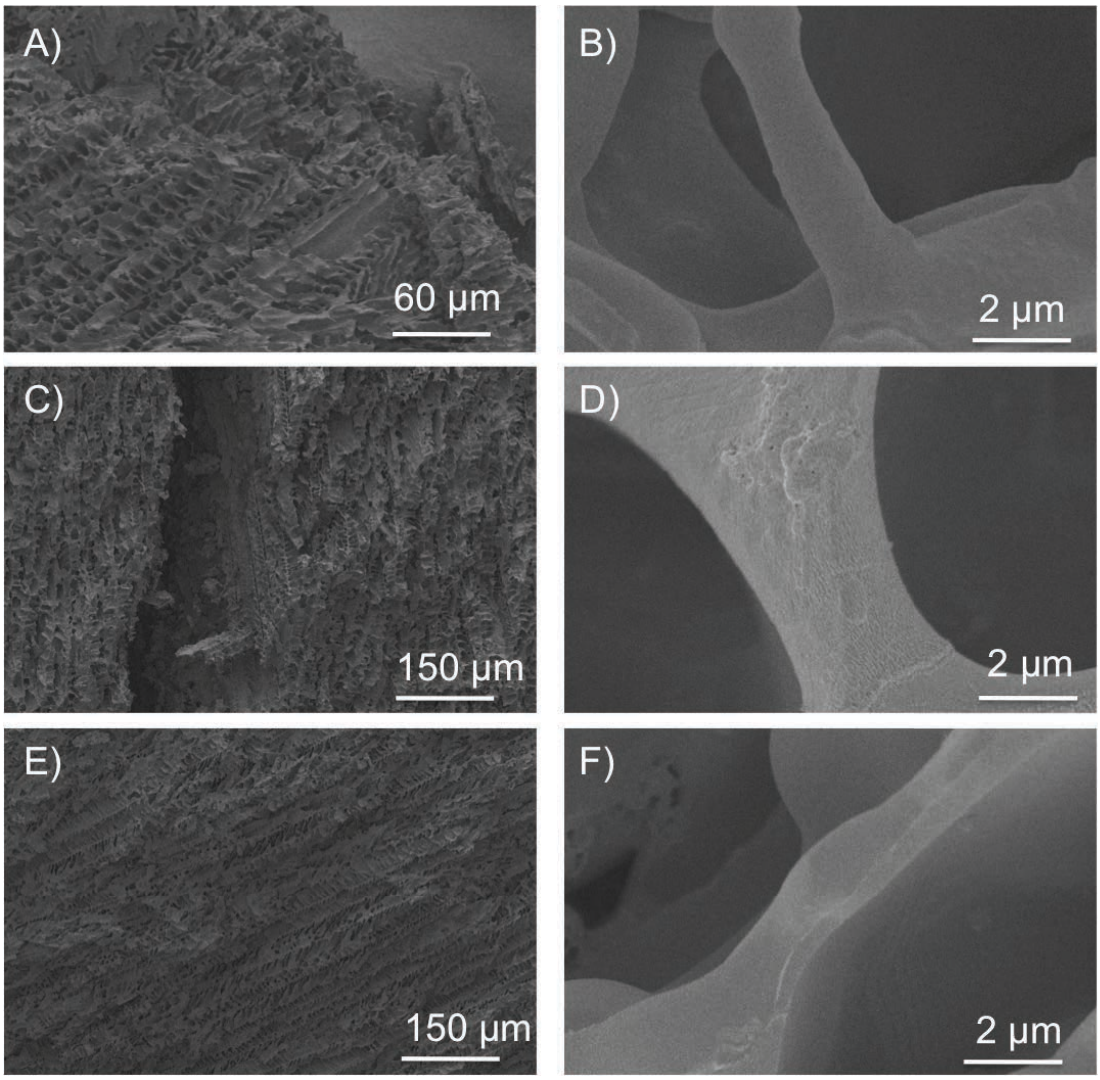

Figure 5.4 Pore morphologies of materials obtained from 1:5 monomer to dioxane (9:1 TMSPMA/EGDMA (v/v) monomer mixture) in dioxane after loading silver on to the surface with different reaction times A) B) 2 hours C) D) 5 hours E) F) 24 hours.

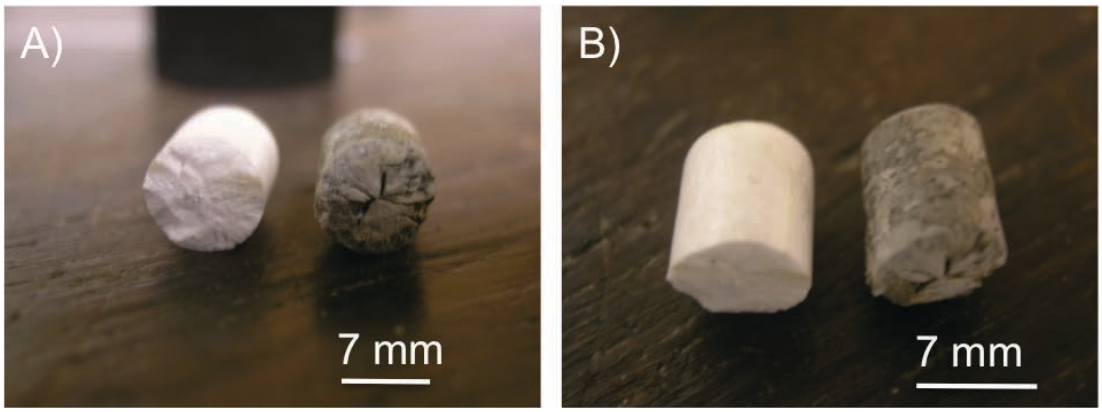

Figure 5.5 A) B) Materials obtained from directional freezing and UV polymerization of solutions of 1:5 monomer to dioxane (9:1 TMSPMA/EGDMA (v/v) monomer mixture) in dioxane and treated with MPTMS (left) and loaded with silver for 24 hours (right). Monoliths are 7 mm in diameter.

5.3.2.2 Scaffolds Prepared from 1:10 Monomer to Dioxane (v/v) Solutions

For scaffolds prepared from 1:10 monomer/dioxane solutions (v/v), four samples of similar mass were used to determine the loading using different amounts of silver nitrate. The samples were soaked in 0.075, 0.15, 0.3 and 2 g of silver nitrate in 10 ml water overnight then hydrothermally reduced in an autoclave at 120 °C for 24 hours.

The mass increases are shown in Table 5.3 show the mass increases with different amounts of silver nitrate in the solution. The percentage increase in mass between samples containing 0.3 g and 2 g of silver nitrate is not as big as expected, which could mean when 2 g of silver nitrate was used the maximum loading for this method could be close to 300% (Table 5.3). The aligned porous morphology is demonstrated as before with smooth pore walls (Figure 5.6).

Table 5.3 Mass increases using different amounts of silver nitrate.

Sample (mass of silver nitrate used in g)	Mass before loading (g)	Mass after loading (g)	% Increase in mass
1 (0.075)	0.0863	0.1508	174.7 %
2 (0.15)	0.0760	0.1525	200.7 %
3 (0.3)	0.0927	0.2277	245.6 %
4 (2)	0.0701	0.2002	285.7 %

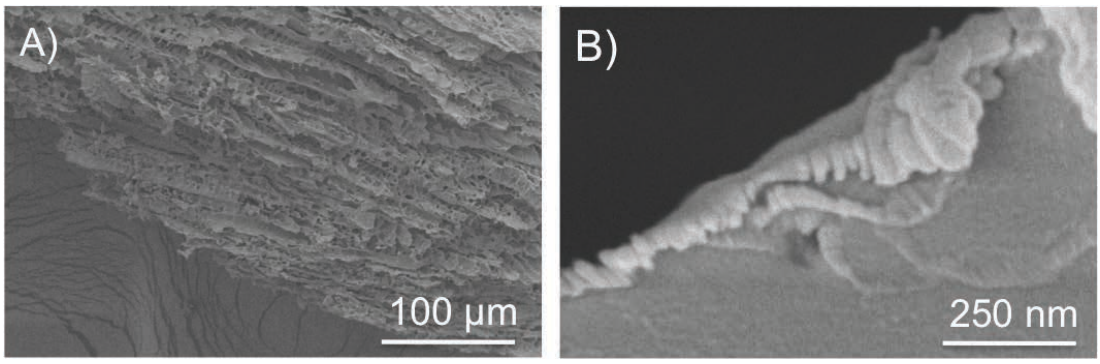

Figure 5.6 A) Pore morphology of materials obtained from directional freezing and UV polymerization of solutions of 1:10 monomer to dioxane (9:1 TMSPMA/EGDMA (v/v) monomer mixture) in dioxane and post functionalized with silver (sample 4 from Table 5.3). B) Highly magnified image of the surface of the material.

Again, when the samples were tested for conductivity the readings on the sourcemeter were out of range indicating that the materials had a very high resistance. This could be because the silver did not form a conductive network on the surface of the scaffold. To better understand the elemental arrangement on the surface energy-dispersive X-ray spectroscopy (EDX) was used. The technique relies on high-energy electron beams exciting characteristic X-rays within a sample which reveal the presence of different elements on a surface. To take an EDX reading first the SEM was used to focus on a flat part of the scaffold. Figure 5.7 shows how each element is distributed with coloured representation. Within a highly crosslinked structure it is likely elements are distributed randomly throughout, this is reflected in the images were each element appears randomly scattered. Figure 5.7G shows that the surface contains silver aggregates which do not appear to be in contact. For conductive materials a more homogenous covering of silver could be required. Figure 5.8 shows the percentage by mass of each element on the surface.

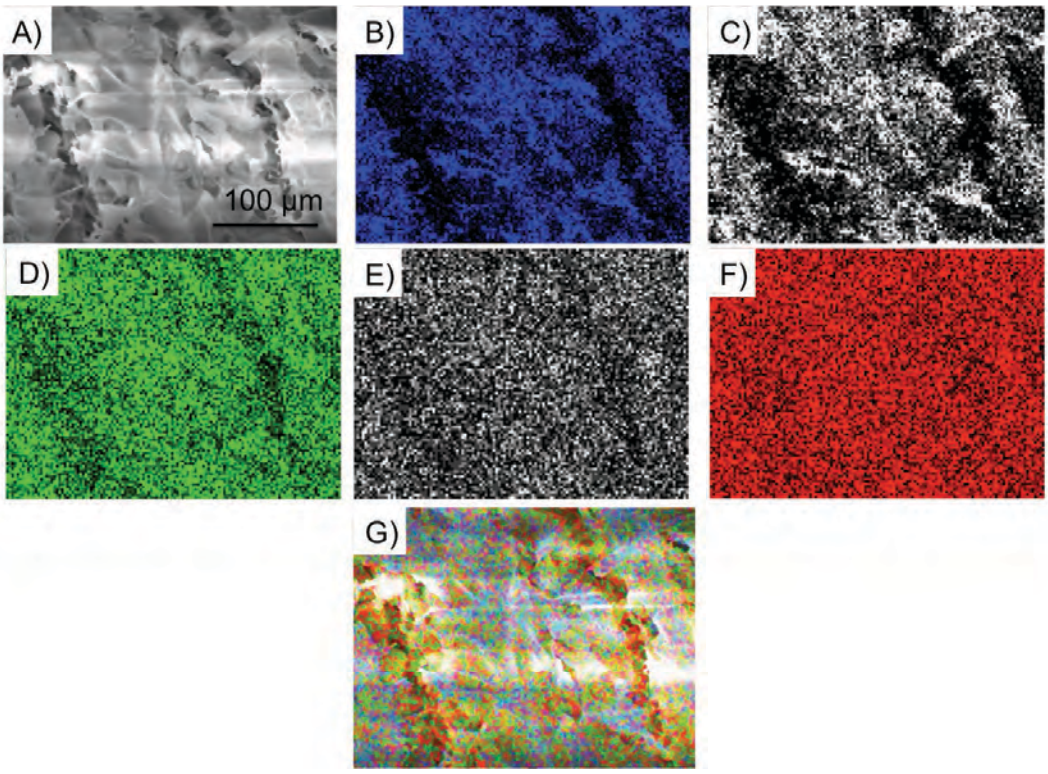

Figure 5.7 EDX surface elemental data of sample 4 from Table 5.2 showing coloured representations of the distribution of elements on the surface of the material A) Original SEM microscope image B) Carbon C) Oxygen D) Silicon E) Sulfur F) Silver G) Combined elements.

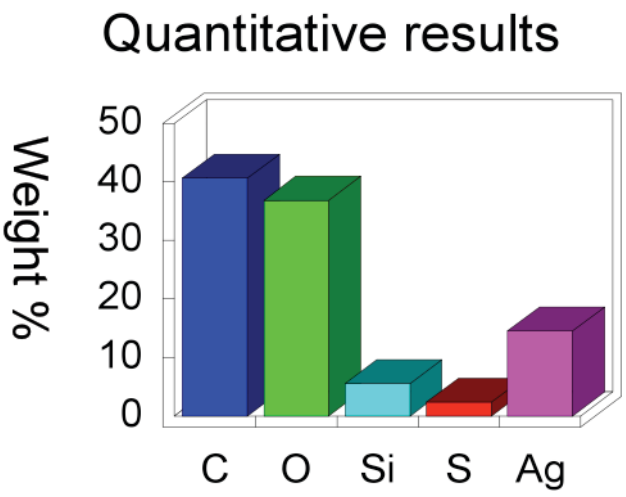

Figure 5.8 Bar chart showing percentage by mass of each element on the surface of the material.

This EDX data gives further confirmation that the functionalization step was successful and the percentage by mass of sulfur on the surface of the composite is 2.32%. The relatively small amount of silver (14.57 %) could be a further reason for low conductivity of samples.

A calcination experiment was carried out to determine if it is possible to create conductive composites, by heat-fusing the soft silver metal on the surface. This method has previously been used to heat-fuse aligned microwires, creating a smooth metallic surface whilst retaining the aligned microwire structure.[38] The four samples from Table 5.3 were calcined at 300 °C overnight and the mass loss was recorded (Table 5.4).

Table 5.4 Mass losses after calcination of samples.

Sample	Mass before (g)	Mass after (g)	% Mass loss
1	0.0093	0.0040	57.0
2	0.0145	0.0063	56.6
3	0.0165	0.0070	57.5
4	0.0155	0.0080	51.6

After calcination the samples shrunk considerably and lost between 51-57% of their mass. The colour changed from silver to a dark blackish colour. The materials

remained intact retaining the monolithic form. However, they became mechanically weak and fragile. When the calcined materials were tested for conductivity the resistance values were again out of range of the sourcemeter. This means that the silver within the composite has not formed a homogenous conductive network. SEM images show how the aligned porous structure was retained after calcination (Figure 5.9A). The images are from sample 4 in Table 5.4 which had the highest mass loss. At higher magnification the surface appears blotchy compared to the samples before calcination which had a smooth surface. This could be due to aggregated silver that has clumped together during heat treatment, or be a result of a high contact angle on the surface preventing formation of a continuous film.

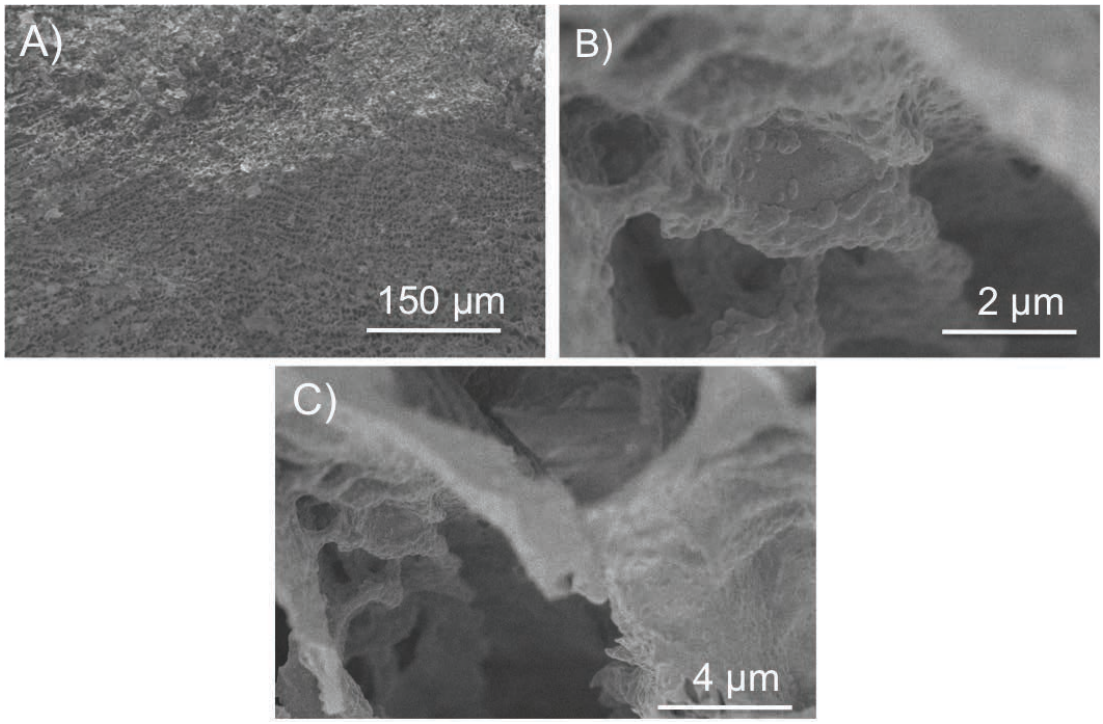

Figure 5.9 SEM images of material obtained after sample 4 from Table 5.4 was heated at 300°C for 15 hours A) aligned porous structure B) C) high magnification images of the surface.

Even though it has proved unsuccessful to construct conductive aligned porous silver composites, it is believed these materials could be investigated for catalytic or antimicrobial applications. Also the thiolated material could be investigated for water treatment as the thiol group has an affinity for many heavy metal ions.[39]

5.3.3 Aligned Porous MOF Composites

HKUST-1 is a thermally stable cubic MOF with a structure $Cu_3(BTC)_2(H_2O)_3$ that can be made from copper nitrate trihydrate and organic linker trimesic acid also known as 1,3,5-benzenetricarboxylic acid (BTC).[40] Surface areas of HKUST-1 can range from between 650-1900 m^2/g depending on the method of production.[40,41] The aim was to maximize the loading of HKUST-1 MOF composites on an aligned porous scaffold and assess the composite materials as a stationary phase for the separation of organic compounds. To maximize the loading, polyTEGDMA scaffolds from chapter 3 were compared with aligned porous organosilica scaffolds containing primary amine groups on the surface after functionalization with APTES. Also, two different solvothermal methods of producing HKUST-1 were compared: an ethanol and water mixture and dimethyl sulfoxide.

5.3.3.1 Ethanol and Water samples

An ethanol/water mixture was used to prepare HKUST-1 and to compare loading on polyTEGDMA and NH_2 functionalized scaffolds. The synthesis was conducted in an autoclave for 16 hours in the presence of each scaffold.[26] Materials were investigated with different porosity to determine whether loading could be increased on a more porous scaffold. To achieve different levels of porosity the monomer solutions were simply varied in concentration before they were directionally frozen and polymerized on ice/dry ice. For this study 1:5, 1:10 and 1:20 (v/v) monomer to dioxane solutions were used. The loading of samples was worked out by weighing the monolith before and after loading with HKUST-1. An average was calculated from 3 samples of the same porosity. The results in Table 5.5 show that on average the NH_2 functionalized scaffolds are loaded with more HKUST-1 than polyTEGDMA scaffolds with the same porosity. The numbers highlighted in yellow show the average percentage by mass of HKUST-1 within the resulting composites. Samples prepared from 1:5 monomer to dioxane (v/v) solutions contain the lowest amount of MOF, which is expected as these are the least porous scaffolds. As the porosity is increased using 1:10 and 1:20 monomer to dioxane (v/v) solutions the loading increases, and the NH_2 functionalized composites contain considerably more HKUST-1 than their polyTEGDMA counterparts. The general appearance of the composites reflects the loading values obtained. The appearance of the scaffolds is white until loaded with HKUST-1 when the scaffolds turn a blue colour reflecting the colour of HKUST-1

crystals. PolyTEGDMA samples loaded with HKUST-1 appear patchy, however NH_2 functionalized scaffolds are covered with more homogenous layer of HKUST-1 (Figure 5.10).

Table 5.5 Mass increases when HKUST-1 MOF is synthesized in an ethanol and water mixture in the presence of the aligned porous scaffolds.

Sample	Mass before (g)	Mass after loading (g)	% Mass increase	% MOF	Average % MOF
1:5 TEG1	0.1314	0.1530	16.0	14.0	18.0
1:5 TEG2	0.1112	0.1220	9.7	8.9	
1:5 TEG3	0.0891	0.1291	44.0	31.0	
1:10 TEG1	0.1589	0.2015	26.8	21.1	22.7
1:10 TEG2	0.1954	0.2700	38.2	27.6	
1:10 TEG3	0.1463	0.1812	23.9	19.3	
1:20 TEG1	0.0998	0.1516	51.9	34.2	32.7
1:20 TEG2	0.1123	0.1947	73.4	42.3	
1:20 TEG3	0.1087	0.1385	27.4	21.5	
1:5-NH_2 1	0.1123	0.1463	30.3	23.2	18.4
1:5-NH_2 2	0.1527	0.1808	18.4	16.1	
1:5-NH_2 3	0.1476	0.1758	19.1	16 .0	
1:10-NH_2 1	0.0560	0.0745	33.0	24.8	26.0
1:10-NH_2 2	0.0752	Solvent evaporated	--------		
1:10-NH_2 3	0.0576	0.0791	37.3	27.1	
1:20-NH_2 1	0.0466	0.0789	69.0 Did not stay intact- crumbled	40.1	40.1

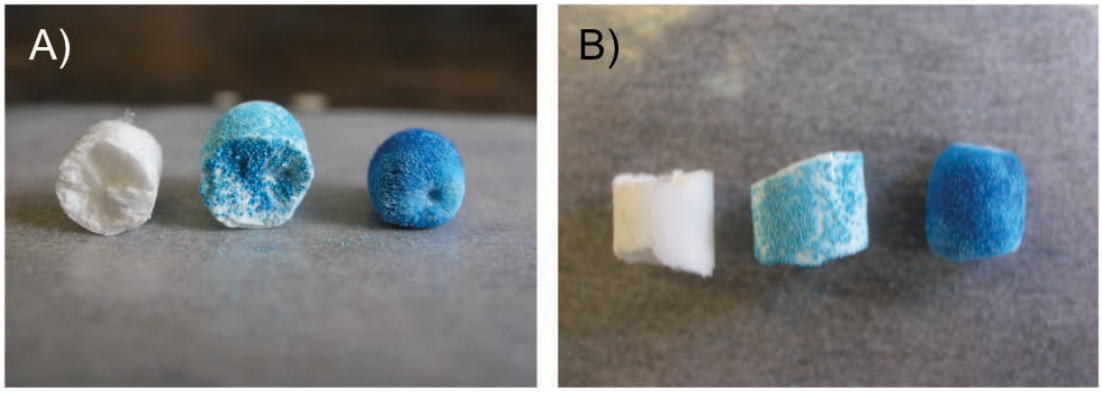

Figure 5.10 A) Cross section B) birds eye view of scaffold and composite materials. The sample on the left is a scaffold prepared from 1:10 TEGDMA/dioxane (v/v), then loaded with HKUST-1 using the EtOH/H_2O method (centre) and a composite material (right) made using 1:10 monomer/dioxane (v/v) of the TMSPMA/EGDMA mixture then NH_2 functionalized before preparing HKUST-1 in the presence of the scaffold. Monoliths are 7 mm in diameter.

SEM images were taken to show that covering of the pore walls with HKUST-1. For polyTEGDMA samples larger crystals have formed on the exterior of the samples (Figure 5.11A), with very small coverage of HKUST-1 on the inside of pores (Figure 5.11B). For NH_2 functionalized scaffolds the loading appeared greater, however complete surface coverage was not achieved (Figure 5.11C & D). This data supports what can been seen with the naked eye (Figure 5.10).

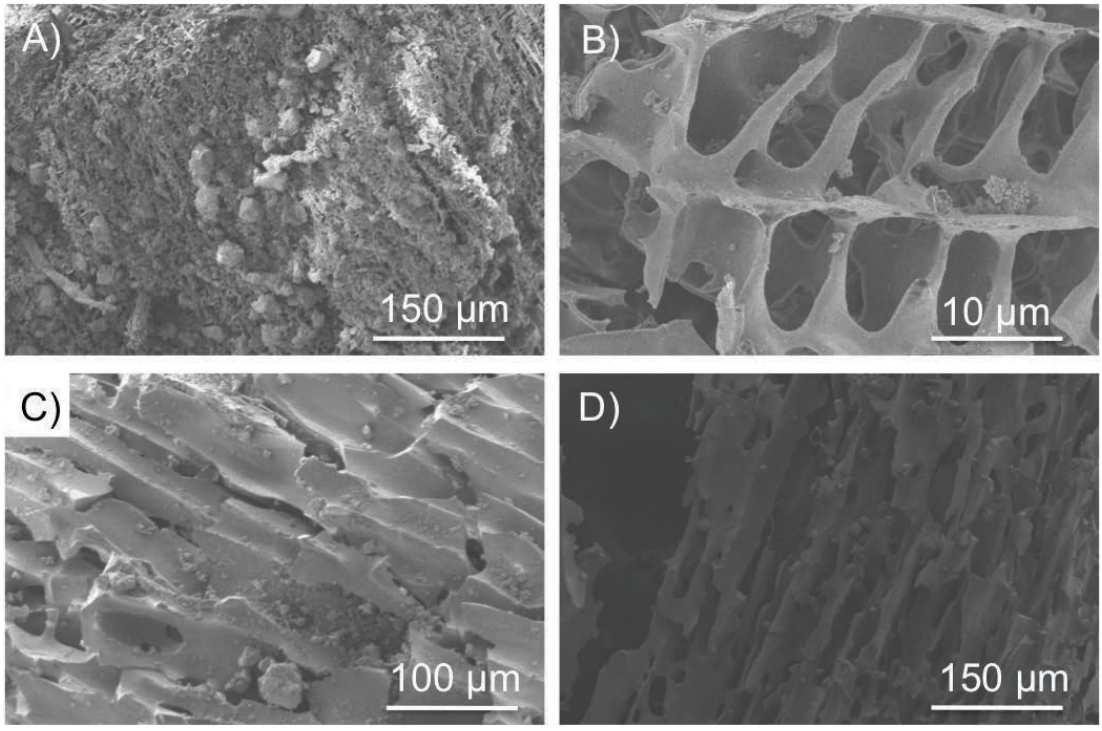

Figure 5.11 SEM images of aligned porous MOF composites prepared using EtOH/H_2O. Scaffolds were prepared from solutions: A) 1:10 TEGDMA/dioxane (v/v) B) 1:20 TEGDMA/dioxane (v/v) and NH_2 functionalized material prepared from solutions of C) 1:5 monomer/dioxane (v/v) D) 1:10 monomer/dioxane (v/v) containing a monomer mixture of 1:1 TMSPMA/EGDMA (v/v).

BET surface areas were taken to show the difference between in surface area between composites when using TEGDMA and NH_2 functionalized scaffolds. When BET measurements were taken on aligned porous polyTEGDMA scaffolds in chapter 3 values of 0-11 m^2/g were obtained. This is characteristic of macroporous scaffolds. As previously stated, surface areas for HKUST-1 can range from between 650-1900 m^2/g depending on the method of production. For hierarchically micro/macroporous composite systems we would expect the surface areas to be somewhere between the BET values for both the micro and macroporous

components individually depending on the ratio of each material. This has been the case for previously prepared micro/macroporous composites.[26,42] For BET surface area measurements 100 mg was taken from the interior of each composite. Table 5.6 shows a big difference between TEGDMA and NH_2 functionalized composites with the same porosity, where the TEGDMA composite has a surface area of 1.77 m^2/g suggesting a very low loading of HKUST-1. The surface areas for NH_2 functionalized composites are considerably higher ranging for 53-201 m^2/g demonstrating that as the porosity of the scaffold and subsequent loading increases, so too does surface area.

Table 5.6 BET surface areas of aligned porous MOF composites prepared using EtOH/H_2O method.

Sample	BET 5 point surface area (m^2/g) to 3 s.f
1:10 TEG HKUST-1	1.77
1:5 NH_2 HKUST-1	53.1
1:10 NH_2 HKUST-1	117
1:20 NH_2 HKUST-1	201

5.3.3.2 DMSO Samples

HKUST-1 can be synthesized using various solvents,[22,26,43] so it is important to compare more than one solvent method for seeding of HKUST-1 within the aligned porous scaffolds prepared using directional freezing and frozen UV polymerization. Moreover, the highly crosslinked scaffolds have been shown to be hydrophobic[10] meaning organic solvents could be better for seeding HKUST-1 and lead to higher loading than composites prepared using an ethanol/water procedure. Table 5.7 shows loading values obtained for aligned porous composite prepared using DMSO.

The loading of HKUST-1 was achieved by soaking the scaffold for 24 hours in a DMSO solution consisting of copper nitrate and BTC. Again the reaction took place in an autoclave at 120°C for 16 hours. Generally, the loading values obtained using DMSO are higher than loadings obtained when using an ethanol/water mixture. This could be due to two factors. The hydrophobic properties of the scaffolds prevent the diffusion of water into all areas including the smaller interconnected pores. Also the DMSO method yields more MOF overall than the ethanol/water method. This study

is focused on the composite material rather than the crystal size so the concentration of precursor solutions were kept constant throughout.

Interestingly, the % loading of HKUST-1 using DMSO was very similar for polyTEGDMA and NH_2 containing scaffolds. In both cases composites prepared from 1:10 and 1:20 (v/v) monomer to dioxane solutions contained between 46-54% HKUST-1. On further inspection of the surface it is clear the loading is more homogenous on the NH_2 containing scaffold. The polyTEGDMA samples higher loading is due to HKUST-1 building up on the exterior of the monolith and the cross-section image shows the loading in the middle of the sample is not uniform (Figure 5.12A).

Table 5.7 Mass increases when HKUST-1 MOF is synthesized in DMSO in the presence of the aligned porous scaffolds.

Sample	Start Mass	After Loading of HKUST-1	% Mass increase	% MOF	Average MOF %
1:5 TEG 1	0.1785	0.2683	50.6	33.5	33.3
1:5 TEG 2	0.0744	0.1131	52	34.2	
1:5 TEG 3	0.1330	0.2055	54.5	35.2	
1:10 TEG1	0.0782	0.1698	117.1	53.9	49.9
1:10 TEG 2	0.1121	0.1907	70.1	41.2	
1:10 TEG 3	0.0469	0.1032	120	54.5	
1:20 TEG 1	0.0352	0.0798	126.7	55.9	53.8
1:20 TEG 2	0.0433	0.0943	117.8	54.1	
1:20 TEG 3	0.0327	0.0673	105.9	51.4	
1:5-NH_2 1	0.1832	0.3050	66.5	39.9	39.1
1:5-NH_2 2	0.2108	0.3424	62.4	38.4	
1:5-NH_2 3	0.1696	0.2779	63.9	38.9	
1:10-NH_2 1	0.1280	0.2492	94.7	48.6	46.6
1:10-NH_2 2	0.0906	0.1639	80.9	44.7	
1:10-NH_2 3	0.1117	0.2091	87.2	46.6	
1:20-NH_2 1	0.0571	0.1122	96.5	49.1	49.7

SEM images show moderate loading of HKUST-1 on the surface of the pore walls of polyTEGDMA scaffolds (Figure 5.13A &B). For scaffolds containing NH_2 groups the loading on the pore walls appears more uniform and in some places the pores are completely covered with HKUST-1 (Figure 5.13C- F). However for separation applications, complete surface coverage must be achieved.

Figure 5.12 Optical image showing cross sections of aligned porous MOF composites prepared using DMSO. The loadings between polyTEGDMA scaffolds (left) are compared with NH_2 functionalized scaffolds (right). Scaffolds were prepared using 1:10 monomer/dioxane (v/v) solutions. Monoliths are 7 mm in diameter.

As before, 100 mg was taken from the centre of the composites for surface area measurements. This means that any extra HKUST-1 on the outside of the monoliths was not included. Table 5.8 shows that in general composites made from NH_2 scaffolds have a higher surface area than polyTEGDMA samples with the same porosity. This was expected because the loading of HKUST-1 appeared more uniform on NH_2 functionalized scaffolds.

The loading of HKUST-1 on polyTEGDMA shows no trend with respect to surface area of the composite. The mass gain experiments show that as the porosity is increased the loading of MOF increased (Table 5.7). However the surface areas obtained do not reflect this because the loading is not homogenous and a lot of MOF was clumped together around the edge of the monolith. Surface areas for NH_2 functionalized composites are slightly higher and range from 265-358 m^2/g as the porosity of the scaffold is increased. They also show a trend, as the % content of MOF is increased the surface area increases. This is consistent with data that suggests the loading of HKUST-1 is more uniform on NH_2 functionalized scaffolds. So far, the data suggests that HKUST-1 formation is more uniform on NH_2 functionalized surfaces and overall loading is higher. It also shows, as expected, that organic solvent DMSO is a better solvent than an ethanol/water mixture in terms of maximizing the loading of HKUST-1 onto aligned porous surfaces.

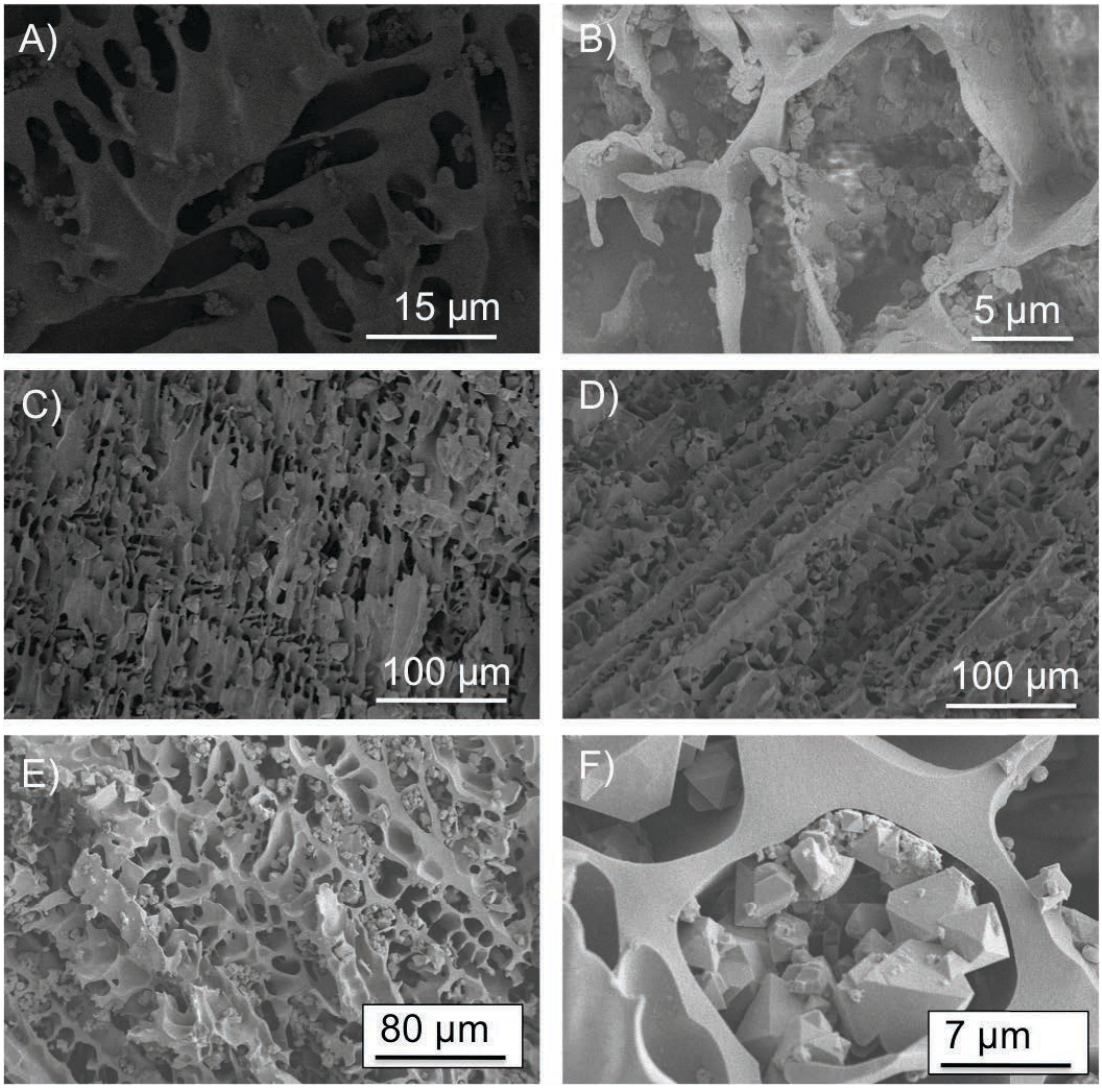

Figure 5.13 SEM images of aligned porous MOF composites prepared using DMSO. Scaffolds prepared from solutions of A) 1:10 TEGDMA/dioxane (v/v) B) 1:20 TEGDMA/dioxane (v/v) NH_2 functionalized material prepared from solutions of C) & D) 1:5 monomer/dioxane (v/v) E & F) 1:10 monomer/dioxane (v/v) containing a monomer mixture of 1:1 TMSPMA/EGDMA (v/v).

Table 5.8 BET surface areas of aligned porous MOF composites prepared using DMSO method.

Sample	BET 5 point surface area (m^2/g) to 3 s.f
1:5 TEG HKUST-1	156
1:10 TEG HKUST-1	158
1:20 TEG HKUST-1	277
1:5-NH_2 HKUST-1	265
1:10-NH_2 HKUST-1	315
1:20-NH_2 HKUST-1	358

5.3.3.3 Powder X-Ray Diffraction (pXRD)

Powder X-Ray diffraction was used to show the presence of crystalline MOF HKUST-1 on the amorphous aligned porous scaffolds. Firstly, aligned porous scaffolds and HKUST-1 scaffolds were tested separately. Amorphous patterns were observed for both polyTEGDMA (Figure 5.14A) and silica containing (Figure 5.14B) aligned porous scaffolds. This is expected as the scaffolds contain a highly crosslinked polymer network which have no periodicity and atoms are randomly distributed. This means X-rays are scattered in many directions leading to a large noisy bump in a wide range of 2θ instead of high intensity peaks observed for ordered crystalline material.

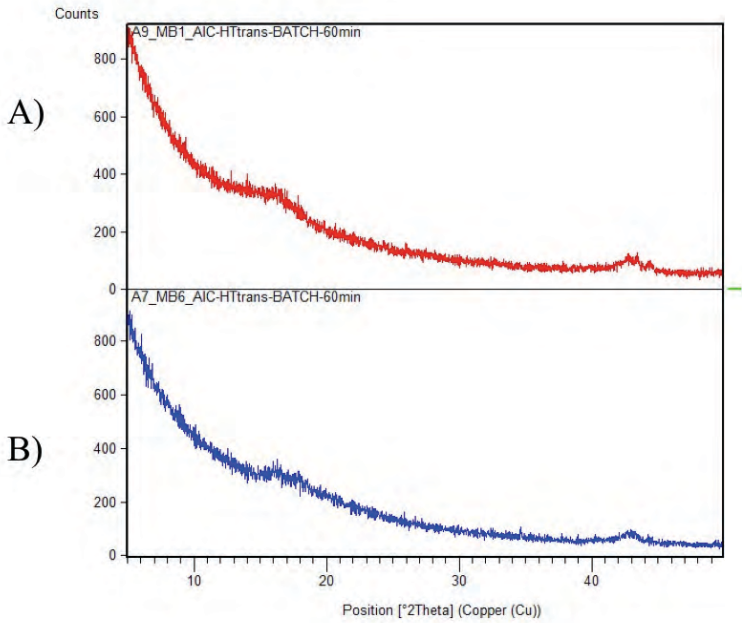

Figure 5.14 X-ray diffraction patterns of A) silica containing monolith before functionalization prepared from 1:10 monomer/dioxane (v/v) solution B) polyTEGDMA scaffold made from 1:10 TEGDMA/dioxane solution

For aligned porous HKUST-1 composites produced using an ethanol/water mixture, the powder X-ray pattern for polyTEGDMA appears to be noisy with no intense peaks, indicating a highly amorphous surface (Figure 5.15A). The mass gain experiments showed that when NH_2 functionalized scaffolds porosity increased, the loading of HKUST-1 increased and so did the surface area. Figure 5.15B-D show increasing amounts of characteristic HKUST-1 peaks as the scaffold porosity and loading increased. The scaffolds were prepared from solutions of 1:5 (Figure 5.15B),

1:10 (Figure 5.15C) and 1:20 (Figure 5.15D) (v/v) monomer to dioxane solutions. Although the cubic structure of HKUST-1 is already well known, the X-Ray pattern of pure HKUST-1 was recorded (Figure 5.15E). The X-Ray pattern of HKUST-1 recorded in Figure 5.15E matches those recorded in previous studies.[17,22,28,43] The patterns can be used to match Bragg reflections with any crystalline material present within the aligned porous composites. The X-Ray patterns for these composites contain amorphous backgrounds as the loading for composites prepared using an ethanol/water mixture was shown to be low compared to composites prepared from DMSO.

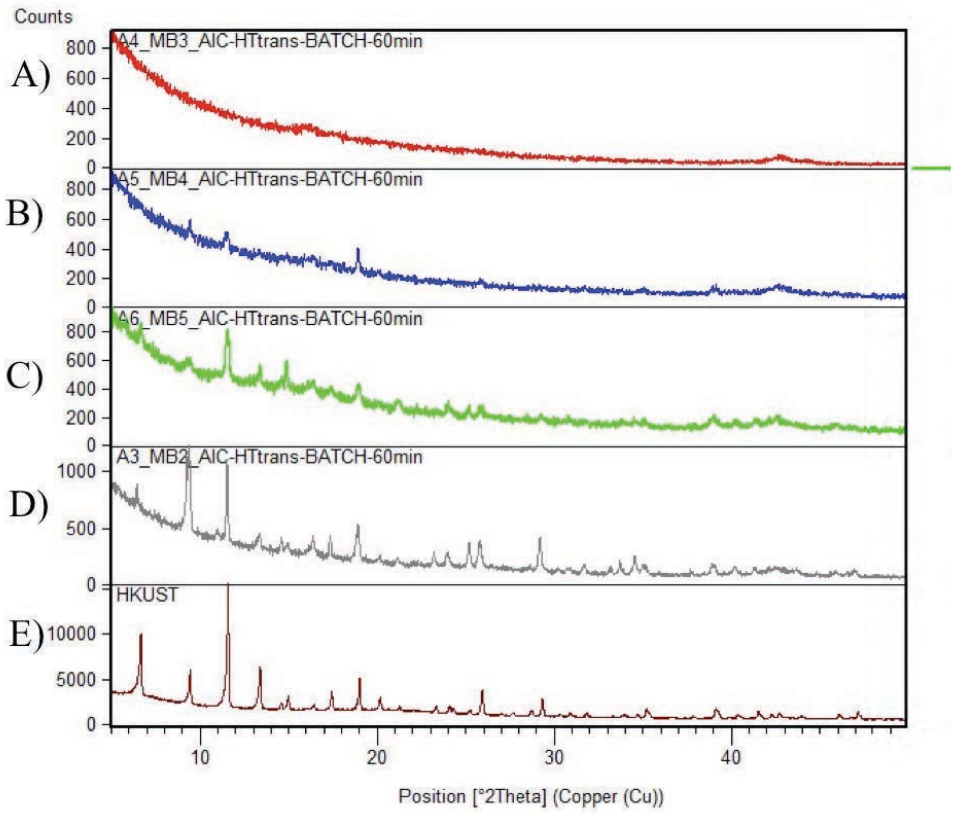

Figure 5.15 X-ray diffraction patterns for and aligned porous HKUST-1 composites prepared using EtOH/H_2O method. Scaffolds were prepared from solutions of A) 1:10 TEGDMA/dioxane (v/v) B) 1:5 C) 1:10 D) 1:20 monomer/dioxane (v/v) containing 1:1 (v/v) TMSPMA/EGDMA monomer mixture that was post functionalized with APTES. E) HKUST-1 metal organic framework

As expected, the peaks observed for composites prepared using the DMSO method appear to be more intense than those prepared using ethanol and water. For polyTEGDMA composites, intense characteristic peaks for HKUST-1 are observed.

The X-Ray patterns also contain small humps indicating the presence of the amorphous polyTEGDMA scaffolds (Figure 5.16A & B). For composites prepared on NH_2 functionalized scaffolds the intense peaks related to HKUST-1 are observed again (Figure 5.16C & D). Interestingly, the 'amorphous humps' observed for polyTEGDMA composites are not present. The X-Ray diffraction patterns for NH_2 functionalized HKUST-1 composites are remarkably similar to X-Ray patterns for pure crystalline HKUST-1 suggesting homogenous loading of MOF on the surface of the scaffold. We can conclude from this data that the best conditions investigated for loading HKUST-1 to aligned porous material are using DMSO solvent and having primary amine groups present on the scaffold surface.

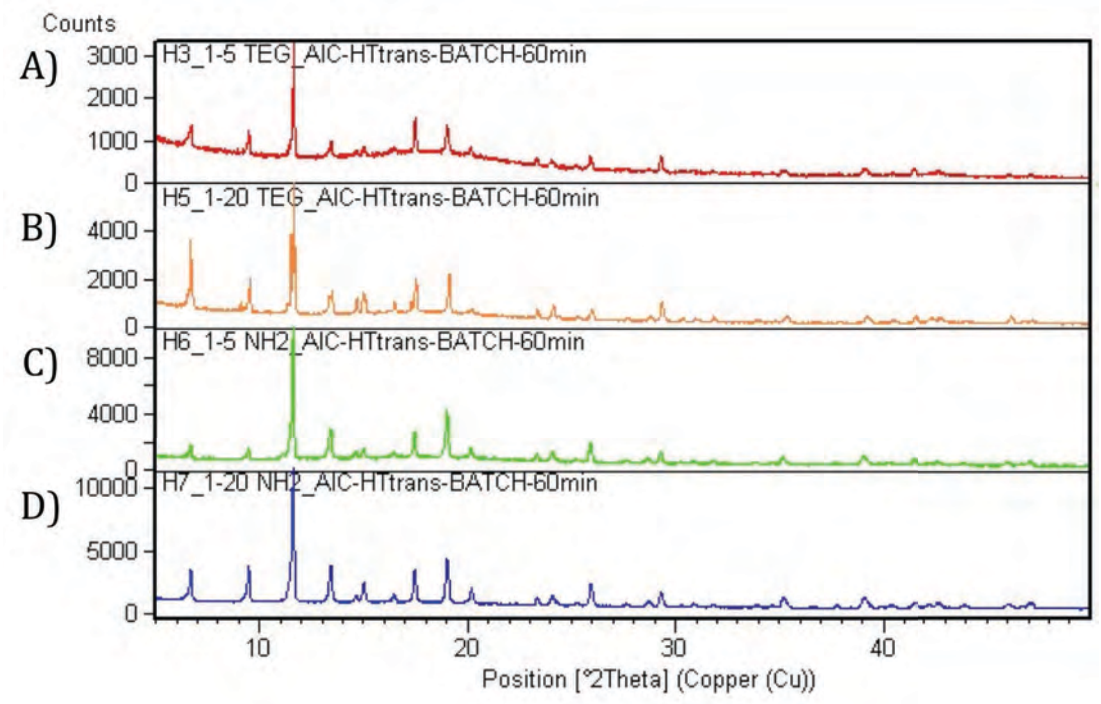

Figure 5.16 X-ray diffraction patterns for aligned porous HKUST-1 composites prepared using DMSO method. Scaffolds were prepared from solutions of A) 1:5 TEGDMA/dioxane (v/v) B) 1:20 TEGDMA/dioxane (v/v) C) 1:5 monomer/dioxane (v/v) D) 1:20 monomer/dioxane (v/v). The monomer mixture was made up of 1:1 TMSPMA/EGDMA (v/v), silica containing materials were post functionalized with APTES to contain NH_2 on the surface.

To improve surface coverage of HKUST-1 of NH_2 functionalized scaffolds one could simply repeat the autoclave synthesis, where the composite solution will be soaked in precursors copper nitrate and BTC before placing the reaction vessel in an oven at 120 °C. Before attempting this synthesis, thermogravimetric analysis (TGA) was used to determine the thermal stabilities of the scaffolds, HKUST-1 and

composite materials. The test measures the % mass loss of a material as the temperature is increased. Figure 5.17A shows TGA graphs for an NH_2 scaffold and HKUST-1 separately. The blue line shows the scaffold is stable up to about 250 °C when organic material is removed by heat up to 600 °C. At this point only 20 % of material is left. This is due to silica content within the material.

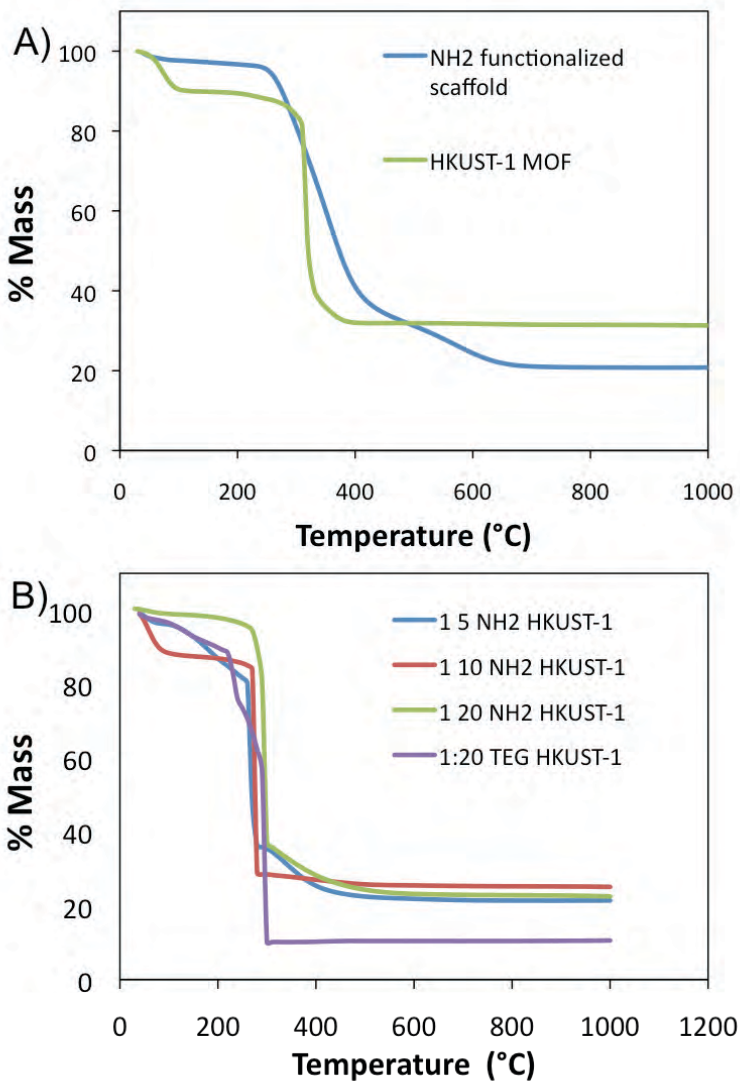

Figure 5.17 Thermogravimetric analysis (TGA) of A) Blue line- NH_2 functionalized scaffold, green line- HKUST-1 MOF B) Aligned porous HKUST-1 composites using NH_2 functionalized scaffolds: blue line-scaffold prepared using 1:5 monomer/dioxane (v/v), red line- scaffold prepared using 1:10 monomer/dioxane (v/v), green line scaffold prepared using 1:20 monomer/dioxane (v/v), purple line- polyTEGDMA HKUST-1 composite (scaffolds prepared using 1:10 monomer/dioxane (v/v)). All composites were prepared using DMSO method.

The initial mass loss observed for HKUST-1 (green line) is commonly observed, and is due to solvent trapped within the micropores of HKUST-1. The MOF is thermally

stable up to around 300 °C when the organic components begin to be removed by heat. After 400 °C, only copper oxide remains which is stable up 1000 °C. For all polymer composites the initial mass loss is again due to any solvent trapped with HKUST-1 (Figure 5.17B). All composites are stable up until 250 °C when the organic components are removed. This means repeated loading should be possible. It is difficult to work out precise loadings of HKUST-1 on NH_2 containing scaffolds as both copper oxide and silica remain after 400 °C. However it is possible to work out loading of polyTEGDMA composites as only copper oxide remains after 300°C after all polymer material is removed (purple line).

5.3.3.4 Multiple Loadings

Due to the thermal stability demonstrated by the composites, multiple loading procedures could be followed without compromising HKUST-1 produced in the previous step. Figure 5.18 shows how surface coverage of HKUST-1 is increased as the loading procedure is repeated. NH_2 functionalized aligned porous scaffolds were used and a DMSO loading method as this led to most uniform loading. Scaffolds prepared from 1:5 and 1:10 (v/v) monomer/dioxane solutions were used, as they are rigid enough to maintain an aligned porous morphology in solution after multiple loadings of HKUST-1. The most rigid samples were prepared from 1:5 monomer/dioxane (v/v) solutions as they contain more crosslinked polymer. Figures 5.18 A-C show increasing amounts of HKUST-1 with each loading step. The more porous scaffold prepared from 1:10 monomer/dioxane (v/v) solutions maintained an aligned porous morphology and monolithic form after multiple loadings. The surface coverage of HKUST-1 also increased with more loading steps (Figure 5.18 D-F). In both instances HKUST-1 is shown to grow on the surface of pore walls and fill the pore voids. BET surface area values given in Table 5.9 show that multiple loading cycles increases the overall surface area of the composites. For NH_2 functionalized composites prepared from 1:5 monomer/dioxane (v/v) solutions the surface area increases from 265 m^2/g after one loading to 612 m^2/g. For composites prepared from 1:10 monomer/dioxane (v/v) solutions, the surface area increased from 315 m^2/g after one loading to 825 m^2/g after three loading cycles. Scaffolds prepared from 1:10 solutions produce more porous material resulting in higher loading of HKUST-1 and overall surface area of the composite.

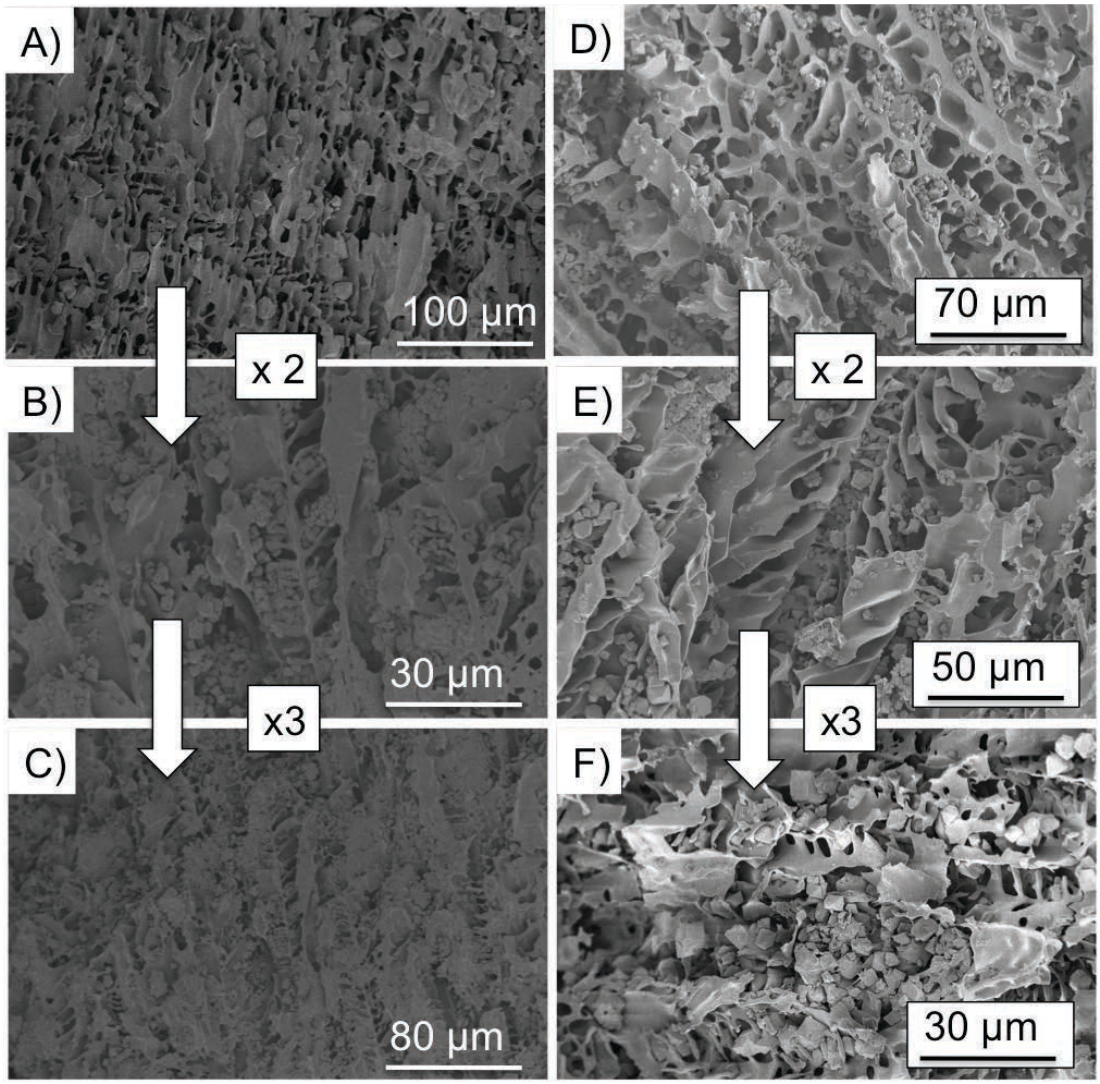

Figure 5.18 SEM images of aligned porous NH_2 functionalized polymer/HKUST-1 MOF composites prepared using DMSO loading method multiple times. Scaffolds were prepared from solutions of 1:5 monomer/dioxane (v/v) and loaded A) 1 B) 2 C) 3 times and a 1:10 monomer/dioxane (v/v) loaded D) 1 E) 2 F) 3 times. The monomer mixture is made up of 1:1 TMSPMA/EGDMA (v/v).

Table 5.9 BET surface areas of NH_2 functionalized scaffolds loaded multiple times with HKUST-1.

Sample	BET 5 point surface area (m^2/g) to 3 s.f
1:5-NH_2 HKUST-1 (one loading cycle)	265
1:5-NH_2 HKUST-1 (two loading cycles)	451
1:5-NH_2 HKUST-1 (three loading cycles)	612
1:10-NH_2 HKUST-1 (one loading cycle)	315
1:10-NH_2 HKUST-1 (two loading cycles)	693
1:10-NH_2 HKUST-1 (three loading cycles)	825
1:20-NH_2 HKUST-1 (one loading cycle)	358

The increase in surface area after multiple loading suggests that the composites are thermally stable and they are also stable under pressure. This could be useful for heterogeneous catalytic purposes where solutions require heat or pressure for chemical reactions to take place. To show the correlation between loadings vs surface area the samples listed in Table 5.9 were correlated with the percentage by mass content of HKUST-1 within the composite material. Each sample in Table 5.9 is colour coordinated with a data plot in Figure 5.19A. The relationship between percentage by mass of MOF within the composite seems to be linear with respect to surface area.

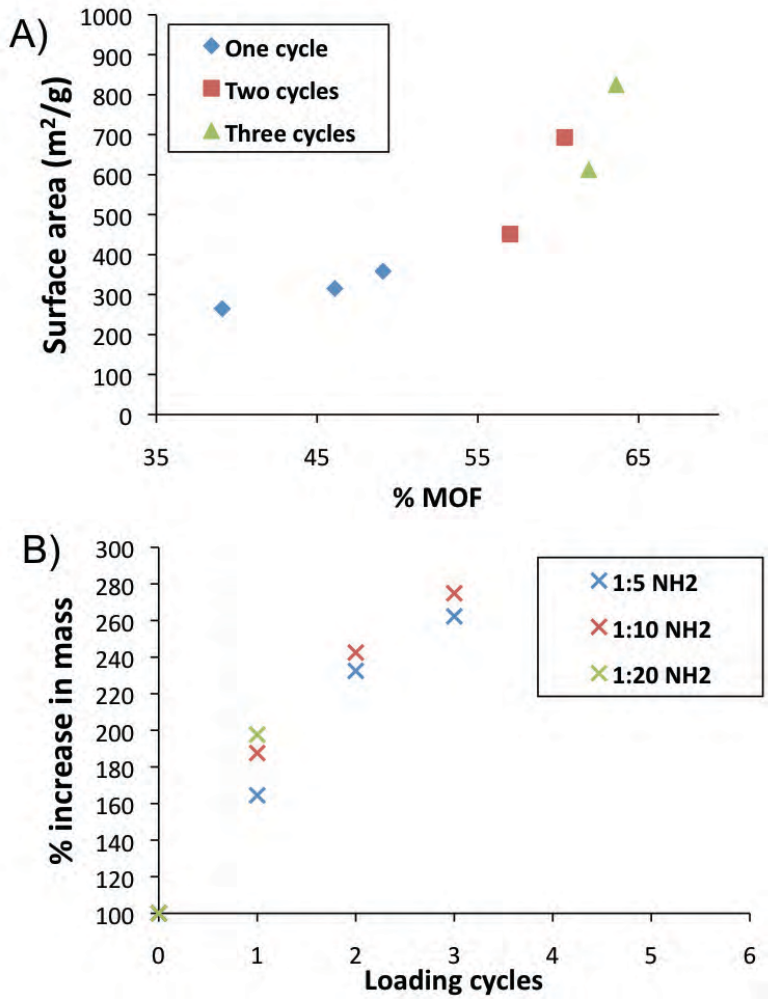

Figure 5.19 Graphs showing A) Relationship between % by mass of MOF within the composites vs BET surface area B) % increase in mass as the amount of loading cycles is increased.

Taking the functionalized scaffolds mass as 100 % the percentage increase in mass with each loading step is given in Figure 5.19B. After each loading excess MOF built up on the surface of the monolith was wiped away with greaseproof paper so the loading refers only to MOF forming within the scaffold. The graph shows that with

each loading step, the percentage increase in mass is lower due to pores becoming more full with HKUST-1 after each loading step. The sample prepared from 1:20 monomer/dioxane crumbled after one loading cycle as the scaffold was too mechanically weak. Therefore multiple loading values and surface areas could not be obtained.

The increase in surface area of composites with each loading cycle suggests that the crystal structure of HKUST-1 is not compromised. It also suggests that HKUST-1 is not simply washed away from the pores. X-Ray diffraction patterns for double (Figure 5.20A) and triple loaded (Figure 5.20B) composites maintain a highly crystalline surface.

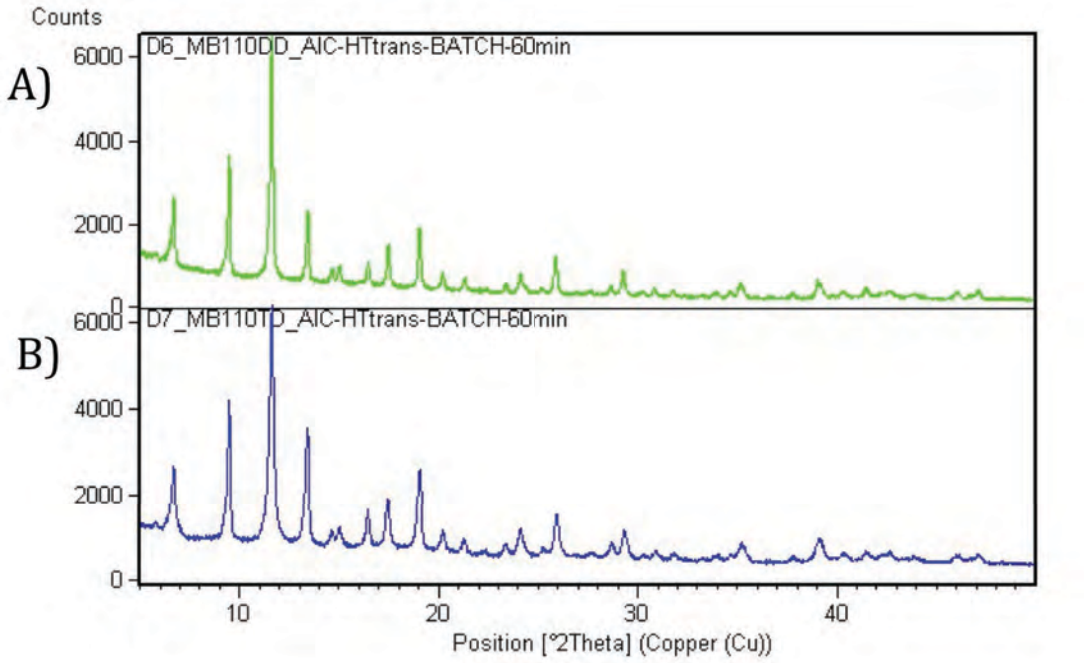

Figure 5.20 X-ray diffraction patterns for NH_2 functionalized polymer/HKUST-1 composites loaded with MOF more than once. Scaffolds were prepared using 1:10 monomer/dioxane (v/v) soluions consisting of 1:1 TMSPMA/EGDMA (v/v) monomer mixture. Samples were loaded using DMSO method A) loaded twice B) loaded three times.

5.3.3.5 Aligned Porous MOF Composite as Stationary Phase for Separation

After finding the best conditions for preparing aligned porous HKUST-1 composites and increasing the surface coverage using multiple loading, the composites were assessed as a stationary phase for HPLC. To do this a triple loaded NH_2 functionalized composite was prepared in the tip of an Eppendorf pipette. Scaffolds

made from 1:5 monomer/dioxane (v/v) solutions were selected because they were the most rigid and therefore easier to handle and could be more reusable. Any shrinkage problems caused by the solvent removal after directional freezing and frozen UV initiated polymerization are minimized as the composite can be pushed further down the pipette tip after loading. After loading three times with HKUST using the DMSO method the sample was glued into the pipette tip with an insoluble resin to stop any leakage down the side of the composite (Figure 5.21A). The bottom of column was plugged with glass wool to stop any HKUST-1 falling into the recorded fractions.

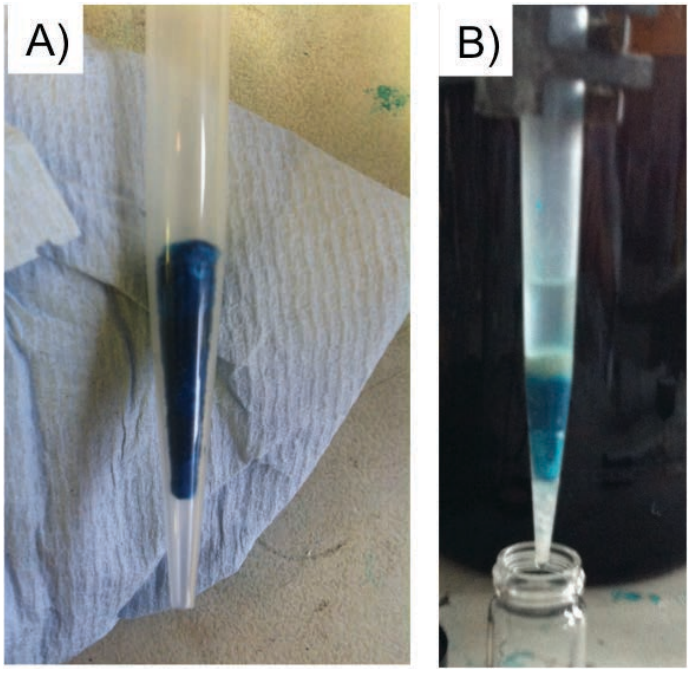

Figure 5.21 Aligned porous HKUST-1 MOF composites prepared in Eppendorf pipette tips using NH_2 functionalized scaffold and 1:5 monomer/dioxane (v/v) ratio. Scaffolds were loaded three times with HKUST-1 MOF using DMSO method. A) Monolith inside pipette tip B) monolith plugged underneath with glass wool and used as stationary phase for separation of organic mixture. Sand was used to stop mixture diffusing into the solvent above.

The separation mixture was placed on top of the dry composite and small amounts of sand placed on top to stop any separation components passing back into the mobile phase as it was passed through the column. The mobile phase could then be passed through the aligned porous HKUST-1 composite by applying small amounts of pressure from the pipette (Figure 5.21B). For this study styrene and ethyl benzene were selected as the separation mixture and heptane selected as the mobile phase. Pure HKUST-1 has been used previously to separate styrene and ethyl benzene

however irregular particle size led to low efficiency and large back-pressures. These parameters were improved significantly when HKUST-1 was incorporated into silica microspheres.[23]

To show that pure HKUST-1 and the aligned polymer composites prepared in this study have an uptake affinity for styrene and ethyl benzene, a preliminary experiment was conducted. Three solutions of 5 µl 1:1 ethyl benzene/styrene (v/v) in heptane were prepared. In one solution 0.3 g of pure HKUST-1 was placed. In another, a 0.3g triple loaded polymer HKUST-1 composite was placed, and the other solution was kept pure. The solutions were left to stir gently for 24 hours in sealed vessels before a 0.5 ml fraction was taken from each solution and injected into the gas chromatography (GC) machine. Figure 5.22 shows GC chromatograms for the three solutions. The retention time of a compound in a GC column is governed by the boiling point. Ethyl benzene has a boiling point of 136 °C and styrene 145 °C, so ethyl benzene (left peak) is eluted slightly before styrene (right peak).

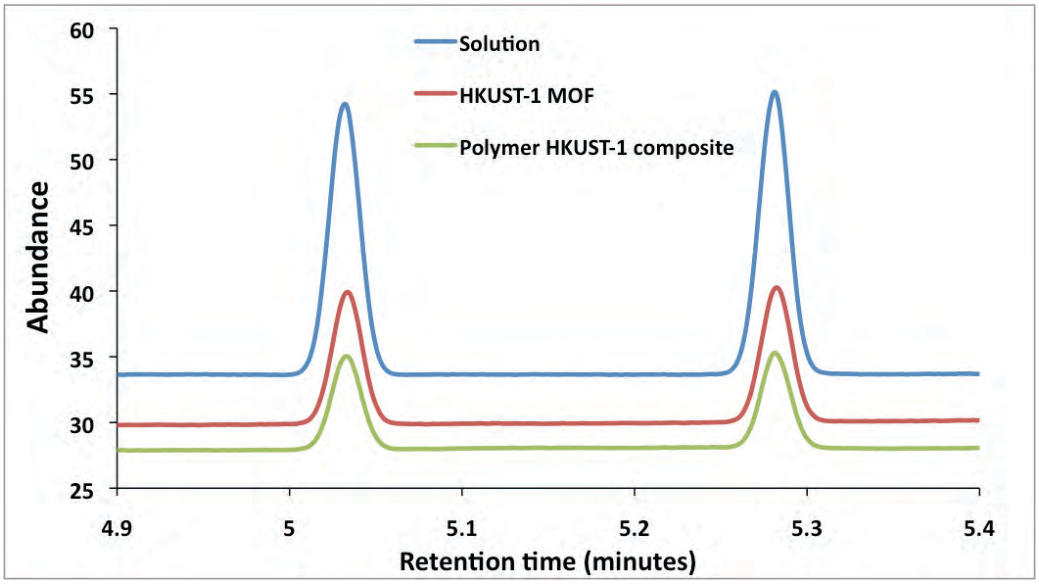

Figure 5.22 GC chromatogram of a solution of 5 µl ethyl benzene/ styrene (v/v) mixture in 5 ml heptane: Blue line-pure solution, red line – after soaking 0.3g HKUST-1 in solution for 1 day, green line-after soaking NH_2 functionalized polymer/MOF composite (loaded three times) in same solution for one day.

The abundance of a compound is proportional to the peak height or peak area given in the chromatogram. The pure solution has peak heights of about 20 for ethyl benzene and styrene, whereas the solutions that had HKUST-1 and polymer-

HKUST-1 materials present had peak heights between 7 and 8 for both compounds. This suggests HKUST-1 uptakes both styrene and ethyl benzene.

An aligned porous NH_2 fuctionalized polymer HKUST-1 composite that was loaded three times with HKUST-1 was loaded into the Eppendorf pipette tip as shown in Figure 5.21B. 5 ml of heptane was used to pass through 5 µl of the separation mixture. Initially ten 0.5 ml fractions were taken and injected into the GC machine. The peak heights given in table show that in the 10 fractions only ethyl benzene was eluted and styrene is retained in the column. This is expected as styrene has a C=C bond and is more likely to have π-π interactions with the BTC component of HKUST-1.

Table 5.10 Peak heights after 5 µl 1:1 ethyl benzene/ styrene (v/v) mixture was passed through a 0.3 g column made from NH_2 functionalized polymer/MOF composite (loaded three times) with 5 ml of heptane. 0.5 ml fractions were taken.

Fraction	Peak Height (ethyl benzene)	Peak height (styrene)
1	48.08	0
2	40.46	0
3	27.66	0
4	24.52	0
5	15.93	0
6	15.37	0
7	13.12	0
8	12.66	0
9	17.86	0
10	16.89	0

In an attempt to isolate styrene as well as ethyl benzene the experiment was repeated. However instead of taking 0.5 ml fractions, ten 1 ml fractions were taken. Figure 5.23 shows the GC chromatograms for the first four fractions. It appears most of the ethyl benzene was eluted in the first fraction with a small amount of styrene. The next three fractions showed small amounts of each compound, and the final six fractions had peak heights of zero for ethyl benzene and styrene. This indicates that whilst ethyl benzene is being eluted from the columns, most of the styrene is retained.

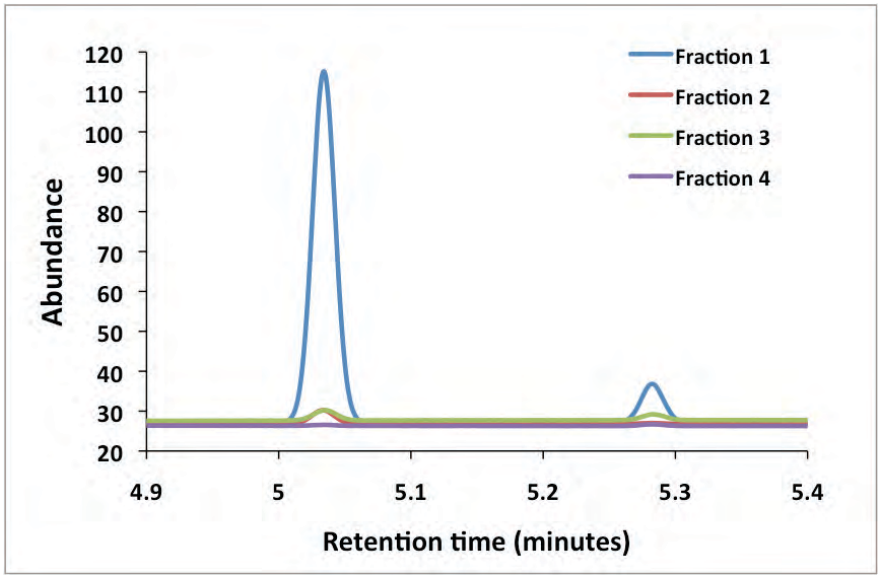

Figure 5.23 GC chromatograms showing peak heights after 5 µl 1:1 ethyl benzene/ styrene (v/v) mixture was passed through a 0.3 g column made from NH_2 functionalized polymer/MOF composite (loaded three times) with 10 ml of heptane. 1 ml fractions were taken.

To show that styrene was being retained within HKUST-1 in the composites, a 50 µl separation mixture was passed through the same column with 15 ml of heptane taking 1.5 ml fractions. The chromatograms of the first two fractions are shown in Figure 5.24. This shows that when a more concentrated solution is passed through the column very low retention of either compound occurs as the pores of HKUST-1 are likely over saturated.

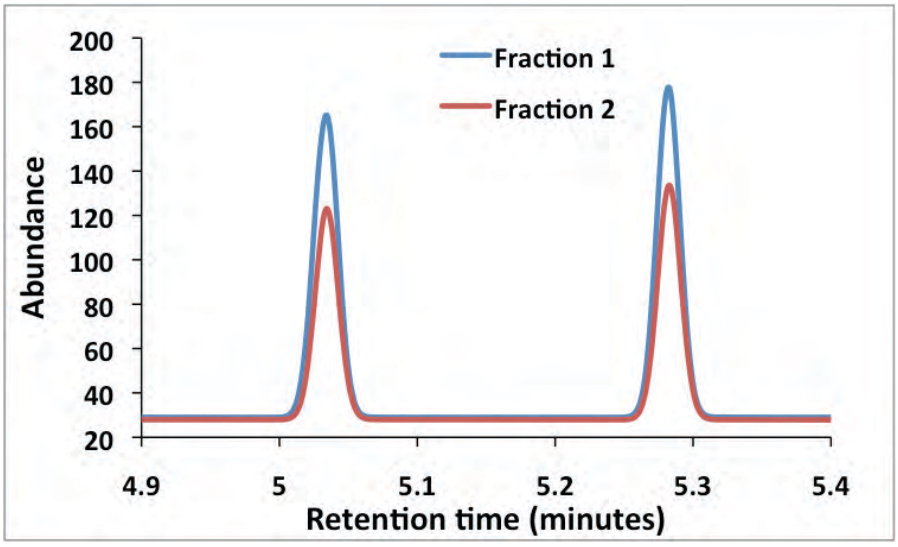

Figure 5.24 GC chromatogram showing peak heights after a solution of 50 µl 1:1 ethyl benzene/ styrene (1:1) in 15 ml heptane was passed through a 0.3 g column made from NH_2 functionalized polymer/MOF composite (loaded three times). 1.5 ml fractions were taken.

To assess aligned porous HKUST-1 composites as stationary phases for HPLC more investigation is required to isolate both ethyl benzene and styrene. From the data collected so far, it appears that using 5 µl for a 0.3 g column is a reasonable ratio for the separation of the two compounds. However a more polar solvent maybe required to isolate the styrene that is retained within the HKUST-1, for example using heptane/DCM mixtures could be beneficial. An interesting property of these composites is that only gentle pressure is required from a pipette to pass liquid through the material. This could be beneficial for any flow through methods such as separation or catalysis.

5.4 Conclusions

The versatility of the directional freezing and frozen UV initiated polymerization method is again demonstrated using another type of methacrylate monomer. TMSPMA and EGDMA can be applied to this method to produce aligned porous scaffolds. The trimethoxysilane groups on the surface of the crosslinked scaffolds can undergo modification reactions to introduce thiol and primary amine functionality. Introducing such functional groups to the surface can enable further surface reactions to take place.

Aligned porous silver composites were prepared by first modifying the surface with MPTMS to anchor thiol groups to the material. The resulting composites were shown to contain moderate amounts of silver, however they were non conductive. Further applications could be investigated using this material for water treatment or catalysis.

The other part of this study involved the attachment of primary amine functionality to the aligned porous silica containing scaffolds. This was achieved using APTES and the resulting scaffold was shown to be a more favourable than polyTEGDMA in terms of uniform growth of HKUST-1 MOF on the surface. DMSO was also found to be a better solvent for uniform loading than an ethanol/water mixture. Once the best conditions were discovered, multiple loadings of HKUST-1 on NH_2 containing scaffolds using DMSO was used to prepare composites for separation of organic

molecules. This was possible due to the stability of the composite material under autogenous pressure and temperatures up 250 °C.

Multiple loading increased surface coverage and BET surface area of composites and the triple loaded composite was used as a stationary phase to attempt to separate an ethyl benzene/styrene mixture. Although complete separation was not achieved, some retention of styrene was observed. Further investigation is required to assess aligned porous MOF composites as stationary phase for HPLC as well as catalysis. This method of producing MOF composites could also be extended to different types of MOF for different applications.

Two examples of aligned porous composites are shown in this chapter. This method could be extended to produce surfaces with functional groups and thus allowing production of a wider catalogue of aligned porous composites.

5.5 References

(1) Yang, Y.; Boom, R.; Irion, B.; van Heerden, D.-J.; Kuiper, P.; de Wit, H. *Chemical Engineering and Processing: Process Intensification* **2012**, *51*, 53.

(2) Meyer, C. *Cem. Concr. Compos.* **2009**, *31*, 601.

(3) Aho, A. J.; Rekola, J.; Matinlinna, J.; Gunn, J.; Tirri, T.; Viitaniemi, P.; Vallittu, P. *Journal of Biomedical Materials Research Part B: Applied Biomaterials* **2007**, *83B*, 64.

(4) Deville, S.; Saiz, E.; Nalla, R. K.; Tomsia, A. P. *Science* **2006**, *311*, 515.

(5) Munch, E.; Launey, M. E.; Alsem, D. H.; Saiz, E.; Tomsia, A. P.; Ritchie, R. O. *Science* **2008**, *322*, 1516.

(6) Gutiérrez, M. C.; Ferrer, M. L.; del Monte, F. *Chem. Mater.* **2008**, *20*, 634.

(7) Abarrategi, A.; Gutiérrez, M. C.; Moreno-Vicente, C.; Hortigüela, M. J.; Ramos, V.; López-Lacomba, J. L.; Ferrer, M. L.; del Monte, F. *Biomaterials* **2008**, *29*, 94.

(8) Gutiérrez, M. C.; Hortigüela, M. J.; Amarilla, J. M.; Jiminez, R.; Ferrer, M. L.; del Monte, F. *The Journal of Physical Chemistry C* **2007**, *111*, 5557.

(9) Katuri, K.; Ferrer, M. L.; Gutiérrez, M. C.; Jiménez, R.; del Monte, F.; Leech, D. *Energy & Environmental Science* **2011**, *4*, 4201.

(10) Barrow, M.; Eltmimi, A.; Ahmed, A.; Myers, P.; Zhang, H. *J. Mater. Chem.* **2012**, *22*, 11615.

(11) Romeo, H. E.; Hoppe, C. E.; López-Quintela, M. A.; Williams, R. J. J.; Minaberry, Y.; Jobbágy, M. *J. Mater. Chem.* **2012**, *22*, 9195.

(12) Du, J.; Kang, D. J. *Mater. Lett.* **2008**, *62*, 3185.

(13) Yang, L.; Ning, X.; Xiao, Q.; Chen, K.; Zhou, H. *Journal of Biomedical Materials Research Part B: Applied Biomaterials* **2007**, *81B*, 50.

(14) Xiao, B.; Wheatley, P. S.; Zhao, X.; Fletcher, A. J.; Fox, S.; Rossi, A. G.; Megson, I. L.; Bordiga, S.; Regli, L.; Thomas, K. M.; Morris, R. E. *J. Am. Chem. Soc.* **2007**, *129*, 1203.

(15) Grant Glover, T.; Peterson, G. W.; Schindler, B. J.; Britt, D.; Yaghi, O. *Chem. Eng. Sci.* **2011**, *66*, 163.

(16) Mueller, U.; Schubert, M.; Teich, F.; Puetter, H.; Schierle-Arndt, K.; Pastre, J. *J. Mater. Chem.* **2006**, *16*, 626.

(17) Munch, A. S.; Mertens, F. O. R. L. *J. Mater. Chem.* **2012**, *22*, 10228.

(18) Xie, S.-M.; Zhang, Z.-J.; Wang, Z.-Y.; Yuan, L.-M. *J. Am. Chem. Soc.* **2011**, *133*, 11892.

(19) Liu, S.-S.; Yang, C.-X.; Wang, S.-W.; Yan, X.-P. *Analyst* **2012**, *137*, 816.

(20) Chang, N.; Gu, Z.-Y.; Yan, X.-P. *J. Am. Chem. Soc.* **2010**, *132*, 13645.

(21) Bradshaw, D.; Garai, A.; Huo, J. *Chem Soc Rev* **2012**, *41*, 2344.

(22) Ahmed, A.; Forster, M.; Clowes, R.; Bradshaw, D.; Myers, P.; Zhang, H. *Journal of Materials Chemistry A* **2013**, *1*, 3276.

(23) Ameloot, R.; Liekens, A.; Alaerts, L.; Maes, M.; Galarneau, A.; Coq, B.; Desmet, G.; Sels, B. F.; Denayer, J. F. M.; De Vos, D. E. *Eur. J. Inorg. Chem.* **2010**, *2010*, 3735.

(24) Tanaka, K.; Muraoka, T.; Hirayama, D.; Ohnish, A. *Chem. Commun.* **2012**, *48*, 8577.

(25) Ahmed, A.; Myers, P.; Zhang, H. *Analytical Methods* **2012**, *4*, 3942.

(26) O'Neill, L. D.; Zhang, H.; Bradshaw, D. *J. Mater. Chem.* **2010**, *20*, 5720.

(27) Schwab, M. G.; Senkovska, I.; Rose, M.; Koch, M.; Pahnke, J.; Jonschker, G.; Kaskel, S. *Adv. Eng. Mater.* **2008**, *10*, 1151.

(28) Sachse, A.; Ameloot, R.; Coq, B.; Fajula, F.; Coasne, B.; De Vos, D.; Galarneau, A. *Chem. Commun.* **2012**, *48*, 4749.

(29) Barrow, M.; Zhang, H. *Soft Matter* **2013**, *9*, 2723.

(30) Savard, S.; Blanchard, L. P.; Léonard, J.; Prud'homme, R. E. *Polym. Compos.* **1984**, *5*, 242.

(31) Venkateswara Rao, A.; Bhagat, S. D. *Solid State Sciences* **2004**, *6*, 945.

(32) Brochier Salon, M.-C.; Bayle, P.-A.; Abdelmouleh, M.; Boufi, S.; Belgacem, M. N. *Colloids and Surfaces A: Physicochemical and Engineering Aspects* **2008**, *312*, 83.

(33) Chojnowski, J.; Rubinsztajn, S.; Wilczek, L. *Macromolecules* **1987**, *20*, 2345.

(34) Jitianu, A.; Britchi, A.; Deleanu, C.; Badescu, V.; Zaharescu, M. *J. Non-Cryst. Solids* **2003**, *319*, 263.

(35) Ahmed, A.; Clowes, R.; Myers, P.; Zhang, H. *J. Mater. Chem.* **2011**, *21*, 5753.

(36) Gordon, O.; Slenters, T. V.; Brunetto, P. S.; Villaruz, A. E.; Sturdevant, D. E.; Otto, M.; Landmann, R.; Fromm, K. M. *Antimicrob. Agents Chemother.* **2010**, *54*, 4208.

(37) Connolly, D.; Twamley, B.; Paull, B. *Chem. Commun.* **2010**, *46*, 2109.

(38) Zhang, H.; Lee, J.-Y.; Ahmed, A.; Hussain, I.; Cooper, A. I. *Angew. Chem. Int. Ed.* **2008**, *47*, 4573.

(39) Brown, J.; Mercier, L.; J. Pinnavaia, T. *Chem. Commun.* **1999**, *0*, 69.

(40) Chui, S. S.-Y.; Lo, S. M.-F.; Charmant, J. P. H.; Orpen, A. G.; Williams, I. D. *Science* **1999**, *283*, 1148.

(41) Klimakow, M.; Klobes, P.; Thünemann, A. F.; Rademann, K.; Emmerling, F. *Chem. Mater.* **2010**, *22*, 5216.

(42) Hasell, T.; Zhang, H.; Cooper, A. I. *Adv. Mater.* **2012**, *24*, 5732.

(43) Majano, G.; Pérez-Ramírez, J. *Helv. Chim. Acta* **2012**, *95*, 2278.

Chapter 6

Conclusions and outlook

The main success of this piece of work is the development of a new directional freezing and frozen UV polymerization method to produce aligned porous materials. The method was used to produce a range of materials with different functionality. When the work began, there were no reports of directional freezing of monomer solutions followed by frozen UV polymerization. However, in the last three years more reports are emerging employing the two methods.[1,2] There has also been reports of directional freezing of monomer solutions followed by redox cryopolymerization.[3,4] Materials prepared using this method were further functionalized to by filling the pores of the material with responsive polymer to make composites with tailored functionality.[5]

6.1 Chapter 3

The first experimental work involved development of the new frozen polymerization technique. Dimethacrylate monomer (TEGDMA) was used to fabricate crosslinked aligned porous structures with significantly improved mechanical stability compared to freeze dried polymer material. As a result of the crosslinked nature and significant mechanical stability, the frozen samples could be warmed up to remove the solvent under vacuum at room temperature, thereby avoiding the use of freeze-drying procedure but maintaining the aligned structures. The aligned porous polymer was further treated with graphene and PEDOT-PSS to produce conductive porous structures. The aligned porous polymer monolith was also assessed for HPLC, demonstrating the separation of the test mixture with well-resolved peaks. This highlights the potential of this material as a stationary phase in reverse phase chromatography. It could be possible to produce a range of functional aligned porous materials for applications in chromatography or porous electrodes by varying the monomers used for frozen polymerization. Using monomers with lower oxygen content could be beneficial for conductive material as carbonization could be used to produce crosslinked conductive material. Also to improve the chromatographic performance, structures with more C-C bonds compared to C-O could be more beneficial as a stationary phase for reverse phase chromatography. Alternatively, using specific monomers or grafted surfaces for a particular mode of chromatography.

The method was expanded to produce aligned porous structures using different methacrylates such as polyHEMA, which is a very hydrophilic polymer. This led to the conclusion that it could be possible to produce aligned porous stimuli responsive structures using other methacrylate monomers.

6.2 Chapter 4

In chapter 4 the new directional freezing and frozen UV initiated polymerization was expanded to produce aligned porous temperature- and pH-responsive polymeric materials. They were prepared using methacrylate monomers OEGMA and DMAEMA and crosslinker EGDMA. The swelling properties of the materials acting as hydrogels was manipulated by changing crosslinker ratio and porosity. Both can were achieved simply by changing the compositions of the monomer solutions. Anisotropic compressive strength and diffusion behaviour were observed with respect to the direction of freezing. The anisotropic properties of these materials could be particularly useful for guiding cell growth or targeted delivery.[6-8] Further studies could be focused on the biocompatibility and cytotoxicity of the hydrogels and also finely tuning the sensitivity for potential biological applications. In terms of tissue engineering, it could be possible to try to prepare aligned porous structures of other biocompatible polymers such as polymethacryloxyethyl phosphorylcholine. Once the biocompatibility of such polymer networks is achieved, *in vivo* testing in various living systems could be attempted and compare results with other polymer scaffolds.

6.3 Chapter 5

In chapter 5 the versatility of the directional freezing and frozen UV initiated polymerization method was again demonstrated using another type of methacrylate monomer. TMSPMA and EGDMA were applied to this method to produce aligned porous scaffolds. The trimethoxysilane groups on the surface of the crosslinked scaffolds could undergo modification reactions to introduce thiol and primary amine functionality. Introducing the functional groups to the surface enabled further surface reactions to take place.

Aligned porous silver composites were prepared. This was possible due to grafting of thiol groups to the material before the silver salt was added. Even though the composites were not conductive, presence of silver on the surface was confirmed. Further work could include attempting to understand why conductive materials were not achieved with high loading of silver. Also attachment of other metals such as gold could be attempted.

The other part of this chapter involved the attachment of primary amine functionality to the aligned porous silica containing scaffolds. This was achieved using APTES and the scaffold was shown to be more favourable than polyTEGDMA in terms of uniform growth of HKUST-1 MOF on the surface. DMSO was also found to be a more a better solvent for uniform loading than an ethanol/water mixture. Once the best conditions were discovered, multiple loadings of HKUST-1 were carried out and the composite material was used for attempted separation of organic molecules. Multiple loadings were possible due to the stability of the composite material under pressure in an autoclave and temperatures up 250°C. More loading cycles increased surface coverage and BET surface area of composites and the triple loaded composite was used as a stationary phase to attempt to separate an ethyl benzene/styrene mixture. Although separation was not completely achieved of both components, retention of styrene was observed. Further investigation is required to assess aligned porous MOF composites as stationary phase for HPLC as well as catalysis. This method could also be applied to other aligned macro/micro porous composites.

It could also be possible to use the raw silica scaffolds for chromatography and attempt to graft functional groups to the surface for specific chromatography modes.

6.4 Outlook

Aligned porous materials made by directional freezing and frozen UV polymerization are still relatively unexplored. In this work functional aligned materials have been prepared and do demonstrate some advantages compared to regularly porous materials and mechanically weak freeze dried materials. Future studies could focus on composition of material, mechanical stability, tissue

engineering, or energy storage. A lot more investigation is required to exploit this method and new breed of material fully.

6.5 References

(1) de Hazan, Y. *J. Am. Ceram. Soc.* **2012**, *95*, 177.

(2) Okaji, R.; Taki, K.; Nagamine, S.; Ohshima, M. *J. Appl. Polym. Sci.* **2012**, *125*, 2874.

(3) Zhu, J.; Wang, J.; Liu, Q.; Liu, Y.; Wang, L.; He, C.; Wang, H. *Journal of Materials Chemistry B* **2013**, *1*, 978.

(4) Wu, J.; Zhao, Q.; Sun, J.; Zhou, Q. *Soft Matter* **2012**, *8*, 3620.

(5) Wu, J.; Lin, Y.; Sun, J. *J. Mater. Chem.* **2012**, *22*, 17449.

(6) Abarrategi, A.; Gutiérrez, M. C.; Moreno-Vicente, C.; Hortigüela, M. J.; Ramos, V.; López-Lacomba, J. L.; Ferrer, M. L.; del Monte, F. *Biomaterials* **2008**, *29*, 94.

(7) Xu, C. Y.; Inai, R.; Kotaki, M.; Ramakrishna, S. *Biomaterials* **2004**, *25*, 877.

(8) Mandoli, C.; Mecheri, B.; Forte, G.; Pagliari, F.; Pagliari, S.; Carotenuto, F.; Fiaccavento, R.; Rinaldi, A.; Di Nardo, P.; Licoccia, S.; Traversa, E. *Macromolecular Bioscience* **2010**, *10*, 127.